NTNU – Trondheim
Norwegian University of
Science and Technology

The impact of wettability alterations on oil release and transport mechanisms in a 2D porous medium

Vegard Flovik

Physics
Submission date: July 2012
Supervisor: Alex Hansen, IFY

Norwegian University of Science and Technology
Department of Physics

The impact of wettability alterations on oil release and transport mechanisms in a 2D porous medium

Vegard Flovik*

July 20, 2012

*Electronic address: vegardflovik@yahoo.no

1 Abstract

The effects of wettability alterations in a 2D network model of a porous media has been studied. By changing the wetting properties of the reservoir through a developed algorithm, previously immobile oil clusters in the network are re-mobilized, leading to significant changes in the steady state flow distribution of the model porous media. This caused de-stabilization of percolating and trapped clusters as the wettability was changed from an oil wet to a mixed wet system.

A critical transition at a certain wetting angle, depending on the initial saturation and lattice size of the system was found. This indicating a possible phase transition from a percolating flow regime to a more uniform flow distribution through the network model. A link between changes in fractional flow and a percolation transition is also suspected, and using the theoretical framework of percolation theory, D.Stauffer and A.Aharony [38], critical exponents were estimated. The best estimate for a critical exponent was $\beta = 0.13 \pm 0.02$, which is close to the result from ordinary percolation: $\beta = 5/36 \approx 0.1388...$ The critical transition in fractional flow, seems to obey similar scaling laws as that of ordinary percolation. The use of finite size scaling theory to investigate the system for various lattice sizes, yielded a rough estimate for the correlation length critical exponent, $\nu \approx 0.4$, which is significantly smaller compared to the result from ordinary percolation, $\nu = 4/3$.

2 Sammendrag

Effekten av å endre fuktegenskapene i en 2D nettverksmodell av et porøst medium har blitt undersøkt. Ved å endre fuktegenskapene i reservoaret gjennom en utviklet algoritme blir tidligere immobile olje-clustere re-mobilisert, og dette fører til signifikante endringer i systemets strømningsegenskaper. Endringene fra et oljefuktende nettverk til en mix av både vann og oljefuktende, førte til sammenbrudd av perkolerende og fangede clustere.

En kritisk overgang ved en viss fuktningsvinkel, avhengig av oljemetning og nettverksstørrelse ble funnet. Dette indikerer en mulig faseovergang fra et perkolerende strømningsregime, til en mer uniform strømningsfordeling gjennom nettverket. En mulig kobling mellom endringer i oljestrømning og perkolasjon er også undersøkt, og ved å bruke det teoretiske fundamentet fra perkolasjonsteori, ble kritiske eksponenter estimert. Stauffer og A.Aharony [38]. Det beste estimatet for en kritisk eksponent var $\beta = 0.13 \pm 0.02$, som er nærme resultatet fra ordinær perkolasjon: $\beta = 5/36 \approx 0.1388...$ Den kritiske overgangen i oljestrøming, oppfyller tilsynelatende lignende skalerings-lover som ordinær perkolasjon. Ved å bruke finite-size skaleringsteori for å undersøke systemet for forskjellige nettverksstørrelser, ble et overslag for korrelasjonslengdens kritiske eksponent estimert til $\nu \approx 0.4$, som er betydelig mindre sammenlignet med resultatet fra ordinær perkolasjon, $\nu = 4/3$.

3 Preface

The following thesis is submitted as part of the requirements for the Master's degree in physics, and concludes my studies at the Norwegian University of Science and Technology, (NTNU). It has been written under the supervision of Professor Alex Hansen, and it was proposed by Erik Skjetne at Statoil ASA. I have also been working in collaboration with post doc. Santanu Sinha at NTNU, whose insight in the subject of network modelling has been most valuable. Computational resources has been found at the department of physics' UNIX cluster.

Complex systems has been a research field in rapid growth the last years, but to our knowledge this kind of simulation haven't been conducted before. This still being a quite simple model, but it captures the essential physics of the system. However, there is still a way to go in further research before a direct comparison with real oil reservoirs.

The fact that something is complicated is not a reason to give up. Rather the contrary. Given the large impact a greater understanding of this topic could yield, it should definitively be a focus area in time to come. In my opinion, the motivation for studying physics is the desire to understand the world. This is why I find the opportunity to work on this topic so rewarding. It is my hope that our work could be part of solving the puzzle, and that continued effort will lead to further progress in times to come.

There are recommendations on further work, and still a lot of questions which needs to be addressed.

Trondheim, july 2012

Vegard Flovik

4 Acknowledgements

First, I would like to thank my supervisor Alex Hansen at NTNU, and Erik Skjetne at Statoil for giving me the opportunity to work on such an interesting problem. They have contributed with valuable input and knowledge, which has inspired me greatly in my work. I would also like to thank Santanu Sinha for his help with the network model and comments on the final manuscript, and the participants at our weekly meetings in the COMPLEX research group at NTNU for interesting discussions.

A thank should also go to the lecturers at Sør-Trøndelag university college who inspired me to go for an education in physics rather than engineering studies as was my original plan. It is a choice I have never regretted.

And to all those who made my student years in Trondheim such an amazing experience, and more then just books and studying. It‘s been a great time!

Finally, special thanks to my family for their support and encouragement. I could not have done it without you.

Contents

List of Figures

5 Introduction

One of the big challenges in the time to come, is to solve the increasing energy demands of the world. Population is increasing, and the standard of living in developing countries is getting higher. Still, there is no way of satisfying this need in terms of renewable energy sources. This means that fossil fuels like oil and gas will still be very important sources of energy in many years to come. The fact that some 20 to 60 percent of the oil remains in the reservoir after the end of oil production, is a challenge of increasing importance in these times of dwindling oil reserves. Roberts [5]. The reason for this loss is the formation of oil clusters embedded in water and held in place by capillary forces, which in turn are controlled by the wetting properties of the reservoir fluids with respect to the matrix rock.

The production from oil reserves that today are considered immobile due to complex reservoirs will then be an important area of focus. The easy accessible reserves are running out, and an increasing amount of the world oil reserves are located in challenging and complex reservoir conditions. Conducting research in this area of improved oil recovery should thus be a focus area in the time to come, and wetting properties of reservoirs is an important topic within the field of Enhanced Oil Recovery, EOR. The role of formation wettability has been reviewed during e.g. Schlumbergers Wettability Workshop in 2007, [2].

Sandstone is strongly water wet before oil migrates from a source rock into the reservoir. When oil enters a pore, it displaces water and forms a water film sandwiched between the oil and rock surface. This film may be several nanometers thick, and results from balancing Van der Waals and electric double layer forces, capillary pressure and grain curvature. Israelachvili [3]. A permanent wettability alteration is believed to take place by adsorption of asphaltenes from the crude oil to the rock, and leads to high but slow recovery through continuous oil films. Kovschek et al. [4], Kaminsky et al. [10]. As the oil saturation drops, these films can become discontinuous, leaving immobile oil clusters held in place by capillary forces.

An important parameter which can determine the wetting properties of the reservoir, is the salinitiy of the pore water. At low salinities, perfect water wetting can be achieved. By increasing the salinity level of the pore water, the wetting angle increase. Also, increase in temperature results in more water wetness of the reservoir, which increase the oil recovery. Skauge et al. [8]. This could also be of great importance during e.g thermal recovery methods.

Changes in the reservoir from strongly oil wet to neutral wet or water wet conditions, show a significant increase in oil recovery depending on the stage of recovery. Tweheyo, Holt and Torster [9]. New production methods, like low salinity water flooding show some promising results in increasing the recovery factor of reservoirs, and many mechanisms explaining this effect have been suggested. Correlations have been shown with wetting behavior to the electrostatic forces between the rock and oil surfaces. Buckley et al. [11]. But there is still no consensus on that what the dominating microscopic mechanism is. Research towards a deeper understanding of these effects could be an important effort

towards a more complete understanding of transport properties in reservoirs, and has been a priority in the industry for years.

In this work, it is assumed that local wettability alterations take place, and the consequences of this on oil recovery by re-mobilizing stuck oil clusters is investigated. To study these effects, a two-dimensional pore scale network simulation model is used. Having bi-periodic boundary conditions, it allows the study of steady state properties, representing the flow behavior deep inside the reservoir. The effect of wettability alteration is introduced in the model through a developed algorithm, continuously adjusting the wetting angles in the network during simulation. The changes in steady state flow properties of the system as a result of this is then studied.

6 Theory

The main focus of this work, is the effect of pore wettability on the transport properties of oil reservoirs. In reservoirs, there is usually a mix of oil, water and gas which leads to multi-phase flow. This cause less efficient recovery due to the immiscibility of the different phases, and surface tensions between the fluids. The effect of wettability alterations in the reservoir is believed to be one of the key parameters in achieving higher recovery. The complete physics governing changes in wettability is not yet fully understood, and this thesis will thus focus on the effects of this change, rather than the underlying physics of wettability alterations itself.

This chapter will discuss the concept of wettability, and also give a general introduction to the topic of fluid flow in porous media. Major parts of the theory introduction is from the book by Dullien, "Fluid transport and pore structure" [1] , and Schlumbergers "Fundamentals of wettability" [2].

6.1 Wettability, introduction

The definition of wettability, is the ability of one of the immiscible fluids in multi phase systems to adhere to the surface of a solid. You have probably witnessed the effect of wettability if you have polished your leather shoes, or waxed your car. This wax layer makes the surface oil wetting, causing water to form droplets on the surface which simply "rolls off", keeping your feet nice and dry, and your car protected from rust.

In the context of reservoirs, this effect has important implications. If the reservoir rock is mainly water wetting, this means is has a higher affinity to water than oil. The result of this, is that water will occupy the smaller pores and also cover most of the pore surfaces in the reservoir. Whereas for an oil wet reservoir, the opposite will happen. Depending on reservoir conditions, rock types, etc. the rock wettability can vary between strongly water wet and strongly oil wet. An important parameter describing wettability, is the wetting angle θ, which ranges from 0 to 180 degrees. As seen in figure 1, in the case of a small wetting angle the system is strongly water wetting, and the oil forms a droplet on the surface. In the complete opposite case with a wetting angle close to 180 degrees, the oil will form a thin film which covers the surface.

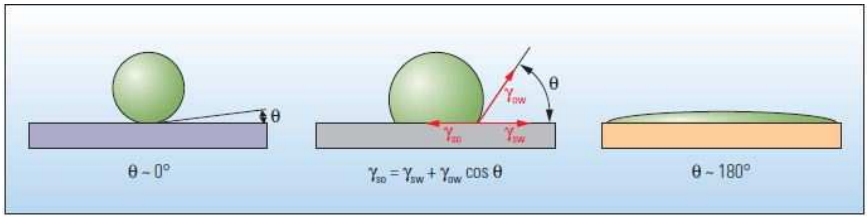

Figure 1: wetting angles ranging from oil wet to water wet, where oil is shown as green. Figure from Schlumberger [2]

Understanding formation wettability is crucial for optimizing oil recovery. The oil versus water wetting preference influence many aspects of reservoir performance, particularly in water flooding and enhanced oil recovery techniques. Making the assumption that a reservoir is water wet when it is not, can lead to irreversible damage to the reservoir. The significant impact on reservoir performance make it one of the most important parameters in reservoir engineering, and is crucial in order to enhance oil recovery.

How to categorize the wettability in different reservoirs is still a major challenge, and there are many conflicting results, showing that the science governing the impact of wettability is very complex. An interesting fact, is that the wettability of a reservoir is not a static property. This means we can attempt to change it in order to increase the reservoir performance, and enhance oil recovery.

In many oil field applications, wettability is considered a binary "switch", meaning the rock is either water wet, or oil wet. This if of course an extreme simplification of the real wetting physics of the reservoir. In real reservoirs, the wettability can be distributed between the two extremes, and will also be a function of position in the reservoir.

6.2 Wettability types

As mentioned, uniform wettability is an idealized condition, and it depends on previous reservoir history on geological time scales. In the case of strongly water wet areas, the pore surface is exclusively in contact with water, while the oil and gas will occupy only the center of larger pores.

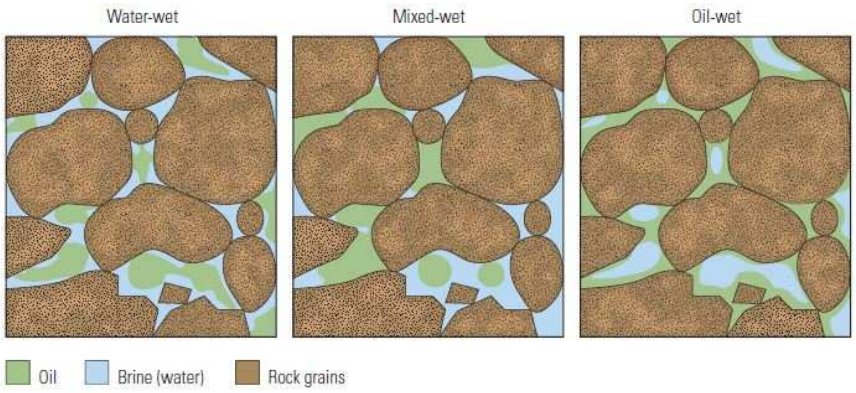

Figure 2: Illustration of pore spaces with different wetting properties, filled by water and oil. The tendency of water films to cover the rock grains in a water wet reservoir is clearly seen, and also the opposite case for oil wet reservoirs. Figure from Schlumberger [2].

In the case of strongly oil wet reservoirs, these properties are simply switched. In more complex reservoirs some regions might have been changed, causing a

mixing of water wet and oil wet regions. These cases are called mixed wet reservoirs, but must not be confused with the case of intermediate wet reservoirs. In the intermediate case, the wetting angle is considered relatively constant throughout the reservoir, with the wetting angle in the range between oil and water wet around 90 degrees. In this case, the rock has an equal affinity to both oil and water. The last classification, is the fractionally wet case. This is considered a special type of mixed wet reservoir, with a mixing of different wetting properties. But in this case with the constraint that there exists a continuous path of oil wet cores in the reservoir. The case of mixed wettability is usually divided in two states, mixed wet small pores (MWS) and mixed wet large pores (MWL), Schlumberger [2] The difference between the MWL and MWS cases is believed to depend on the saturation history of the reservoir. An originally water filled reservoir is believed to initially have been strongly water wet. Oil migration into this reservoir will thus displace the brine into the smaller pores, and oil will only be present in the larger ones. It is then believed that the oil present in the larger pores change the wettability to more oil wet in these pores, and is then what cause the MWL vase. In the opposite case with an initially oil wet reservoir, we would get the MWS case.

The case which usually gives the lowest residual oil saturation, is the mixed wet reservoir. This due to the occurrence of spontaneous imbibition of both oil and water.

6.3 Surface roughness and apparent wetting angles

The idea of a specific wetting angle θ, is derived assuming a smooth surface. However, the real pore space in a reservoir is far from a smooth surface. The apparent wetting angle can thus differ significantly from the real wetting angle, as seen in figure 3. Schlumberger [2]

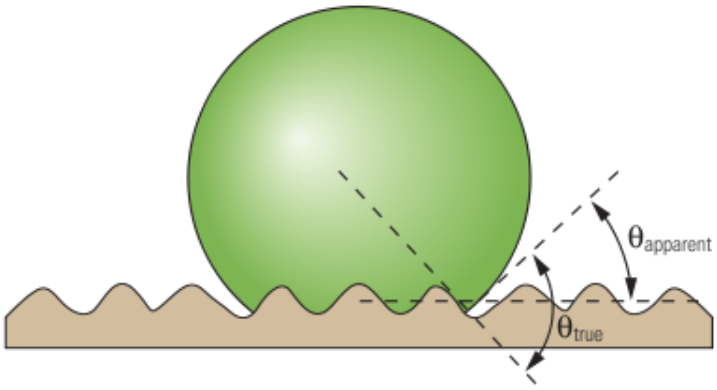

Figure 3: Wetting angle of a fluid droplet at a rough surface, showing the difference between the true and the apparent wetting angle. The apparent wetting angle, $\theta_{apparent}$, indicates a non wetting fluid, whereas the true wetting angle, θ_{true}, indicates intermediate wetting,($\approx$ 90 degrees). Figure from Schlumberger [2]

The difference between apparent and real wetting angle can be significant when the surface area of the pore surface is large compared to the idealized smooth surface. This is described by Wenzel's equation, Wenzel [25].

$$cos\,\theta_{apparent} = r \cdot cos\,\theta_{true} \tag{1}$$

where $\theta_{apparent}$ is the apparent wetting angle corresponding to the stable equilibrium state and r is the roughness ratio, defined as the ratio between the true area of the solid surface to the apparent area.

6.4 Wettability alteration by low salinity water injection

Many suggestions are proposed as the main mechanisms for incremental oil recovery by low salinity water injection, and it is obvious that the working mechanisms of the method is not well verified. Sorbie and Collins [26], Rivet, Lake, Pope [27]. However, wettability alteration is considered a key factor to affect fluid distribution in a porous media. The change of electrical charge at oil/brine and brine/rock interfaces is one of the proposed mechanisms. Nasralla, Bataweel, Nasr-El-Din [24].

Rock wettability is a function of the sign and magnitude of the electric charge at oil/brine and brine/rock. These repulsive or attractive forces between the interfaces are described by Coloumb's law for electric fields. A charge of same sign at both interfaces, will result in repulsive force proportional to the multiplication of the magnitude of the charges. In the case of opposite sign, the force will be attractive.

In experiments performed by Nasralla et al [24], the electrical charge at oil/brine interfaces was measured against different brine ionic strengths using a zeta potential technique. The change of the electro-kinetic charge of the oil/brine interface is related to the wettability alteration caused by low salinity water. The stability of the water film is depending on the electrical double layer repulsion resulting from surface charges at the rock/water and water/oil interfaces. If these interfaces have similar charges, it will result in a repulsive force that maintains a stable water film, giving a water wet surface. The zeta potential is the potential at the shear plane of the electrical double layer. The magnitude of this potential depends on the charge at the oil/brine and brine/rock interfaces, and the thickness of the double layer. The zeta potential in Berea sandstone, silica and kaolinite were highly negative in fresh water. Nasralla, Bataweel, Nasr-El-Din [24]. Low ionic strength of the NaCl solutions (low salinity) resulted in stronger negative charges of brine/oil interfaces, which could be caused by changes in the screening length of the electrical potential depending on the ionic strength of the water. It is evident that electro-kinetic charges of both oil/brine and brine/rock interface are of great importance for wetting properties, even though the full theoretical description is still not completely understood.

6.5 Surface tension and capillary pressure

The capillary pressure is defined as the pressure across the interface between two immiscible fluids, and thus defined as $p_c = p_{non-wettingphase} - p_{wettingphase}$. The starting point to obtain the expression for the capillary pressure in this network model, is from deriving the Young Laplace equation, Laplace [12]. This is a non linear partial differential equation, that describes the capillary pressure across an interface of two static fluids due to the phenomenon of surface tension. The Young Laplace equation relates the pressure difference between the two fluids, to the shape of the surface separating them. This equation is thus a statement of normal stress balance for static fluids meeting at an interface, where this interface is treated as a surface (zero thickness).

An arbitrary surface, where gravitational effects are neglected is considered in this case. Dullien [1].

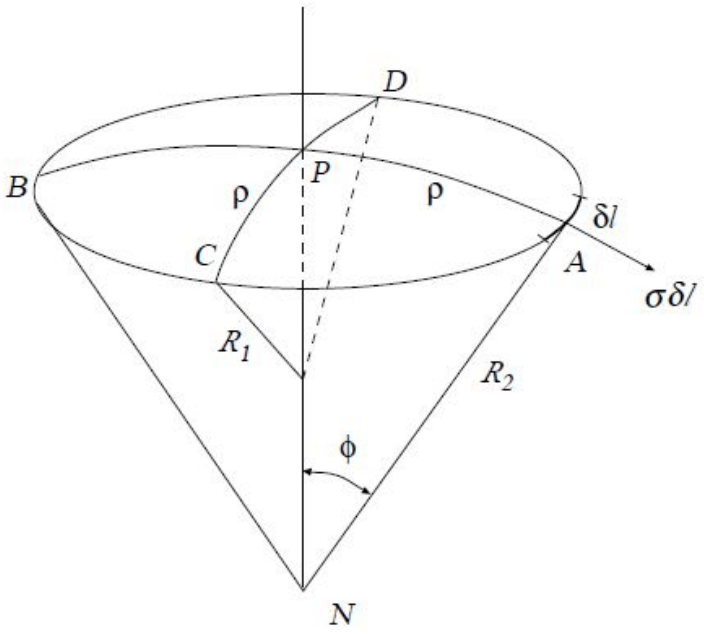

Figure 4: Capillary equilibrium of a nonspherical cap. Figure from Dullien [1].

Consider a point P on the surface (see figure 4) and draw a curve at a constant distance ρ from P. This curve forms the boundary of a cap, spanned by the points A, B, C, D, for which we shall find the equilibrium condition as ρ tends to zero. Through P we draw the two principal curvature sections AB and CD on the surface. Their radii of curvature at P, are R1 and R2. At the point A, an element δl of the boundary line is subjected to a force $\sigma\delta l$, where σ is the surface tension. ϕ is defined in figure 4 and is considered to be small, as one let ρ tend to zero. The projection of this force along the normal PN is then:

$$\sigma\delta l sin\,\phi \approx \sigma\frac{\rho}{R_2}\delta l \tag{2}$$

If one consider four elements δl of the periphery at A, B, C, and D, they will contribute with a force:

$$\rho\sigma\delta l\left(\frac{2}{R_1}+\frac{2}{R_2}\right) \tag{3}$$

This expression is independent of the choice of AB and CD, and can thus be integrated around the circumference. Since four orthogonal elements are considered, the integration is performed over one quarter revolution, giving:

$$F_1 = \pi\rho^2\sigma\left(\frac{1}{R_1}+\frac{1}{R_2}\right) \tag{4}$$

The force on the surface element caused by the pressure difference over the surface, Δp , is given by $F_2 = \Delta p \pi \rho^2$. Equating these forces to each other, gives the Young Laplace equation. Laplace [12]

$$\Delta p = \sigma \left(\frac{1}{R_1} + \frac{1}{R_2} \right) \tag{5}$$

A simple and widespread model representation of reservoir rocks, is a bundle of capillary tubes. If a non wetting fluid is to displace a wetting fluid in these tubes, a pressure difference Δp, called the capillary pressure has to be overcome.

$$\Delta p = p_c = p_{nw} - p_w \tag{6}$$

Where the subscripts nw and w refer to the pressures of non wetting and wetting phases. An increase in capillary pressure, allows more of the non wetting fluid to penetrate into the system. By measuring the pressure difference between the phases, the capillary pressure can be determined. The capillary pressure in a tube is found from the Young Laplace equation, and depends on the contact angle between the two fluids, θ (shown in figures 1 and 5), and the interfacial tension σ.

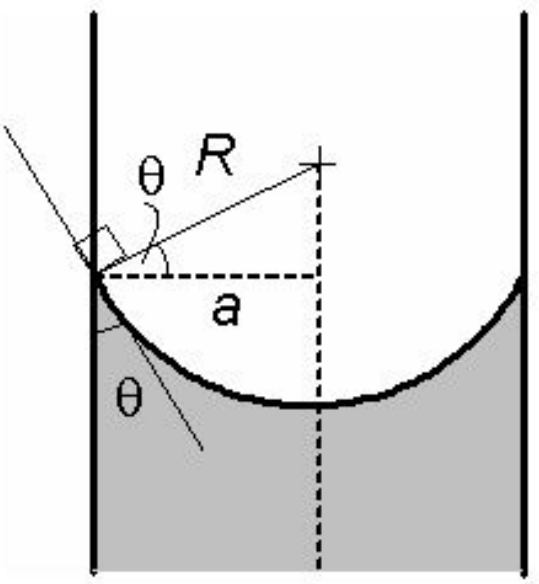

Figure 5: Menisci in a capillary tube. R is the radii of curvature, a is the tube radius and θ the wetting angle

In a sufficient narrow tube with a circular cross section, the fluid interface forms a meniscus that is part of a surface of a sphere with radius R (figure 5). From eq.(5), the pressure drop across the surface will then be:

$$\Delta p = \frac{2\sigma}{R} \tag{7}$$

The radius of this sphere will depend on the contact angle θ and the radius of the capillary tube, a, as seen in figure 5.

$$R = \frac{a}{cos\theta} \tag{8}$$

The pressure drop can thus be written as:

$$\Delta p = p_c = \frac{2\sigma cos\theta}{a} \tag{9}$$

6.6 Displacement in two phase flow in porous media

The two essential types of displacement in two phase flow in porous media are drainage and imbibition. Drainage means that a non wetting fluid displace a wetting fluid. E.g, if a reservoir is originally water filled and considered water wet, drainage is the process when oil is entering the pore space. For imbibition it's the opposite case, that wetting fluid displace a non wetting fluid. As would be the case during water injection into an oil filled water wet reservoir.

The capillary pressure curve seen in figure 6 show the displacement of the wetting phase by the non wetting phase, starting from full saturation to irreducible saturation (point A). This is the process called primary drainage and is, as mentioned above, the equivalent of the process where oil migrate from the source rock into a water filled reservoir. The term irreducible wetting saturation, is when the wetting phase saturation seems independent of further increase in the capillary pressure. This means the remaining water in the pore space is trapped at this point.

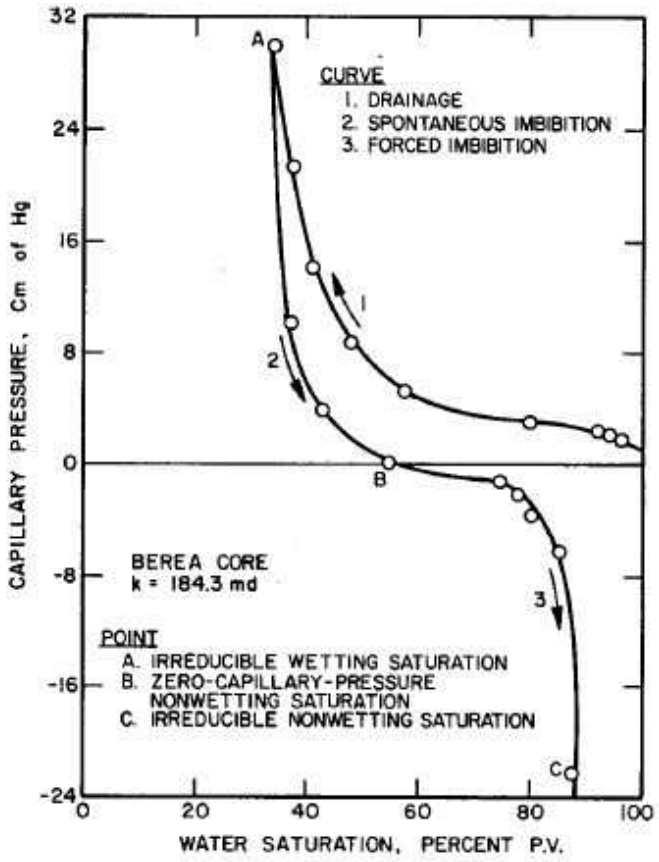

Figure 6: Capillary pressure curve for a water wet system showing both drainage, spontaneous imbibition and forced imbibition. Capillary pressure on the y-axis, and water saturation given by percentage of the total pore volume on the x-axis. Figure from Anderson [13].

If the capillary pressure, initially at a large positive value is gradually decreased to zero, this will allow the wetting phase (water) to imbibe. (Curve from point A to B in figure 6). The non wetting residual saturation reached when $p_c = 0$ (residual oil saturation) is referred to as the zero-capillary-pressure non wetting saturation. Curve 3 in this figure is the forced imbibition curve, where the capillary pressure is decreased from zero to a large negative value. When the capillary pressure is negative, this cause the pressure of the wetting phase (water) to be greater than in the non wetting phase (oil), forcing water into the core. This will continue up to the point of irreducible non-wetting phase saturation, where the non wetting phase looses its hydraulic continuity. That is, the saturation of the non wetting phase reaches the level where it is no longer continuously connected through the reservoir. In the case of a wa-

ter flooding process to displace oil, this is the point where the remaining oil is trapped as clusters held in place by capillary forces. Further oil recovery is then only possible by enhanced recovery methods.

6.7 Relative permeability

Permeability in fluid mechanics and the earth sciences, is a term used to describe the conductivity of a porous media with respect to flow by a Newtonian fluid. However, permeability used in this general sense is of limited usefulness because its value in the same porous medium may vary with the properties of the fluid present, and the mechanism of permeation. It is more useful to separate out the parameter which measures the contribution of the porous medium to the conductivity, and is independent of both fluid properties and flow mechanisms. This is a purely geometrical quantity, and is uniquely determined by the pore structure of the reservoir. This quantity is the specific permeability, often denoted by k. In the following this is referred to as simply the permeabiltiy, and it is defined by Darcy‘s law: Dullien [1].

$$Q = -\frac{kA}{\mu}(\nabla P - \rho g) \tag{10}$$

Where Q is the volumetric flow rate, A the normal cross section area of the sample, k the permeability tensor, μ the fluid viscosity, ∇P the pressure gradient, ρ the fluid density and g the gravitation vector.

Relative permeability on the other hand, is an important quantity which not only depends on the pore geometry, but also which fluids are present in the system. The relative permability is expressed as fractions of the permeability k of the system. For instance, the relative permeability of oil is defined as the following:

$$k_{ro} = \frac{k_o}{k} \tag{11}$$

Where k_{ro} is the relative permeability of oil, k_o is the permeability of oil and k is the absolute permeability. Thus, the relative permeability of oil describes the effective permeability of the oil phase compared to the absolute permeability of the system.

If one assumes that the effect of gravity is negligible and that the pressure gradient across the system is linear, one gets another version of Darcys law:

$$u_0 = -\frac{kk_{ro}}{\mu_0}\frac{\delta P}{\delta x} \tag{12}$$

Where u_o is the flow velocity of oil, driven by the pressure gradient across the system, $\delta P/\delta x$.

When studying recovery methods, relative permeability curves are of great importance. The relative permeabilities are dependent on the wetting properties of the fluids, and changes in the wettability have significant impact on the effect

of water flooding. In the case of water wet cores, they will produce a very low water fraction until water breakthrough, and then experience a sudden increase in water production. Mixed wet systems will produce oil with a higher but more constant water fraction until the oil saturation becomes very low. Water flooding of a neutrally wet reservoir gives the highest total oil recovery, while oil wet systems give the lowest recovery after flooding of a few pore volumes.

There exists several contradictory results on how to relate wettability and permeability, and the relevant transport mechanisms are not as easy to understand as first assumed. The coupling between wettability and permeability might not be a direct link, but a more indirect effect from which the dominant mechanisms are still unknown.

6.8 Washburn equation

To calculate the flow rates in the model, a version of the Washburn equation is used. For small capillaries, one may assume Hagen-Poiseuille flow. White [28]. This takes the following form when neglecting air resistance: Washburn [19]

$$dV = \frac{\pi \sum P}{8\mu l}(r^4 + 4\epsilon r^3)dt \tag{13}$$

where dV is the volume flowing through a cross section of the capillary in a time dt, l is the length of the column of liquid in the capillary, μ the viscosity, $\sum P$ the total effective pressure acting on the liquid, and ϵ the slip coefficient (see eq.(15) and figure 7). By using that the permeability is given by $k = r^2/8$, one gets the following expression for the flow rate q:

$$q = \frac{\pi r^2 k \sum P}{\mu l}(1 + \frac{4\epsilon}{r}) \tag{14}$$

The last term in eq.(14) can be of great significance in flow through nanoporous media, where the effective permeability can vary in orders of magnitude depending on the wetting properties of the liquid. Barrat and Bocquet [20]. Experiments have been performed where this effect can be seen also in the case of pore sizes in the micro meter range. The presence of thin wetting films covering the pore surface leads to slip boundary conditions, which is believed to significantly increase the relative permeability of the non-wetting phase. Berg, Cense, Hofman, Smits [21].

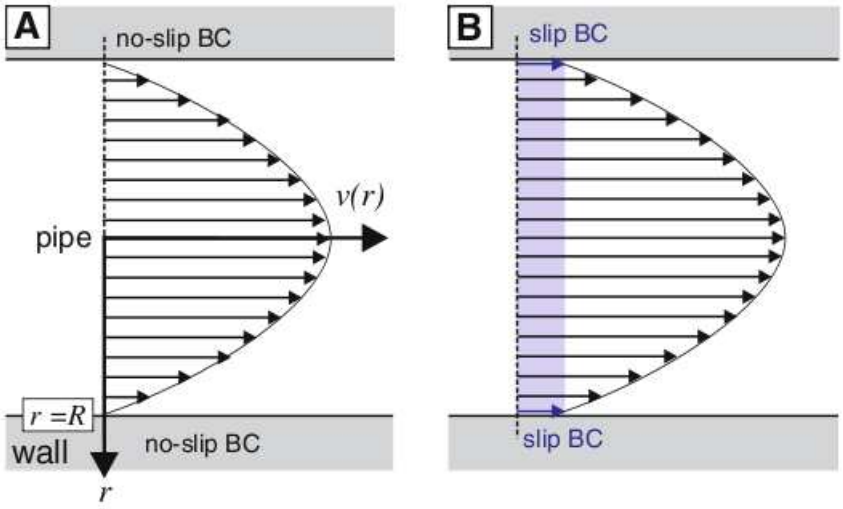

Figure 7: Velocity profiles showing the difference between no slip boundary conditions, and slip boundary conditions. Figure from Berg, Cense, Hofman, Smits [21]

From the velocity profile seen in figure 7, the slip length ϵ is defined as:

$$\epsilon \equiv -v(r=R)\left(\frac{\partial v}{\partial r}\bigg|_{r=R}\right)^{-1} \tag{15}$$

For simplicity, it is initially assumed that the slip length ϵ is small compared to the typical pore radius r. Meaning that in the following, no slip boundary conditions for both the wetting and non-wetting phase is used. The last term is then assumed to be insignificant, and can dropped from the expression.

$$q \approx \frac{\pi r^2 k \sum P}{\mu l} \tag{16}$$

6.9 capillary and viscous forces

The interplay between the capillary and viscous forces in a system is very important, and is characterized through the capillary number.

$$Ca = v\frac{\mu_{eff}}{\gamma} \tag{17}$$

Where the velocity v is the mean velocity through the porous media, and is defined as the total flow rate Q_{tot} divided by the inlet area $\sum$, $v = Q_{tot}/\sum$. γ is the interfacial tension between the two phases, and μ_{eff} is the effective viscosity, defined as the weighted average of the different fluid viscosities present in the system, $\mu_{eff} = S_w\mu_w + S_{nw}\mu_{nw}$.

The capillary number can be used to classify systems into different flow regimes. There is usually a crossover point at a capillary number of approximately 10^{-4}, indicating the transition between a capillary dominated flow regime for lower values of Ca, and one dominated by viscous forces for higher values of Ca. Also, in the capillary dominated flow regime, thin film flow is important and needs to be accounted for. Another important parameter in addition to the effective viscosity of the system, is the viscosity contrast between the wetting and non wetting phase.

$$M = \frac{\mu_{nw}}{\mu_w} \tag{18}$$

The viscosity ratio is of great importance when estimating the behavior of injecting one fluid into a system containing the other fluid. Depending on the viscosity ratio the system can behave very differently, and end up in various regimes like viscous fingering, stable piston like displacement, etc.

6.10 Displacement mechanisms

6.10.1 Pore level

Usually, displacement in two phase flow in porous media is divided into essentially two different categories. In the case of drainage displacement, the non wetting invading fluid displaces the wetting fluid. This is the case for the simulations performed in this thesis, where water is displacing oil in an initially oil wet reservoir. In the opposite case of imbibition, the wetting fluid displace the non wetting phase. The mechanisms behind the displacement in these two regimes are quite different, and they should not be confused.

Imbibition is defined as the displacement of one fluid by another immiscible fluid. This process is controlled and affected by a variety of factors. In spontaneous imbibition of wetting liquids into porous media, the capillary pressure created as a result of interplay between the liquid and solid surface energies at pore level, is responsible for the spontaneous suction of the liquids. The capillary number (Ca) and the mobility ratio (M) have the greatest importance.

Typically, the process of slow displacement is characterized by a piston like motion inside the pores, where the invading non-wetting fluid only enters the pore if the capillary pressure is equal to or greater than the threshold pressure of that pore. Lenormand, Zarcone, Starr [29]. The threshold pressure corresponds to the capillary pressure in the narrowest part of the pore. However, during imbibition at low injection rates, the invading fluid will enter the most narrow pores first as the injected fluid is the wetting phase, and thus displace the non wetting phase from these pores. Lenormand, Zarcone, Starr [29]

6.10.2 Transient flow conditions

Multiphase flow in porous media is usually divided into different subgroups of transient and steady state flow conditions. The initial injection of a fluid into a

system saturated with another fluid, will cause a transient displacement structure. For a drainage process, the transient displacements are usually divided in different flow regimes depending of the capillary number. The main flow regimes are viscous fingering (high Ca nr.), stable displacement (intermediate Ca nr.) and capillary fingering (low Ca nr.).

Lenormand et al. [30] introduced the concept of "phase diagrams" for drainage displacements, where various experiments and simulations were plotted on logarithmic scale in a plane with Ca along the y-axis and the viscosity ratio M along the x-axis. see figure 8.

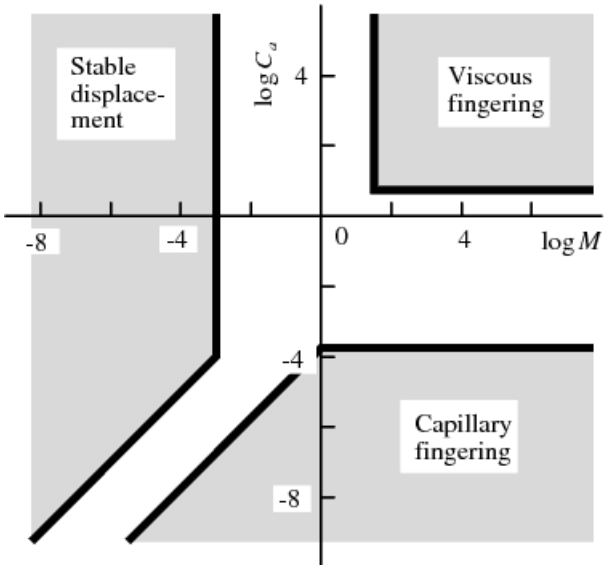

Figure 8: Phase diagram of various flow regimes as a function of Ca and mobility ratio M. Figure from Lenormand, Touboul and Zarcone [30].

Viscous fingering

In the case of high Ca number where the viscous forces of the defending fluid are dominant, one is in the viscous fingering regime. As seen from the formula for capillary number, eq.(17), this condition can be obtained by the injection of a fluid with low viscosity into a medium of higher viscosity at a high rate. The resulting displacement front will have the shape of fluid fingers invading the system, as seen in figure 9

Figure 9: Numerical simulation of viscous fingering. Injection of a fluid of low viscosity (black) into a fluid of higher viscosity (white). Figure from Homsy [44]

in 1987, Paterson [31] was the first to discover a remarkable parallel between the behavior of viscous fingering in porous media and diffusion limited aggregation, DLA. DLA is a process in which particles are left to wander at random far away from initial placement in the system. If the random walker collide with the initial particle, they stick together. This leads to an aggregate of particles to form (the invading fluid). This structure looks surprisingly like viscous fingering. In the continuum limit, DLA is described by the diffusion equation

$$\frac{\partial C}{\partial t} = D\nabla^2 C \tag{19}$$

Where C is the concentration of particles as a function of time and position. With a steady flux of particles from a source far away from the aggregate of stuck particles, we have that $\frac{\partial C}{\partial t} = 0$. This results in the reduction of the DLA equation to the Laplacian:

$$\nabla^2 C = 0 \tag{20}$$

This is the equivalent of viscous fingering in porous media when the defending fluid has a much greater viscosity than the invading fluid. ($M \to 0$). In this limit, the pressure gradient of the invading fluid can be approximated by zero. The fluid flow is then described by Darcy‘s equation applied to the defending fluid only.

$$Q = -\frac{k}{\mu}\nabla p \tag{21}$$

Where Q is the flow rate, k is the permeability, μ the viscosity and ∇p the pressure gradient across the defending phase. Then, by assuming an incompressible fluid ($\nabla \cdot Q = 0$), one gets the following:

$$\nabla^2 p = 0 \tag{22}$$

Which is the same as eq.(20), with C being replaced by p. But, even though there are similarities, there is still a big difference. The disorder of the DLA process is caused by random walkers, while the disorder in the porous media is given by the pore size distribution. There is no one to one correspondence between DLA and the viscous fingering process, but simulations and experiments have found that the fractal dimension of the structures produced by DLA is similar to that found in experiments in porous media. Chen and Wilkinson [33]. Måløy, Feder, Jøssang [34].

Stable displacement

Also in the stable displacement regime the main force involved is the viscous force, but in this case of the invading fluid, meaning the process is basically the opposite of that for viscous fingering. The displacement structure is an almost flat front between invading and defending fluid. The cluster size is limited by the roughness of the displacement front, and only small clusters are able to develop. See figure 10.

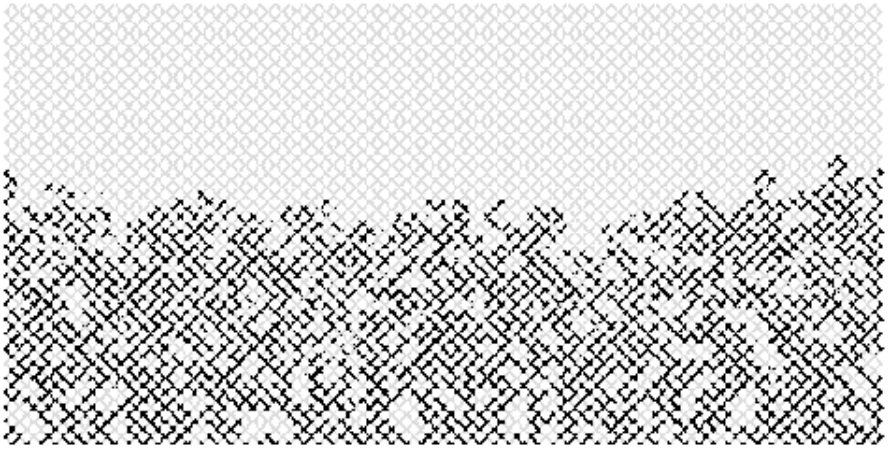

Figure 10: Stable displacement front. Figure from Aker [43]

The connection between Anti-DLA and stable displacement was also found by Paterson in 1984, [31]. The anti-DLA process consists of having a compact aggregate of initial particles (the defending fluid) and leave random walkers close by. The particles then move until they reach an initial particle of the aggregate. In this case, both the random walker and the aggregate particle are removed,

causing the aggregate to be "eaten away". The anti-DLA process is only valid in the limit $M \to \infty$, where the viscosity of the invading fluid is much higher than that of the defending fluid. The structures obtained from anti-DLA and stable displacement have been confirmed by Lenormand et al. in 1988, [30]. As for the DLA process, there is no one to one correspondence between anti-DLA and stable displacement, and the reason for these similarities is not well understood.

Capillary fingering

Capillary fingering is obtained by injecting the invading fluid at a very low injection rate. This causes the viscous forces to become negligible, and the dominant force is due to capillary forces of the interface between the invading and defending fluid. This cause a displacement structure consisting of a wide and rough front, with trapped clusters of defending fluid ranging from pore size to system length, see figure 11. Due to the increased dominance of capillary forces, the wetting properties of the two fluids become very important.

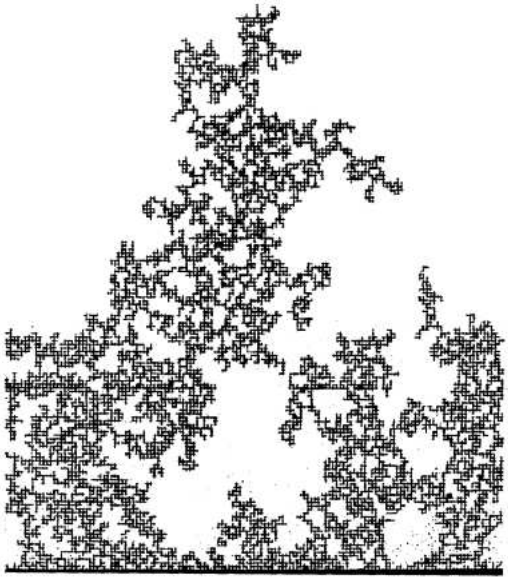

Figure 11: Cluster generated by injecting a non-wetting fluid (white) in a network filled by a wetting fluid (black). Figure from Lenormand and Zarcone [36]

There has been much effort in relating the structures observed during capillary fingering to percolation theory. Inspired by the study of flow in porous media, invasion percolation was developed to take into account the fluid transport process. Wilkinson and Willemsen, [35]. The idea is to map the threshold pressure of each pore to an occupation probability. In an ideal medium, the pore

network may be viewed as a regular lattice where the sites and bonds represent the pores and throats. The random structure of a pore network is implemented by assigning a random nr. f_p to each site and bond, corresponding to the threshold pressure. Thus, f_p is analog to the occupational probability indicating whether the actual site/bond is filled with the invading fluid at the capillary pressure corresponding to f_p. The invasion percolation process proceeds by letting the displacing fluid grow each time step by occupying accessible sites along the front having the smallest nr., f_p. This will cause regions of defending fluid to become disconnected from the outlet, and the sites of these trapped clusters can then not be invaded. The process is stopped when the invading fluid first percolates the system (forms a connected path through inlet and outlet). This process is only valid in the case of very slow displacement ($Ca \to 0$). In this limit, the capillary pressure due to the pore interface is only invaded by the displacing fluid if the pressure is equal to or larger than the corresponding threshold pressure.

6.10.3 Steady state

Steady-state two-phase flow in porous media has received very little attention compared to the instabilities that occur in connection with flooding, i.e. when the porous medium is initially saturated with one of the fluids whereas the other fluid is injected into it displacing the first, leading to e.g. viscous fingering. However, inside a real reservoir the flow is described as a steady state, where the configuration of the phases entering an element is the same as the ones leaving it. At low flow rates, steady state flow essentially consists of one fluid being held in place by capillary forces whereas the other fluid moves. At higher flow rates, both fluids will move and there will be an increasing breakup and merging of fluid clusters. In this regime, the flow settles into a state which is independent of the initial conditions, and determined only by the flow parameters. In this state, the fluids rearrange and flow simultaneously. There will be fluctuations in the global pressure around a mean value, and a fractional flow condition of the phases will settle. The fractional flow is defined as follows: $F_{nw} \equiv Q_{nw}/Q_{tot}$ and $F_w \equiv Q_w/Q_{tot}$, and is among the key properties investigated in this thesis.

6.11 Fractional flow

Darcy‘s equation, eq.(10), derived earlier is a macroscopic equation based on average quantities, and derived for one phase flow. When describing two phase flow in porous media some difficulties arise. The microscopic interactions between the fluids (capillary pressure) cause fluctuations in the pressure gradient on a local level inside the sample. Also, when two fluids are present, the ability of one fluid to flow is depending on the local configuration of the other fluid. A famous way of describing two phase flow, incorporating these effects in Darcy‘s equation, is the Buckley-Leverett displacement. Buckley and Leverett [47].

Consider a reservoir filled with oil, which is displaced by water. The absolute permeability of the reservoir is k, and the viscosities of oil and water is denoted

as μ_o and μ_w. Initially, only the defending phase (oil) flows out of the medium until the invading phase (water) breaks through, and both phases are produced at the outlet. The system eventually reaches a steady state where both oil and water flow through the system in a fixed configuration. Thus, water and oil basically flow in an effective porous medium that does not have the full pore space available. If Q_w is the flow of water, and Q_o is the flow of oil, Darcy's equation for the two phases become (when neglecting gravity effects):

$$Q_w = -k\frac{k_{rw}A}{\mu_w}\nabla P_w \tag{23}$$

$$Q_o = -k\frac{k_{ro}A}{\mu_o}\nabla P_o \tag{24}$$

where k_{rw} is the relative permeability of water defined as $k_{rw} = \frac{k_w}{k}$, and similarly for k_{ro}. The pressure in water, p_w, differs from that of oil, p_o, but the exact difference is only known when there is no flow. Then the menisci between the fluids will be adjusted due to interfacial tension between the water and oil phase, as derived in section 6.5

The saturations are defined as S_w and S_o, and is the volume fraction of each liquid in the system. The effective permeabilities depend on the corresponding saturations. In the limit where water displaces all the oil, $S_w = 1$, one expect $k_{rw} = 1$ and $k_{ro} = 0$, as only water is present in the system. Conservation of pore volume then give:

$$S_w + S_o = 1 \tag{25}$$

As long as the fluids are flowing in steady state, these equations are valid. In Buckley-Leverett displacement the idea is to use these equations outside the stationary regime and solve them for one dimensional flow, where the flow rates and saturations are a function of the position along the system. Buckley and Leverett [47].

To keep track of the changes in saturation, one requires the mass balance equations for water and oil:

$$\phi \sum \frac{\partial S_w}{\partial t} + \frac{\partial Q_w}{\partial x} = 0 \tag{26}$$

$$\phi \sum \frac{\partial S_o}{\partial t} + \frac{\partial Q_o}{\partial x} = 0 \tag{27}$$

Where ϕ is the porosity, defined as ϕ = pore volume/matrix volume, $\sum$ is the cross sectional area of the sample and x is the position along the system.

Now, the five equations (23)-(27) contain 6 unknowns. To obtain the final equation needed, Buckley and Leverett suggested that the capillary pressure p_c is a function of the saturation of water only, $S \equiv S_w$.

$$p_c(S) = p_w - p_o \tag{28}$$

Also, they assumed $dp_c/dS = 0$ is a sufficient approximation, causing the pressure gradients of water and oil to be equal:

$$\frac{\partial p_w}{\partial x} = \frac{\partial p_o}{\partial x} + \frac{\partial p_c}{\partial x} = \frac{\partial p_o}{\partial x} + \frac{dp_c}{dS}\frac{\partial S}{\partial x} = \frac{\partial p_o}{\partial x} \tag{29}$$

Having introduced the concept of fractional flow, Buckley and Leverett derived the equation for the saturation of water $S(x,t)$, often called the Buckley-Leverett equation: Buckley and Leverett [47].

$$\frac{\partial S}{\partial t} + U(S)\frac{\partial S}{\partial x} = 0 \tag{30}$$

Where

$$U(S) \equiv \frac{Q}{\phi \sum}\left(\frac{df}{dS}\right) \tag{31}$$

Here, f denotes the fractional flow of water, and Q is the total volume flow rate, $Q = Q_w + Q_o$. Thus, $f \equiv f_w = Q_w/Q$. The fractional flow of water is a function of saturation S, since the relative permeabilities k_{rw} and k_{ro} are assumed to depend only on the saturations S_w and S_o.

The relative permeabilities as a function of water saturation behave typically as shown in figure 12.

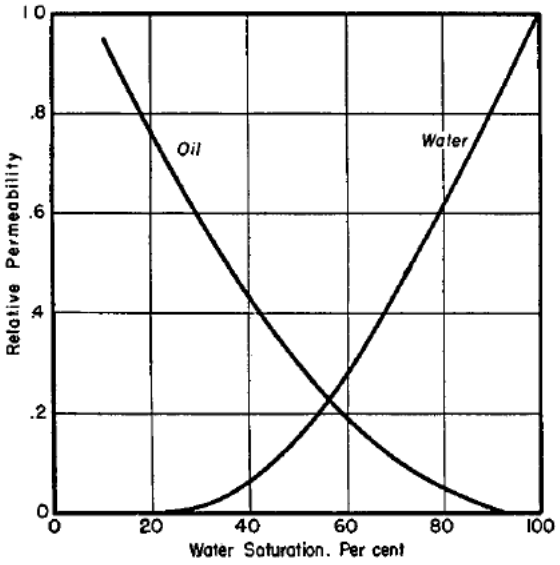

Figure 12: Rel. perm. of water and oil as a function of water saturation. k_{rw} is the curve "Water", and k_{ro} the curve "Oil". Figure from Buckley and Leverett, [47]

If only oil is being produced and no water flows out of the system, $k_{rw} = 0$ and $k_{ro} \approx 1$. As the water first breaks through, k_{rw} starts to increase towards 1. As water displaces oil, the relative permeability of oil goes to zero, and when all oil has been displaced, $k_{ro} = 0$ and $k_{rw} = 1$. Usually, not all oil will be produced and some will be left in the system at the water saturation S_{oc}, where $k_{ro} = 0$. Further injection of water is not able to displace more oil, causing the residual oil in the system to become $S_{or} = 1 - S_{oc}$.

From Darcy's equations for oil and water, eq.(23) and (24), the fractional flow of water is given by the following:

$$f = f(S) = \frac{Q_w}{Q_w + Q_o} = \frac{1}{1 + \frac{k_{ro}}{k_{rw}} \frac{\mu_w}{\mu_o}} \tag{32}$$

Where one has used that the pressure gradient in the water is equal to the one in oil, as shown in eq.(29). The fractional flow is given by using the expected functions for $k_{rw}(S)$ and $k_{ro}(S)$, and a typical fractional flow curve $f(S)$, can be seen in figure 13.

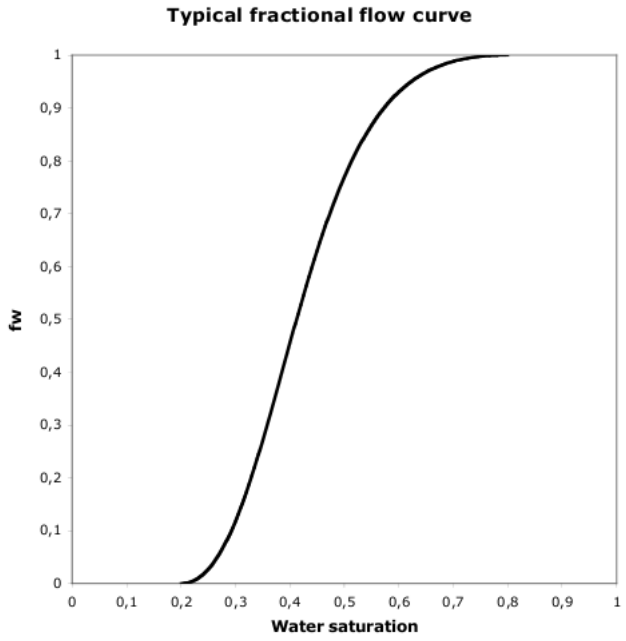

Figure 13: The fractional flow of water, $f(S)$, as a function of water saturation. Figure from Kleppe [48].

6.12 Percolation theory

The application of percolation theory in the context of transport properties of porous media is a well established area. A nice introduction to percolation theory can be found in the book by Shauffer and Aharony, "introduction to percolation theory" [38], and for a closer link to applications in porous media, a paper by Berkowitz and Ewing [41] is recommended. The main use of percolation theory in this thesis, is the application of finite size scaling theory to investigate critical transitions at the percolation threshold p_c. This can relate how quantities of interest behave in a finite system compared to an infinite system. In the following, a brief introduction to finite size scaling of a site percolation problem will be outlined.

We consider a percolation problem for $p \neq p_c$, where the correlation length ξ is finite.

$$\xi \propto |p - p_c|^{-\nu} \Rightarrow |p - p_c| \propto \xi^{-1/\nu} \tag{33}$$

Where ξ is the correlation length, p is the site occupation probability, p_c is the critical site occupation probability, and ν is the correlation length critical exponent.

The strength,$P(p)$ of the infinite network, is defined as the probability that an arbitrarily selected site is connected to infinity by occupied sites. This can then be expressed in terms of the finite correlation length:

$$P(p) \propto (p - p_c)^{\beta} \propto \xi^{-\beta/\nu} \tag{34}$$

Where β is defined as the critical exponent for the percolation strength.

These results are in infinite lattices with $L = \infty$. The interesting thing in our case is what happens when $L < \infty$. As long as $L \gg \xi$ nothing happens, as ξ is still the only relevant length scale. However, if $L \ll \xi$, L will set the length scale. Thus, one expects it to obey the following: Shauffer and Aharony, [38].

$$P(L, \xi) = \xi^{-\beta/\nu} f(L/\xi) \tag{35}$$

Where the scaling function is defined as

$$f(L/\xi) \propto \begin{cases} (L/\xi)^{-\beta/\nu} & \text{for} \quad L/\xi \ll 1 \\ const & \text{for} \quad L/\xi \gg 1 \end{cases} \tag{36}$$

An example of the strength, $P(p)$, measured in a 2d square lattice as a function of occupation probability p, can be seen in figure 14.

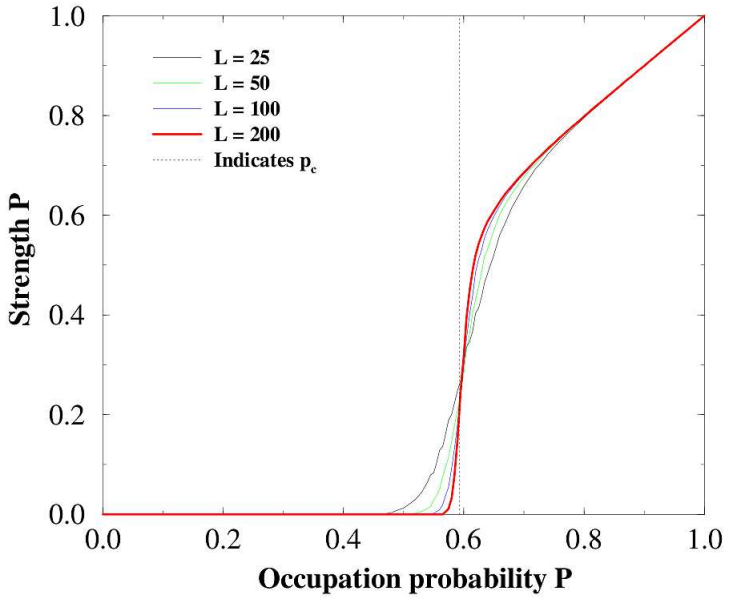

Figure 14: Percolation strength as a function of site occupation probability for different lattice sizes. Figure from Christensen [42]

When p is far away from the threshold p_c, $L \gg \xi$, and the strength is determined by $\xi^{-\beta/\nu}$. When one approaches the transition point p_c however, one can see the finite size effect, (figure 14). $P(p)$ then decay with system size as $L^{-\beta/\nu}$. The importance of this finite size effect, is that by investigating the percolation transition at various lattice sizes and using results from finite size scaling theory, one can extract the exponent β/ν.

However, when using a relatively small lattice size, it is found that the data fit the expected laws of $P(p) \propto (p - p_c)^\beta$ better if one uses a shifted value of p_c instead. Since the sample is finite, there is finite probability of finding a spanning cluster at any finite concentration. To generalize, let $\Pi(p, L)$ be the probability that a lattice of size L percolates at p. for a system where $L = \infty$, Π will be a simple step function with $\Pi = 0$ below p_c, and $\Pi = 1$ above p_c. The quantity $d\Pi/dp$ then gives the probability that the lattice percolates if p is increased from p to $p + dp$. One then gets the following more general expression:

$$\Pi = \Phi[(p - p_c)L^{1/\nu}] \tag{37}$$

Where the scaling function Φ increase from 0 to 1 if the argument increase from $-\infty$ to $+\infty$ (from far below the percolation threshold to far above the threshold). The derivative then gives:

$$\frac{\partial \Pi}{\partial p} = L^{1/\nu}\Phi'[(p - p_c)L^{1/\nu}] \tag{38}$$

Which approach a delta function in the case of an infinite lattice. The average value, p_{avg}, where a percolating cluster appear the first time is defined as:

$$p_{avg} = \int_0^1 p \left(\frac{\partial \Pi}{\partial p} \right) dp \tag{39}$$

By doing several experiments for the same value of L and check when the system percolates for the first time, one can determine p_{avg}. The effective percolation threshold p_{avg} for system size L approach the exact value p_c for infinite systems. This connection can be found from combining eq.(37), (38) and (39):

$$p_{avg} - p_c \propto L^{-1/\nu} \tag{40}$$

This means that from plotting p_{avg} vs $L^{-1/\nu}$ for various trial values for ν until one finds a linear fit for large L, the exponent ν can be estimated.

Not only p_{avg} approach p_c as $L^{-1/\nu}$. If one defines an effective percolation threshold for finite lattices as the point where curve $P(p)$ has an inflection point, (maxima of $\frac{\partial P}{\partial p}$), this threshold will approach the true p_c as $L^{-1/\nu}$.

Also the width of the transition region depends on system size. The width, Δ, of the transition region between large and small probabilities Π can be defined simply as the difference between the value of p where Π is 0.1 and 0.9, or any other suitable numbers to define the width. However, from eq.(37) one gets that Δ, independent of the details of its definition, varies for large L as $L^{-1/\nu}$. This means that by investigating the width of the percolation transition, one can estimate the correlation length critical exponent ν. Shauffer and Aharony [38]

$$\Delta \propto L^{-1/\nu} \tag{41}$$

7 Numerical techniques

7.1 Conjugate gradient method

In mathematics, the conjugate gradient method is an algorithm to obtain a numerical solution to systems of linear equations. A introduction to the method can be found in e.g the book "Numerical recipes" [52]. The method can be applied to systems whose matrix is positive definite and symmetric. The conjugate gradient method is an iterative method, and is suited to sparse systems that are to large to be handled by direct methods. Consider the following system of linear equations:

$$Ax = b \tag{42}$$

It is assumed that A is a $n \times n$ matrix which is symmetric and positive definite. That A is positive definite, means that $x^T Ax > 0$ for all non zero vectors x in R^n. In the following, it will not actually be proven that the system of equations to be solved for this network model fulfills these properties. The goal is rather to explain the basics of the numerical methods used, starting with some linear algebra needed. This can be found in any standard textbook on linear algebra, e.g H.Anton and C.Rorres: "Elementary Linear Algebra with Supplemental Applications" [14].

That two vectors u and v are conjugate with respect to the matrix A, means that $u^T Av = 0$. Since it is assumed that A is symmetric and positive definite, this defines the inner product:

$$\langle u, v \rangle_A = \langle Au, v \rangle = \langle u, A^T v \rangle = \langle u, Av \rangle = u^T Av \tag{43}$$

Two vectors are considered conjugate if they are orthogonal with respect to the inner product. Assume $\{p_k\}$ is a set of n conjugate directions. This set will then form a basis of R^n, and the solution $\tilde{x}$ to the problem $Ax = b$ can be expanded in this basis.

$$\tilde{x} = \sum_{i=1}^{n} \alpha_i p_i \tag{44}$$

The expansion coefficients α_i are given by:

$$b = A\tilde{x} = \sum_{i=1}^{n} \alpha_i Ap_i \tag{45}$$

$$p_k^T b = p_k^T A\tilde{x} = \sum_{i=1}^{n} \alpha_i p_k^T Ap_i = \alpha_k p_k^T Ap_k \tag{46}$$

The last step following from the fact that the set of basis vectors $\{p_k\}$ are mutually conjugate. From this, the expansion coefficients α is found:

$$\alpha_k = \frac{p_k^T b}{p_k^T A p_k} = \frac{\langle p_k, b\rangle}{\langle p_k, p_k\rangle_A} = \frac{\langle p_k, b\rangle}{\|p_k\|_A^2} \tag{47}$$

Using these properties, the conjugate gradient method can be implemented as an iterative method to solve these kinds of problems by choosing the conjugate vectors p_k carefully. This choice can then give a good approximation to the solution $\tilde{x}$, without the need of all the vectors p_k.

The starting point for the iteration process is an initial guess, x_0, for the real solution $\tilde{x}$. Starting from this x_0, the search for the solution starts, and in each iteration one needs a metric to tell if one is getting closer to the solution or not. The idea is now that the solution $\tilde{x}$ for the initial problem $Ax = b$, is also the minimizer of the quadratic function $f(x)$:

$$f(x) = \frac{1}{2}x^T A x - x^T b,\ x \in R^n \tag{48}$$

From this, one take the first basis vector p_1 to be $-\nabla f(x)$ at $x = x_0$. x_0 can be set to 0 without any loss of generality, meaning that $p_1 = b$. The other vectors in the basis will be conjugate to the gradient, which is the reason for the name conjugate gradient method.
For the exact solution, one has that $b - A\tilde{x} = 0$. In the iteration, r_k is defined to be the residual at step k, $r_k = b - Ax_k$. The search directions for each iteration, p_k, is conjugate to each other, and are also required to be built out of the current residue and all previous search directions. From these conditions, one gets the following expression for the search vectors p_k.

$$p_{k+1} = r_k - \sum_{i \leq k} \frac{p_i^T A r_k}{p_i^T A p_i} p_i \tag{49}$$

Following this search direction, one gets the new value for x:

$$x_{k+1} = x_k + \alpha_{k+1} p_{k+1} \tag{50}$$

with α given by:

$$\alpha_{k+1} = \frac{p_{k+1}^T b}{p_{k+1}^T A p_{k+1}} = \frac{p_{k+1}^T (r_k + A x_k)}{p_{k+1}^T A p_{k+1}} = \frac{p_{k+1}^T r_k}{p_{k+1}^T A p_{k+1}} \tag{51}$$

The last step following from the fact that p_{k+1} and x_k are conjugate.

The above algorithm gives a straightforward explanation of the conjugate gradient method. But, the required storage of all previous search directions and residue vectors, and many matrix multiplications can result in a computationally expensive code. Doing a slight modification of the condition to obtain the last residue vector, not by minimizing the metric following from the total previous search direction, but rather by making it orthogonal to the previous

residue does the trick. Minimizing the metric, $f(x)$, is then automatically obtained. The algorithm then only requires storage of the two previous residue vectors, r_{k-1} and r_k, and the previous search direction p_k. Pseudocode for the algorithm can then be written as the following.

$r_0 = b - Ax_0$
$p_0 = r_0$
$k = 0$
repeat:
$\alpha_k = \frac{r_k^T r_k}{p_k^T A p_k}$
$x_{k+1} = x_k + \alpha_k p_k$
$r_{k+1} = r_k - \alpha_k A p_k$
if $r_k < presicion$ **exit loop**
$\beta_k = \frac{r_{k+1}^T r_{k+1}}{r_k^T r_k^T}$
$p_{k+1} = r_{k+1} + \beta_k p_k$
$k = k + 1$
if $k > max\,iterations$ **end repeat**
return x_k

The conjugate gradient method can theoretically be viewed as a direct method as it produces the exact solution after a finite number of iterations, which is limited by the size of the matrix. Unfortunately, this is in an ideal world without any roundoff errors in the calculations. In reality, the method is unstable to small perturbation caused by these errors, and the exact solution will never be obtained. However, the conjugate gradient method used as an iterative method will produce monotonically improved approximations, x_k, to the exact solution, $\tilde{x}$. This solution may reach the required accuracy for the problem after a relatively small number of iterations compared to the problem size.

7.2 Runge-Kutta method

Assume one has the derivative of a function $y_n(x_n) : \frac{dy}{dx} = f(x_n, y_n)$. One then wants to obtain the solution y_{n+1} at the position x_{n+1}. The formula for the Euler method is simply:

$$y_{n+1} = y_n + h \cdot f(x_n, y_n) \tag{52}$$

Where h is defined as the step-size in x, Δx. This is the simplest Runge-Kutta method, but is not very accurate. This method will advance the solution through an interval h, but uses the derivative of the function only at the beginning of the interval. However, for the application in this network model it is considered sufficient.

7.3 Central difference approximation

The derivative of a function f at a point x, is defined by the limit:

$$f'(x) = \lim_{h \to 0} \frac{f(x+h) - f(x)}{h} \tag{53}$$

If one has a set of discrete values for $f(x)$, one needs an estimate for the derivative given these data. When using a dataset of discrete values with spacing h, the derivative can be estimated using the central difference approximation:

$$f'(x) = \frac{f(x+h) - f(x-h)}{2h} + O(h^2) \approx \frac{f(x+h) - f(x-h)}{2h} \tag{54}$$

Where the error scales as h^2.

7.4 Box-Muller algoritm

The idea behind the Box-Muller algorithm is to take two samples from an uniform distribution on the interval [0, 1] (from a standard random nr. generator), and map them to two standard, normally distributed samples. Box and Muller [46].

In many cases, it would be convenient to get a standard normal distribution from a standard uniform distribution by inverting the distribution function. However, the problem is that such a closed form formula for this distribution does not exist.

$$P(X < x) = \frac{1}{\sqrt{2\pi}} \int_{-\infty}^{x} d\tilde{x}\ e^{-\tilde{x}^2/2} \tag{55}$$

The Box-Muller method is a trick to overcome this problem, by using two independent standard uniform distributions to produce two independent standard normal distributions. It is based on the 1D to 2D transformation of Gaussian integrals of the form:

$$I = \int_{-\infty}^{+\infty} dx\ e^{-x^2/2} \tag{56}$$

This integral does not have an algebraic solution of elementary functions. The trick is to rather calculate I^2:

$$I^2 = \int_{-\infty}^{\infty} dx\ e^{-x^2/2} \int_{-\infty}^{\infty} dy\ e^{-y^2/2} = \int_{-\infty}^{\infty} \int_{-\infty}^{\infty} e^{-\frac{x^2+y^2}{2}} dxdy \tag{57}$$

This can be evaluated using polar coordinates and a simple substitution, giving:

$$I^2 = 2\pi \int_{u=0}^{\infty} e^{-u} du = 2\pi \tag{58}$$

The Box Muller algorithm then uses this trick. If one has 2 independent standard normals (X,Y), then the probability density is a product:

$$f(x,y) = \frac{1}{\sqrt{2\pi}}\, e^{-x^2/2} \times \frac{1}{\sqrt{2\pi}}\, e^{-y^2/2} = \frac{1}{2\pi}\, e^{\frac{-(x^2+y^2)}{2}} \tag{59}$$

This is radially symmetric, and one uses the same trick as before, using polar coordinate random variables (R, Θ). Θ is uniformly distributed in the interval $[0, 2\pi]$, and can be mapped using $\Theta = 2\pi U_1$. Where U_1 is a random nr. from the uniform distribution. Unlike the original distribution function $P(X < x)$, there now exists a simple expression for the R distribution function. This can be solved using a simple substitution, and give the following:

$$P(R < r) = \int_{\tilde{r}=0}^{r} \int_{\Theta=0}^{2\pi} \frac{1}{2\pi} e^{\frac{-\tilde{r}^2}{2}} \tilde{r} d\tilde{r} d\Theta \; = 1 - e^{\frac{-r^2}{2}} \tag{60}$$

R can then be sampled from solving the distribution function equation:

$$1 - e^{\frac{-R^2}{2}} = 1 - U_2 \tag{61}$$

Where U_2 is a random nr. from the uniform distribution. This is then solved for R, giving:

$$R = \sqrt{-2log(U_2)} \tag{62}$$

The Box Muller algorithm then uses these independent uniform variables U_1 and U_2, and map them to the independent standard normal variables X and Y using the formulas: $\Theta = 2\pi U_1$, $R = \sqrt{-2log(U_2)}$, $X = R\,cos\,\Theta$, $Y = R\,sin\,\Theta$.

8 Pore network model

To build models representative of fluid transport in porous media is not a straight forward task. In the study of fluid dynamics for intermediate capillary numbers, network models have proven to be a good solution. They are built up by using various nodes and tubes, with different connectivities. The pressure distribution among these tubes then has to be solved to obtain the dynamical evolution of fluid flows by integrating the local flow rates. The numerical models used, represents a simplified ideal model of a porous media. They do not include all details of microscopic structures, but still prove to be a good approximation which is able to replicate the main features of fluid transport in porous media. Also, as this is a 2D model, it is not able to capture effects of thin film flow. This could be important to capture all effects of wettability, as the presence of wetting films covering the rock surface would be more physically correct compared to real reservoir conditions. However, to capture this the model would have to be on a whole other level of complexity. It is believed that a simple 2D model is still able to capture the dominant effects of transport properties in the porous media, and this is thus the scope of this work.

8.1 Initializing the model

The model is based on the idea of using a 2D network of tubes to represent the porous media. The disorder of the system is incorporated using tubes of random radii from a chosen pore radius distribution. The network consists of capillary tubes oriented 45 degrees relative to the overall flow direction from bottom to top. The volume of both throats and pores is contained in the tubes, which then intersect in volumeless node points. (See figure 15).

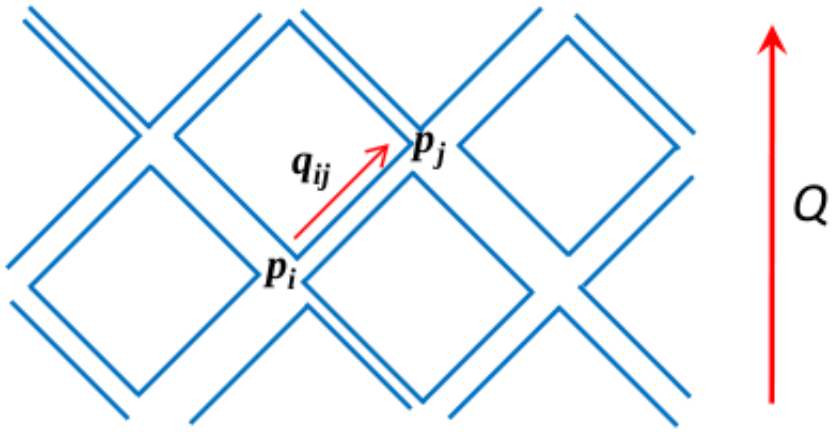

Figure 15: Network of capillary tubes oriented 45 degrees to the overall flow direction shown as Q, where the tubes intersect in volumless node points. p_i and p_j is the pressures at node i and j, and q_{ij} is the flowrate between node i and j.

A simple 2d representation of a porous media consist of grains with channels in between, as seen in figure 16.

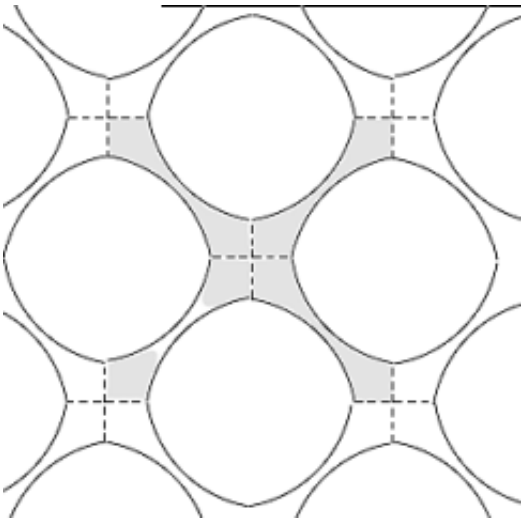

Figure 16: Simple model of a 2d pore space, consisting of grains with channels in between. Figure from Tørå, Ramstad and Hansen, [39].

From this, one can see that the channels connecting the regions between the grains, have an hour glass shape. This is incorporated in the model such that

with respect to the capillary pressure of menisci, the tubes are hour glass shaped. That is, the local capillary increase when menisci move into narrower parts of the tubes are taken into account. This makes the model closer to dynamics of drainage dominated flow, where thin film flow can be neglected. A modified Young Laplace equation give: Dullien [1]. Aker et al. [17]

$$p_c = \frac{2\gamma cos\theta}{r}(1 - cos(2\pi x)) \tag{63}$$

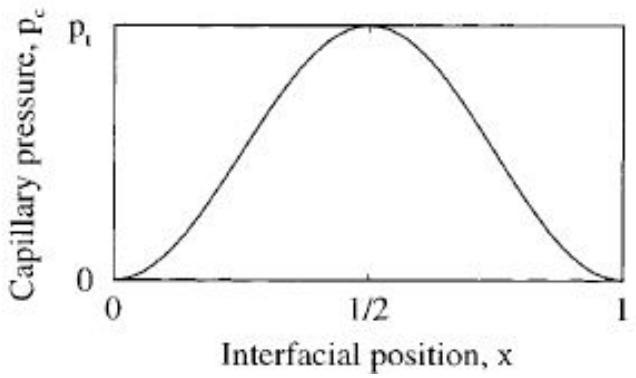

Figure 17: Capillary pressure in an hourglass shaped tube as defined in eq (63). With x running from 0 to 1, and θ denoting the wetting angle

Such a network of tubes corresponds to the pores and throats in a real porous medium. The radii of the pores, r_{ij} are either randomly distributed within chosen boundaries, $r_{ij} = [\lambda_1, \lambda_2]d$ Where the disorder of the porous medium is represented by the width of the radii distribution (see figure 18), or given by a Gaussian distribution with defined mean value and variance. (see figures 19 and 20)

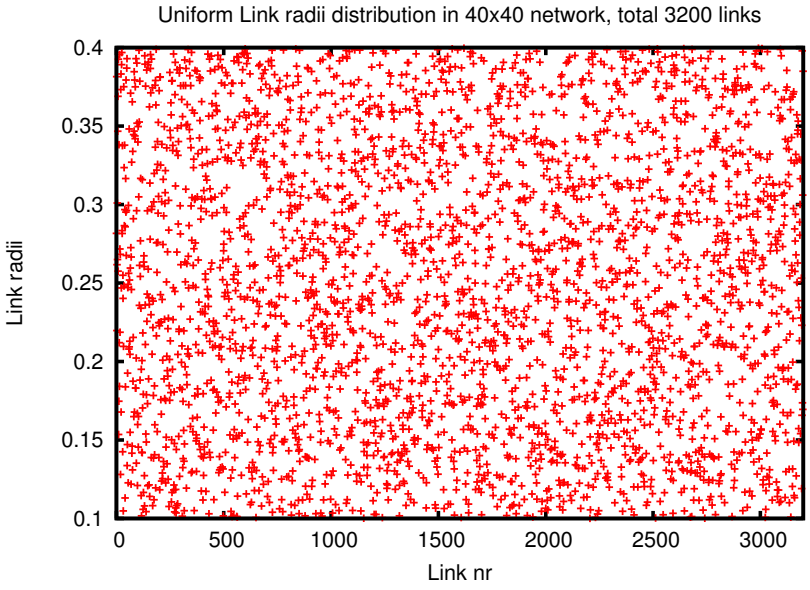

Figure 18: Tube radii, [mm], uniform distribution

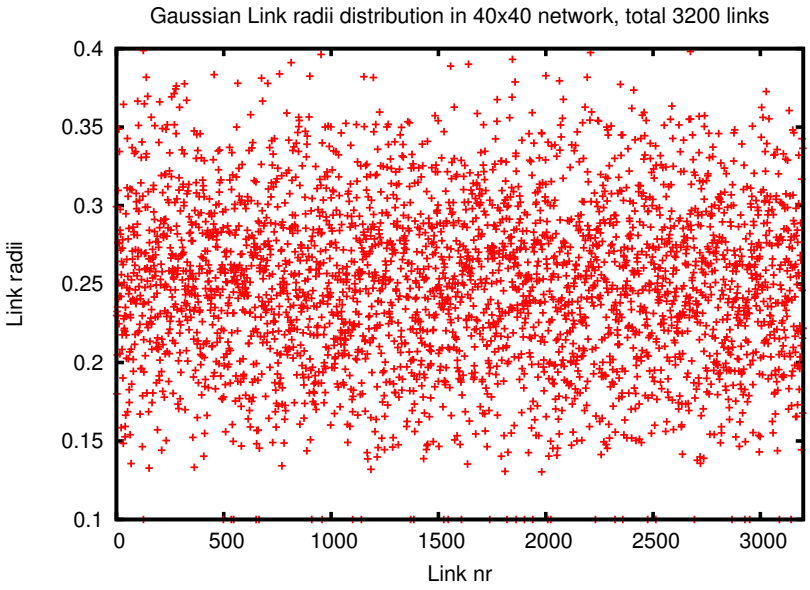

Figure 19: Tube radii, [mm], Gaussian distribution

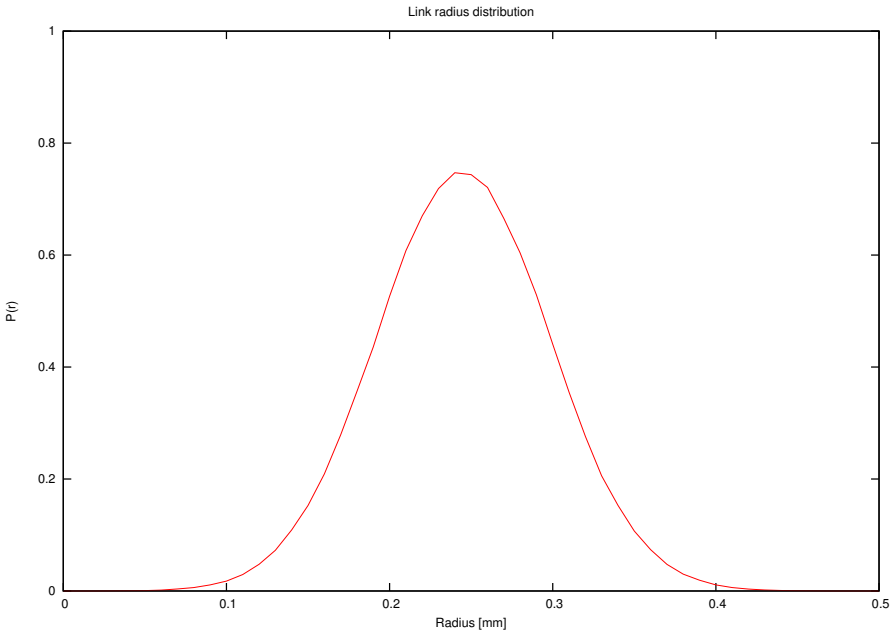

Figure 20: Gaussian distribution of tube radii

With the capillary pressure given by eq.(63), the local flow rate q is given by the Washburn equation: (see derivation of eq.(16) in section 6.8)

$$q_{ij} = -\frac{k_{ij}\pi r_{ij}^2}{\mu_{eff}} \frac{(\Delta p_{ij} - \sum p_c)}{l} \tag{64}$$

Where $k_{ij} = r_{ij}^2/8$ is the permeability, r_{ij} is the radius of the tube connecting node i and j, and $\Delta p_{ij} = p_j - p_i$ is the pressure difference between node i and j. $\sum p_c$ is the sum of the capillary pressures of the menisci in the tube and μ_{eff} is the weighted viscosity according to the volume fraction at the beginning of each time step in each tube. The reason for summing over the capillary pressures of the menisci, is because the present model allows for a total of 3 bubbles of oil/water in each tube. This is illustrated in figure 21.

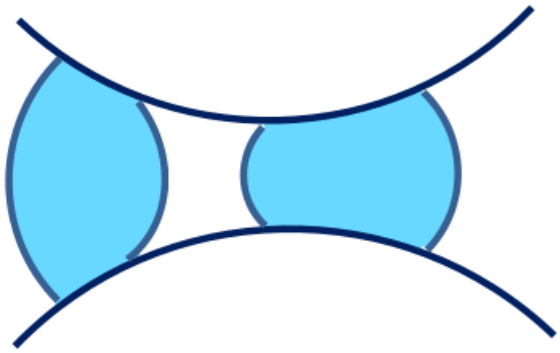

Figure 21: Presence of bubbbles in the hourglass shaped tubes.

In this case, the area of interest is what happens in a system far from inlets and outlets. That is, given a very large system, a small piece located somewhere in the middle is taken out, and its properties investigated. This is done by implementing bi-periodic boundary condition (2d lattice forms a torus, see figure 22). As the network is connected between the inlet and outlet row, time evolution of the system is done by applying the global pressure field, ΔP over the row where the original outlet and inlet row meets.

The straightforward appliance of a global pressure between the inlet row and the outlet row in invasion simulations needs modification. One could do this by adding one row of ghost nodes on both sides of the system. The pressure would be fixed on these two rows as before. The equations would be solved as before, only with the additional constraint that the outgoing flux in each tube between the last row and its ghost row should equal the incoming flux in the respective tube between the other ghost row and the first row. This method works, but has two drawbacks. One is that it gives more complicated computer code. The other is the fact that the pressure is still fixed to have the same value along a straight line through the system, thus giving a boundary effect. Therefore, instead of using ghost nodes with fixed pressures as the driving force, a jump in the pressure over all the tubes on the boundary has been made. This has previously been implemented in random resistor networks, Batrouni and Hansen [32].

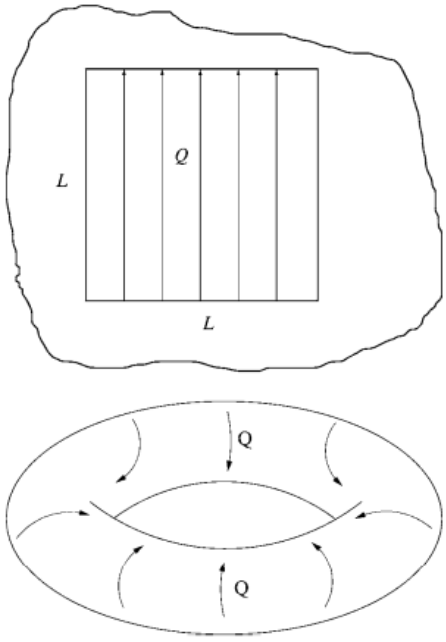

Figure 22: Biperiodic boundary conditions, 2d network forms a torus. Figure from Ramstad and Hansen [40]

In practice, these boundary conditions works such that simulation can go on forever, and still conserve the volume of the two fluids during simulation. From this, the system will reach a steady state after a certain amount of time. The intrinsic properties of the system can then be investigated, giving information about properties like fluid distribution within the pore space, fractional flow, etc.

8.2 solving the flow field

Since the fluids are considered incompressible, Kirchoff's law is applied, and net flux in a single node is set to zero due to mass conservation.

$$\sum_j q_{ij} = 0 \tag{65}$$

Where q_{ij} is the flow through a tube connecting nodes i and j, and the summation j runs over the nearest neighbors of i. This give a large set of linear equations to be solved. By inserting eq.(64) in the Kirchoff equation, one gets the following expression:

$$\sum_j g_{ij}(p_j - p_i - \sum p_c) = 0 \tag{66}$$

Where the tube mobility $g_{ij} = \pi r_{ij}^2 k_{ij}/\mu_{eff}$, has been introduced.

These equations and assumptions, give a large set of linear equations to be solved in order to calculate the local pressures in the nodes with respect to the global pressure drop ΔP across the network. These sets of equations are solved using a conjugate gradient method. (Batrouni and Hansen [16]). If a constant total flow Q is imposed, the flow can be written as:

$$Q = A\Delta P + B \tag{67}$$

Where the first term is from Darcy's equation, and the second term is from capillary effects. The unknown parameters are found from calculating nodal pressures for two different global pressure with corresponding injection rates. Global pressure is then found from $\Delta P = (Q - B)/A$. Global capillary pressure is defined as $P_c = -B/A$

Menisci positions are changed according to a forward integration of eq.(64) (explicit Euler integration). There is a limit of maximum menisci movement of one tenth of the length of a single tube, l_{ij}, which limits the size of the time steps. When a menisci reaches the end of a tube it is redistributed among the neighboring tubes, where the basic processes of snap off and coalescence of bubbles have been considered. See Knudsen, Aker, and Hansen [22] for more detailed information.

8.3 wettability alterations

The theoretical explanation behind increased oil recovery due to wettability alterations is still not fully understood. Many believe that it is associated with electrostatic forces depending on the ionic strength of the water. See section 6.4 for a brief discussion.

In previous work by Ødegården [15], the wettability altering mechanism was a simple flipping of the sign of the capillary pressure to mimic a change in the wetting angle θ from 0 to 180 degrees in eq.(63), and occurred in randomly chosen capillary tubes. In this model, a more physical plausible mechanism to alter the wettability of the system is introduced. Instead of using a simple flip of the sign of the capillary pressure, a distribution function to mimic the effect of continuously changing wetting angles is implemented.

The idea behind this algorithm is that for wettability alterations to occur, low salinity water needs to be in contact with the pore space. This claim is rather trivial, as one can not expect any change if the wettability altering agent is not present in the reservoir. The next assumption, is that the magnitude of change in the wetting angle depends on the cumulative flow of low salinity water that has passed through each pore. This means that if a certain pore is flooded by large amounts of fresh water, the wetting angle should change more than in a pore which has very little water flooded through. That is, all tubes in the model are initially oil wet, and by tracking the flow of low salinity water through each

tube, a new wetting angle is assigned depending on this cumulative flow value, $Q_i(t)$ for tube i at time t.

This is implemented by summing up the flow rates in each capillary tube over a certain "wettability altering time span", $\tau = [t_0, t_1]$ (Illustrated in figure 31). t_0 is the time when the injection of low salinity water is initiated, and the algorithm starts tracking the flow rates in each tube. At time t_1, the system reaches a state with a static wetting angle distribution. To make sure that only the flow of low salinity water affects the wettability, and not the flow of oil, the flow rate in tube i at time t, $q_i(t)$, is multiplied with the water saturation in the tube at the same time step, $\Gamma_i(t)$. This gives the cumulative flow of low salinity water in tube i at time t:

$$Q_i(t) = \sum_{t_0}^{t \leq t_1} q_i(\tilde{t})\Gamma_i(\tilde{t})\Delta\tilde{t} \tag{68}$$

$Q_i(t)$ is then used to assign a continuously changing wetting angle for each tube, updated every time step in the range $[t_0, t_1]$ during simulation. This was done by replacing the $cos\,\theta$ term in eq.(63) by a distribution function depending on $Q_i(t)$. The distribution chosen has approximately the range [-1,1], to represent the $cos\,\theta$ term with θ in the range [180,0].

$$cos\,\theta \rightarrow \frac{2}{\pi} tan^{-1}\left[\frac{20}{Q_i^{thr}}(Q_i(t) - Q_i^{thr})\right] \tag{69}$$

The pre-factor $\frac{2}{\pi}$ is a normalization constant to set the range [-1,1], the nr. 20 is just a parameter to adjust the slope of the distribution function, and Q^{thr} a certain threshold value needed to significantly change the wetting angle.

The idea behind the Q^{thr} factor, is that in order to alter the pore wettability by injecting low salinity water, a certain amount needs to be injected before it significantly affects the wetting angle. Because of the random size distribution of the pore space in a porous media, this threshold value should also depend on the pore size. Intuitively, one expects that more low salinity water needs to be injected in a large pore compared to a small pore to alter the wettability significantly. This threshold value is thus defined as a constant η, times the corresponding pore volume.

$$Q_i^{thr} = \eta\pi r_i^2 l \tag{70}$$

where r_i is the pore radii of tube i, l is the pore length, and η is the parameter defining how many pore volumes of low salinity water needs to be injected through each pore to reach the threshold value.

As this model does not include thin film flow, the wetting angle will not be either 0 or 180 degrees. Rather, the starting point of $\approx$ 165 degrees was chosen. In this case, the threshold value Q^{thr} is the zero point of the distribution function, and represents the state when θ is changed from the initial value to 90 degrees.

This distribution gives the wetting angle for tube nr. i at time t, as a function of the amount of low salinity water injected, $Q_i(t)$. See figure 23.

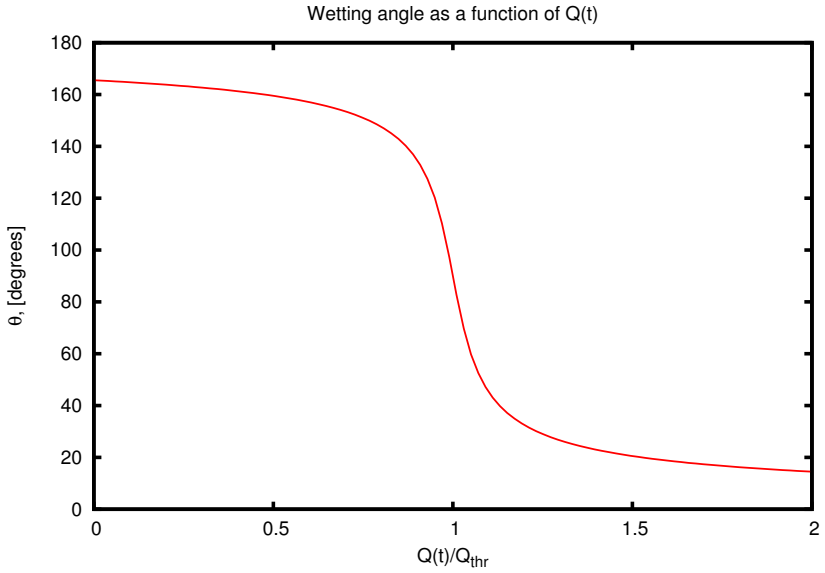

Figure 23: Wetting angle for each tube as a function of $Q_i(t)$

With these changes, the capillary pressure given by eq.(63) is replaced by:

$$p_c(t) \approx \frac{4\gamma}{\pi r_i} tan^{-1}\left[\frac{20}{Q_i^{thr}}(Q_i(t) - Q_i^{thr})\right](1 - cos(2\pi x)) \tag{71}$$

Where $Q_i(t)$ is given by eq.(68). The value of $Q_i(t)$ is updated between each time step, meaning that the wettability is continuously changing as a function of time. This represents that the wetting angles are gradually changing in the various tubes, as more low salinity water has been in contact with the reservoir surface.

Q_{thr} is a fitting parameter, depending on how much low salinity water needs to be injected through a pore to cause significant changes to its wetting properties. This is a parameter which could possibly be fitted against experimental results. But, as such experiments have not been performed yet, this was treated as a tuning parameter in the following work.

The model is first run for a sufficient amount of time steps to reach steady state conditions. Then, the effect of wettability alterations is introduced following from the described algorithm. After a significant amount of time the system is set to static wetting properties, and the model is again run to steady state. This wettability alteration causes a perturbation to the system, which leads to permanent changes in the static flow properties.

9 Simulation procedure

In these kind of simulations computational time is a big issue, as large models are very demanding, and the computational time incrase significantly with larger lattice sizes. The most time consuming part of the program, is the solution of the flow equations using the conjugate gradient algorithm (see section 7.1). The goal is then to find the balance between sufficient size to obtain good results, but still small enough as to limit the computational time.

It was found that a network size of 40x40 was sufficient to obtain good results, and most simulations was thus limited to this size. However, for some of the illustrations (Figures 24, 25, 27, 28, 29, 30, 35, 36, 37, 38, 39, 52), the lattice size was increased to 80x80 in order to make the details more visible. For these figures only a few simulations had to be performed, and computational time was thus not an issue. However, in order to gather statistical data for the fractional flow curves etc, several thousand simulations were performed. The simulations were performed using 5 different seeds, giving new network geometries. This was done to get a better statistical average for the data obtained in the various simulations.

All simulations were performed with $Ca = 10^{-3}$, viscosity contrast $M = 1$, and surface tension $\gamma = 3$ dyne/mm.

For a 40x40 network, using 600.000 time steps and 5 runs with different seeds, the simulation time for each parameter set was in the order of 24 hours. When doing thousands of these simulations, computational time is obviously an issue. However, access to the department of physics UNIX cluster made it possible to run several simulation jobs at the same time, limiting the total computational time.

The results for fractional flow plotted in 2d is showing either the maximum change in fractional flow as a function of oil saturation, or the change in fractional flow as a function of time steps/injected pore volumes. The results plotted in 3d, show the changes in fractional flow as a function of both oil saturation and wetting angles. When calculating the maximum change in fractional flow, this was taken as the difference in fractional flow at steady state before and after wettability alterations. This was done by first taking the mean value over 10.000 time steps before the change, and then over the last 10.000 time steps of the simulation. This then gave the discrete values as shown in e.g figure 34.

10 Results

10.1 Transient to steady state flow: Imbibition and Drainage

At initialization, the system is divided in two separate regions of oil/water. Following from a simultaneous process of drainage and imbibition (caused by the bi-periodic boundary conditions), the two fluids will distribute themselves in the network. After sufficient amount of time, the system will ultimately reach a steady state. This process can be seen in figure 24.

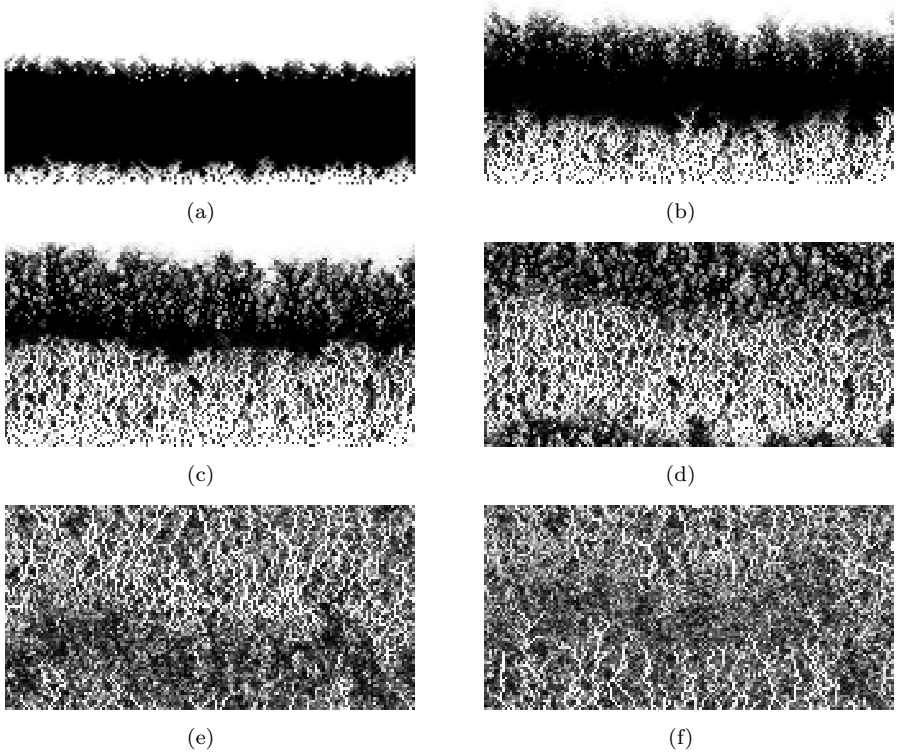

Figure 24: Showing a combined drainage and imbibition process with oil as black, and water as white. The network is oil wetting, and the difference in fluid invasion by a wetting vs. non-wetting fluid is clearly visible.

In the last picture of figure 24, one can see the starting development of percolating paths of water, shown as the white branch-like structures. This will cause trapping of oil clusters in the regions between these paths, which will then be basically immobilized. This topic will be discussed in detail in section 10.2.2.

10.2 Uniform radii distribution

10.2.1 Wettability alteration

Using the algorithm described in section 8.3, wettability alterations was introduced in the model. Initially all tubes were oil wet ($\theta \approx 165$ degrees). The system then gradually transforms to a mixed wet system with some tubes still being oil wet, while others are changed to intermediate or water wet. This effect can be seen in figure 25. The wetting angle is drawn on a grey-scale, where white corresponds to 180 degrees, and black to 0 degrees. This shows how the wettability is first altered in the percolating paths in the network which dominate the total flow rate. After some time, the wettability starts changing also in regions with lower flow rates.

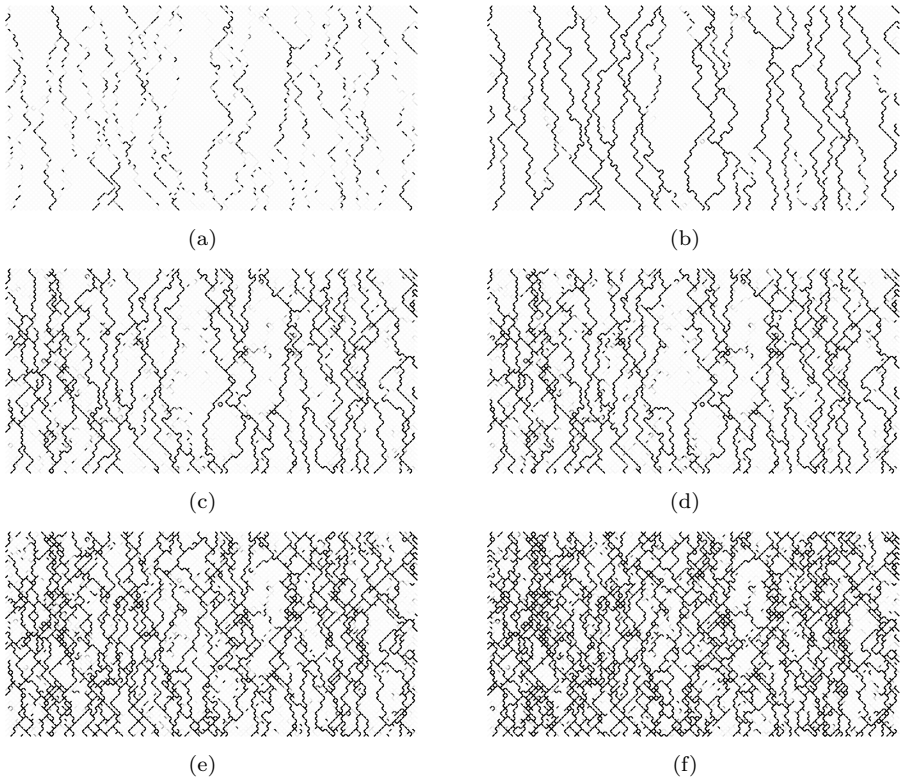

Figure 25: Wetting angles in network at various time steps, starting in upper left corner. Final state in last figure at bottom right. Shown on a grey-scale where white corresponds to 180 degrees, and black to 0 degrees.

As mentioned in section 8.3, the degree of wettability alteration in the network is controlled by the fitting parameter Q_i^{thr}. It was found that by setting $Q_i^{thr} = 150 \cdot \pi r_i^2$ (see section 8.3 for closer description of this parameter), the

wettability was significantly changed in about half of the tubes. Initially, all tubes had a wetting angle of $\theta \approx 165$ degrees . In the final state, wetting angles are distributed in the range $\theta \approx [0, 165]$ degrees, as can be seen in figure 26.

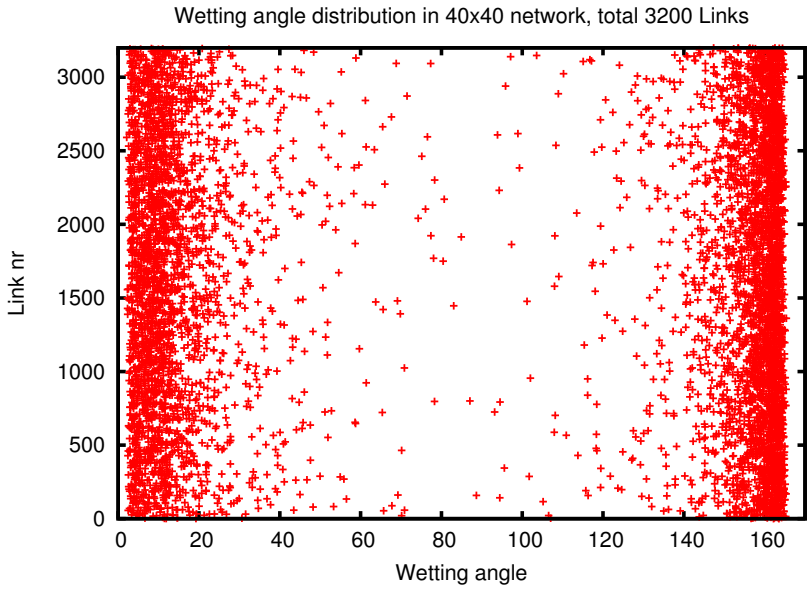

Figure 26: Final wetting angle distribution for 40x40 network, with a total of 3200 tubes.

From this angle distribution, one can define an "average wetting angle" for the network, defined as

$$\theta_{avg} = \frac{1}{N_{tubes}} \sum_{i=1}^{N_{tubes}} \theta_i \tag{72}$$

This parameter will depend on the value of Q_i^{thr}, and also on the lattice disorder. For initial tests giving angle distributions like the one in figure 26, it was found to be in the range $\theta_{avg} \approx 90 - 100$ degrees. However, the idea is that the spatial correlations between regions of different wettability is of greater importance than simply the overall average wetting angle.

10.2.2 Flowdistribution perturbation

The wettability alterations significantly affect the flow properties of the system. figure 27 is showing the oil saturation in the network at steady state, where oil is black and water white. If one looks closely, one can notice that there exists a structure of narrow white paths percolating the system.

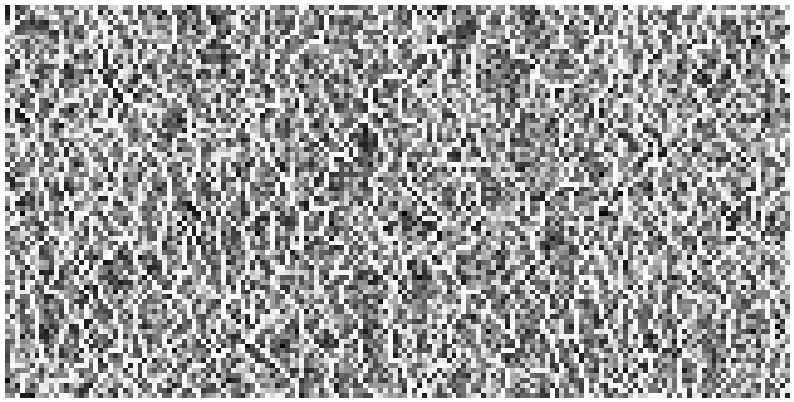

Figure 27: Oil saturation in network at steady state before wettability is altered.

These paths dominate the total flow rate through the system, and the oil in the regions between them are basically immobile. Comparing with the oil saturation in the network at steady state after the wettability alteration, it is clear that this has a great impact on the system. See figure 28.

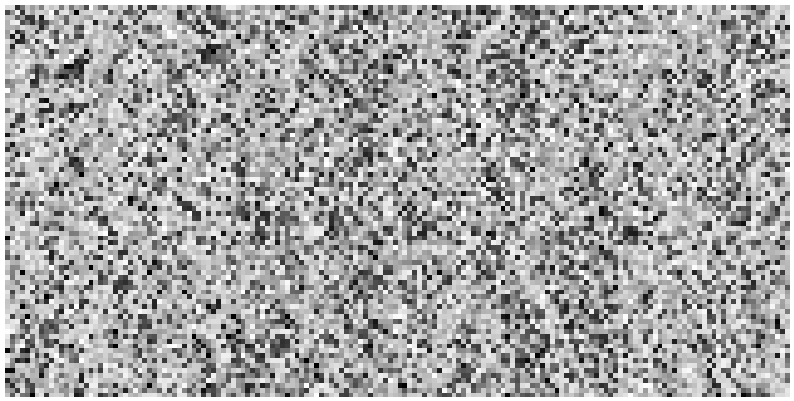

Figure 28: Oil saturation in network at steady state after wettability has changed to a mixed wet system

The white percolating paths seen in figure 27 have now broken down, and it seems to be a more uniform mix of oil and water, where both phases contribute to the total flow. These changes can easier be seen by investigating the flow rate distribution in the network, as this shows which regions flow, and which are basically stuck. The flow rates in the system at steady state before wettability alterations is seen in figure 29.

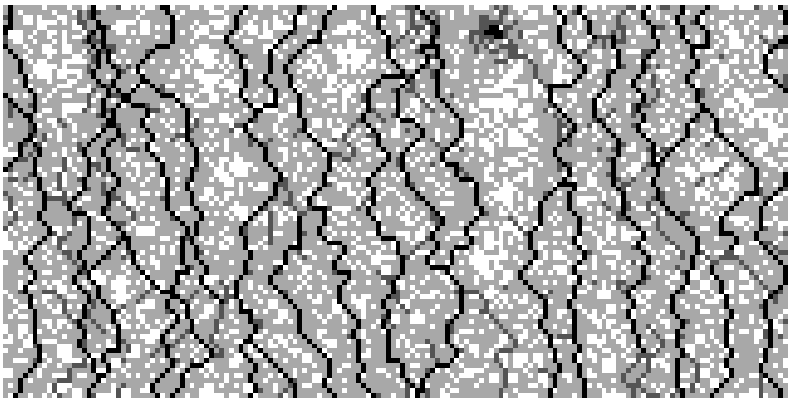

Figure 29: Flow rates in oil wet network. On normalized logarithmic scale with 1 (black) corresponding to the maximum flow rate through any tube, and white corresponding to a flow rate of less than 10^{-4} compared to max flow rate.

As in figure 27 of the oil saturation, one can see the percolating paths where the flow rate is orders of magnitude greater then in the immobile regions, which is basically stuck (seen as white). However, as the wettability of the network is changed to a more mixed wet system, these dominating paths appear to break down, and is replaced by a more uniform flow distribution. The large white regions in figure 29 which were previously "stuck", are now mobilized and these regions also contribute significantly to the total flow rate. This can be seen in figure 30, which is the flow rate corresponding to the final wetting state shown in figure 25.

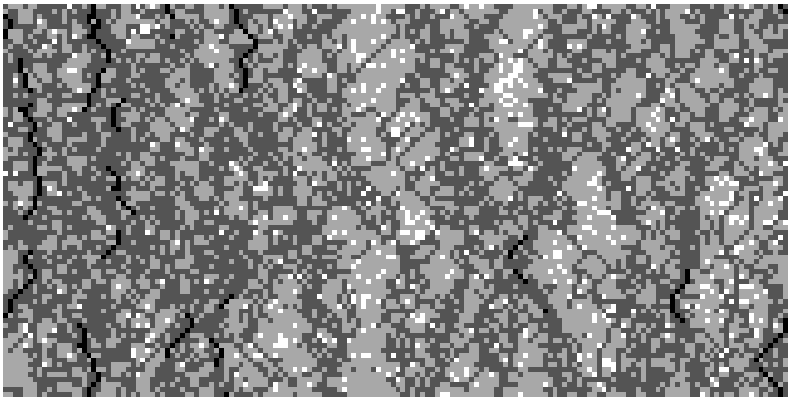

Figure 30: Flow rates in mixed wet network. On normalized logarithmic scale with 1 (black) corresponding to the maximum flow rate through any tube. And white corresponding to a flow rate of less than 10^{-4} compared to max. flow rate.

10.2.3 Fractional flow

The re-mobilization of oil can also be seen as an increase in the fractional flow of oil, see figure 31. For a 40x40 network with $S_{oil} = 0.3$, the system is starting to reach steady state after the injection of approximately 5 pore volumes (total pore volume of the network). The wettability altering algorithm is activated after the injection of ≈ 8 pore volumes (t_0, as defined in section 8.3), causing a significant and permanent change in the fractional flow of oil.

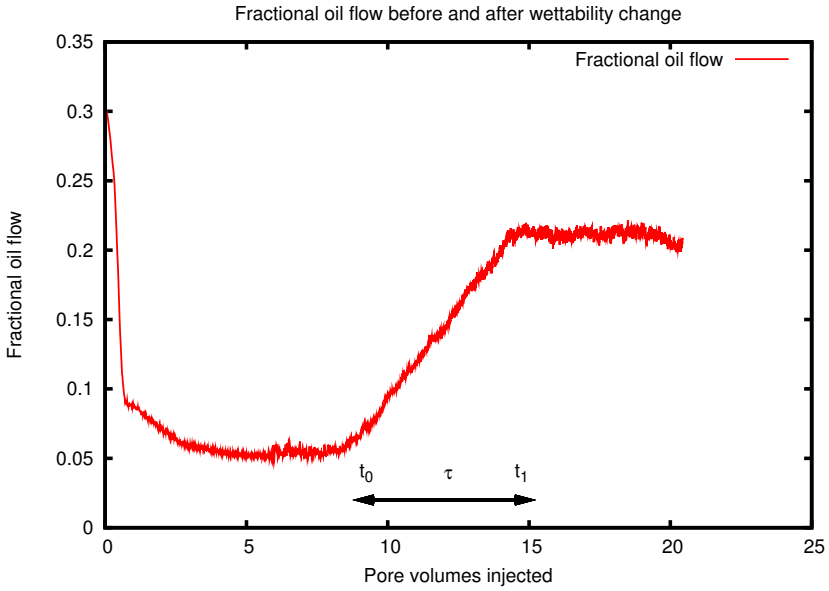

Figure 31: Fractional flow of oil. After injection of approximately 8 pore volumes, wettability alterations is introduced in the model following from the algorithm described in section 8.3. From that definition, the wettability altering time span τ, is between $\approx 8 - 15$ in terms of injected pore volumes.

At steady state conditions, if one of the phases spans throughout the system with a single phase dominated flow path, the motion of this phase require less global pressure then the motion of two phases with interfaces. Therefore, as single phase percolating paths break down there should be an increase in the global pressure across the system, as there are a greater number of interfaces moving through the network. This effect of pressure increase due to breakdown of the percolating paths of water can be seen in figure 32.

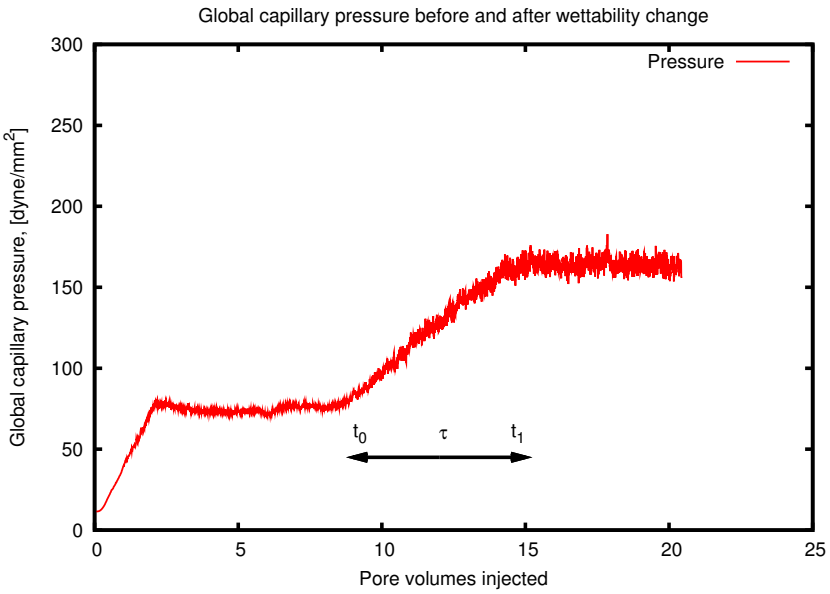

Figure 32: Pressure increase due to oil mobilization

The results shown so far, are for an oil saturation $S_o = 0.3$. Also for different oil saturations, there is an increase in the fractional flow of oil in a mixed wet network compared to an oil wet network. For various oil saturations, this can be seen in figure 33.

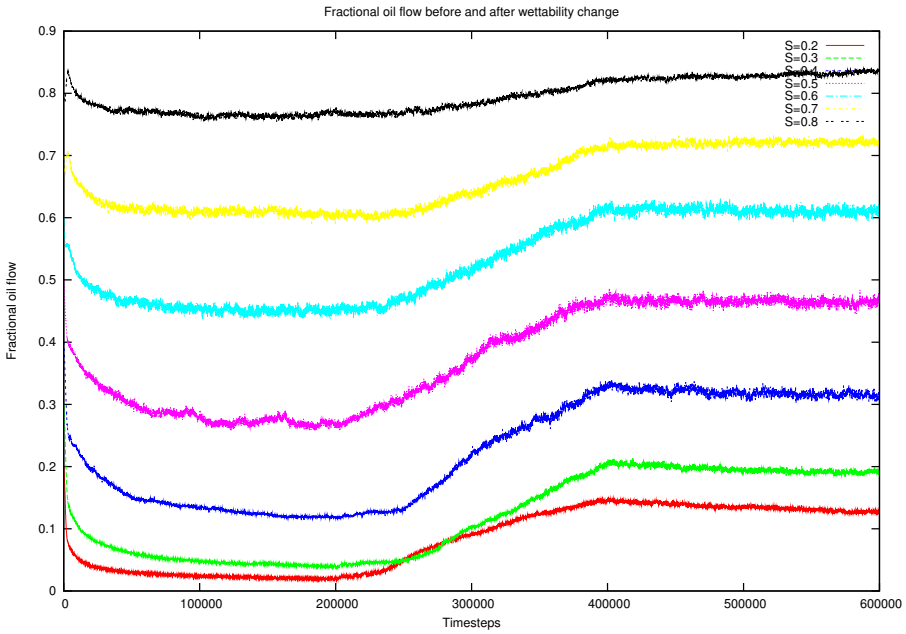

Figure 33: Fractional flow of oil before and after wettability alteration for various oil saturations in the range 0.2-0.8. At t=200.000 time steps, the wettability altering algorithm starts simulating the injection of low salinity water, causing an increase in F_{oil} as the network wettability changes to a mixed wet system. At t=400.000 time steps, the system reaches a state of a static wetting angle distribution. The system then settles in a new steady state with a significant increase in F_{oil} compared to the initially oil wet system. In this figure, time steps rather then injected pore volumes are used as the time scale. This to easier compare the results for various oil saturations, as the number of injected pore volumes differ as S_{oil} is changed.

These results can be summarized in a plot showing the change in fractional oil flow before and after wettability alteration.

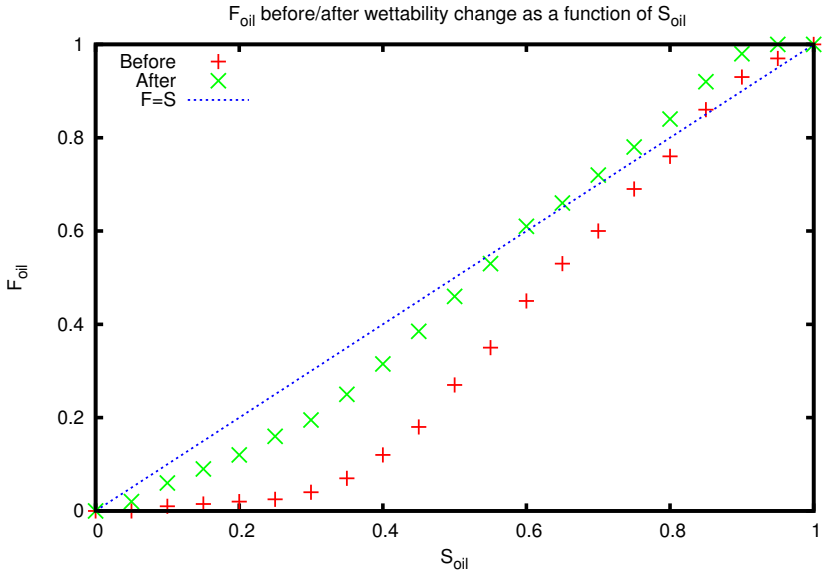

Figure 34: Fractional flow of oil as a function of oil saturation in the range 0.1-0.9

The S-shape of these curves is resemblant of the ones found in Buckley-Leverett fractional flow. Dullien [1], Buckley and Leverett [47]. In figure 34, a diagonal line is added. This is the line where the fractional flow is equal to the oil saturation. A miscible fluid mixture would follow this line, and it is interesting to use as a reference to compare how the data points lie above or below this line.

10.3 Gaussian radii distribution

10.3.1 Wettability alteration

Simulations using a Gaussian radii distribution was also performed, to see how the tube radii distribution affected the results. Following the same procedure as for the uniform distribution, gave the following snapshots of the wettability alteration:

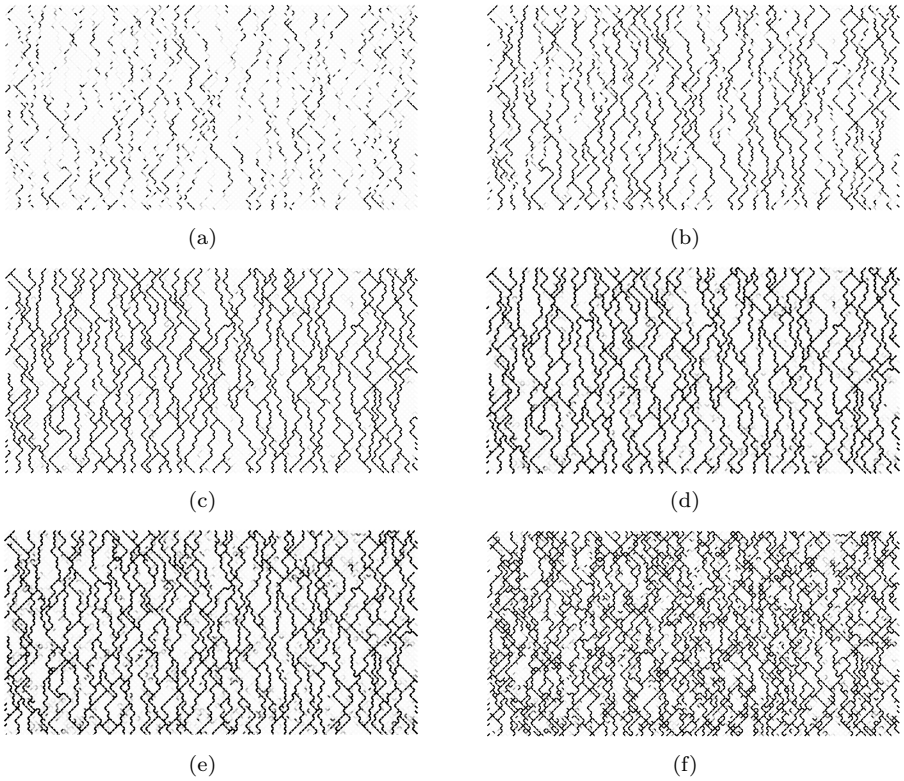

Figure 35: Wetting angles in network at various time steps, starting in upper left corner. Final state in last figure at bottom right. Shown on a grey-scale where white corresponds to 180 degrees, and black to 0 degrees.

Compared to the results from the uniform radii distribution, the wettability alteration also in this case first occur in the percolating paths spanning the network. However, these paths are distributed more uniformly throughout the network than in the uniform radii case.

10.3.2 Flow distribution perturbation

Comparing the figures of oil saturation in the networks, the results are similar for both the uniform radius distribution (figure 27) and the Gaussian distribution (figure 36). However, the size of the stuck clusters is smaller in the Gaussian case, as the number of percolating paths through the network is larger.

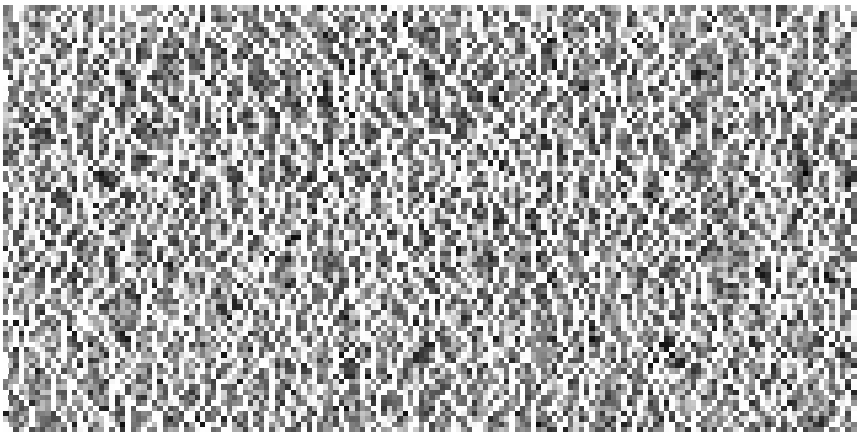

Figure 36: Oil saturation in network at steady state before wettability in altered.

Comparing with the oil saturation in the network at steady state after the wettability alteration, it is clear that this has a great impact on the system also in the Gaussian case. See figure 37.

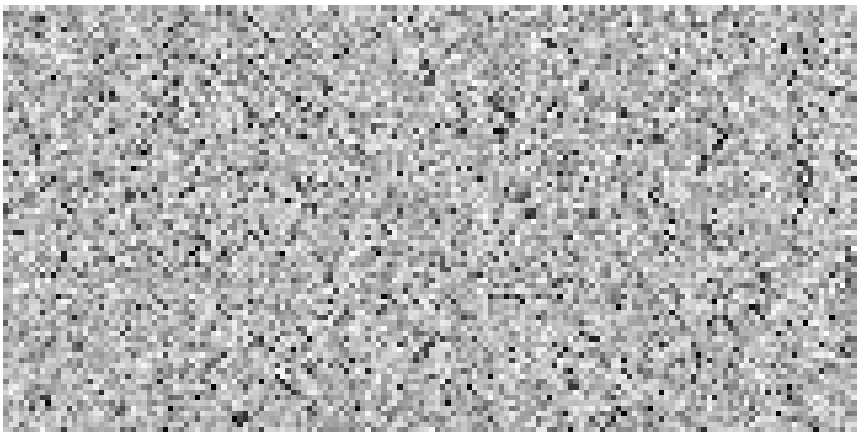

Figure 37: Oil saturation in network at steady state after wettability has changed to a mixed wet system

Since the clusters are smaller in the Gaussian system, it seems to make the

wettability alteration able to break up basically all the clusters, causing an even more uniform mix of oil and water in this network compared to the one with an uniform radii distribution.

As for the uniform radii case, these changes are easier to notice when investigating the flow rates instead of the oil saturation. In figure 38 you see the flow rates in the network at steady state before the wettability alteration.

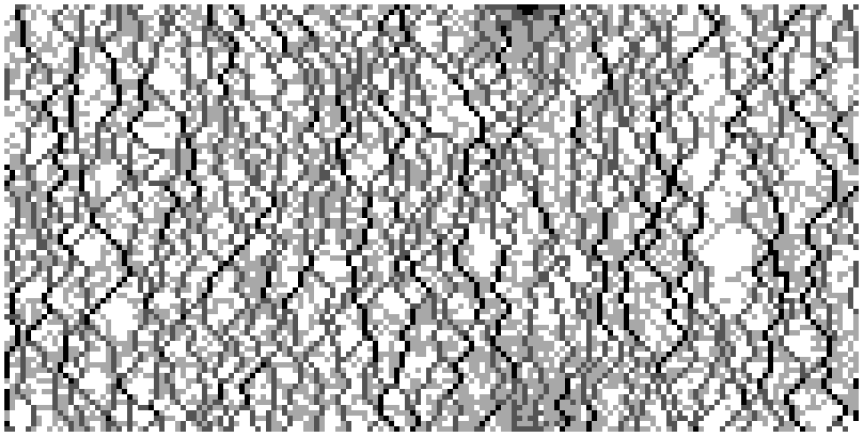

Figure 38: Flow rates in oil wet network before wettability is altered. On normalized logarithmic scale with 1 (black) corresponding to the maximum flow rate through any tube, and white corresponding to a flow rate of less than 10^{-4} compared to max. flow rate.

Using a Gaussian radii distribution, the flow pattern is more uniform than for the uniform radii network.(See figure 29), with a higher number of percolating paths. However, the existence of white regions representing stuck clusters is still present in this case. Changing the wettability to a more mixed wet system cause perturbations also to this system, leading to a more uniform flow distribution in the network (figure 39).

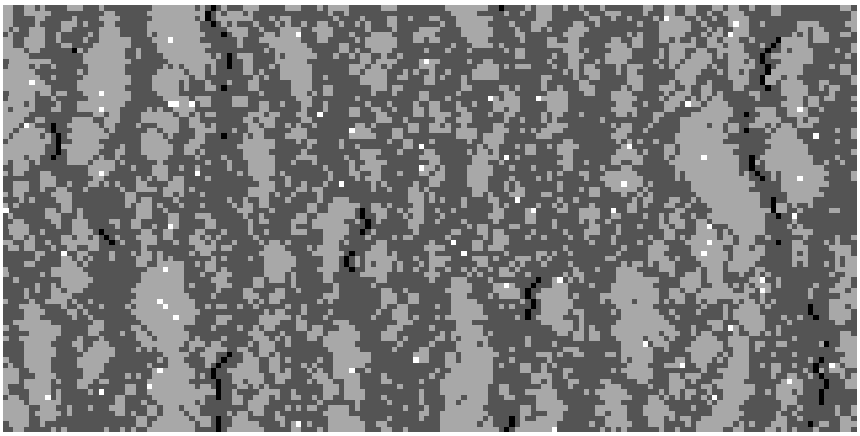

Figure 39: Flow rates in mixed wet network after wettability alteration. On normalized logarithmic scale with 1 (black) corresponding to the maximum flow rate through any tube, and white corresponding to a flow rate of less than 10^{-4} compared to max. flow rate.

The reason for the initially more uniform flow patterns in the Gaussian case, is probably from the reduced disorder of the network. From the tube radii distribution (figure 20), the probability for the radii to be located in the middle of the distribution is a lot larger than being close to the upper/lower limit. This will thus cause a less disordered system than for the uniform radii model. Considering this, the results are not that surprising. However, investigating the effect of changing the tube radii distribution is still interesting, as this distribution is what one actually use to represent the physical reservoir rock with a certain pore radius distribution which may, or may not, be known.

Investigating the changes in fractional flow using the Gaussian distribution compared to the uniform radii case, did not show any big differences. Since these results did not show anything perticularly interesting, it was decided to not perform a more detailed investigation at this point.

10.4 Critical behavior

In the simulation results shown so far, the wetting angles of the final mixed wet system are in the approximate range of [165,0]. However, the magnitude of wettability alteration due to low salinity water injection is not well understood. It is thus interesting to investigate how much the wetting angles have to change to cause any significant effect on the system. In previous work by Ødegården [15], the fractional flow of oil was found to depend linearly with the wettability w of the system. $F^w(S) \propto w$, where w is defined as the ratio between the number of oil wet tubes and total number of tubes, $w = N_{oil-wet}/N_{total}$. From this, and from the expression for the capillary pressure, eq.(63), one could expect a similar connection between fractional flow and wetting angle, $F^\theta(S) \propto cos\theta$. One should then get smooth changes in the fractional flow as the wetting angles of the system change. Instead of having the wettability altering algorithm operating in the full range as shown in figure 23, a cutoff angle θ_{min} was introduced. As before, all angles initially start at 165 degrees. However, as the wetting angles change according to the algorithm, they are not allowed to change to values lower than θ_{min}. By doing many simulations with θ_{min} in the range between the initial 165 degrees and 0 degrees, a critical wetting angle was found. At angles above this critical value, the system is basically unaffected by wettability alterations. When the wetting angles reach the critical value, this suddenly cause dramatic changes to the system, see figure 40.

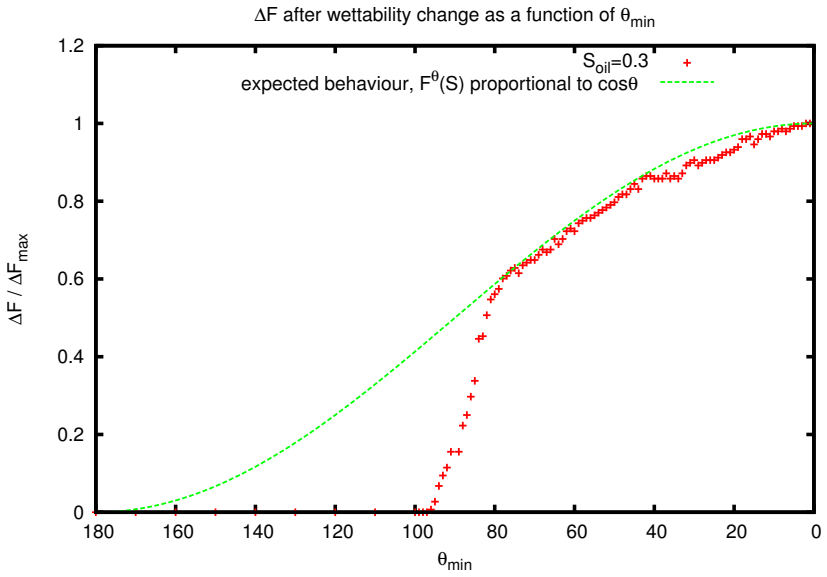

Figure 40: Critical transition in fractional flow as a function of θ_{min}, indicating possible relations to a percolation threshold

Comparing this result with the percolation strength measured in a 2d square lattice (figure 41), there are several similarities.

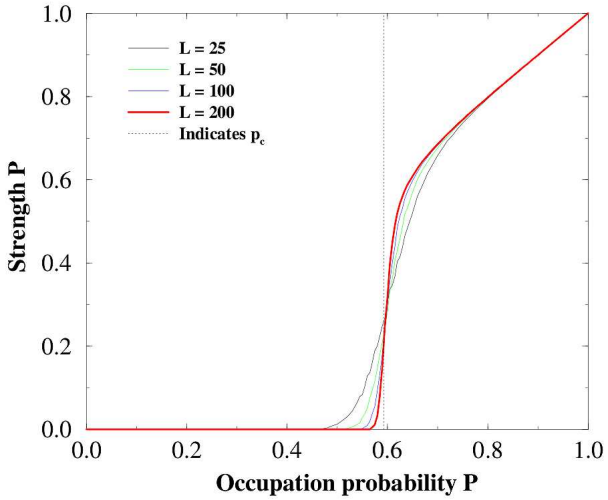

Figure 41: Percolation strength as a function of occupation probability. Figure from Christensen [42]

The transition is not as sharp as the one in the main red line in figure 41, but this could be caused by finite size effects (see section 6.12) "smoothing the transition", since the lattice size in this case is only 40x40. This behavior could indicate some kind of phase transition at the critical point. The idea of phase transitions of flow regimes in porous media has also been addressed by previous work. Cieplak and Robbins [37], Koiller, Ji and Robbins [49]. During capillary displacement in a 2D porous media, they found indications of a dynamical critical transition as the contact angle of the invading fluid varies. This transition causing a divergence of the invading fingers, transforming the system from one dominated by fractal growth patterns as in the invasion percolation model, to a uniform flooding of the system. See figure 42.

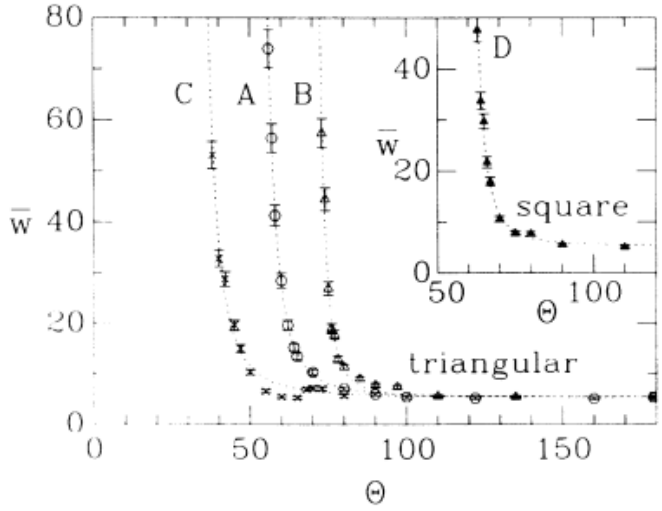

Figure 42: Divergence of invading fingering width at a critical angle. Where the curves A,B and C are for different porosities. Figure from Cieplak and Robbins [42]

From their work, they also estimated critical exponents at the transition point. They found the transition to shift depending on the lattice disorder, and that the critical exponents estimated also depend on the amount of disorder, believed to be caused by finite size effects from percolation theory. Ji and Robbins [49].

If the changes in fractional flow can be described as a percolation transition, one can use relations from percolation theory to investigate the system. Possibly obtaining estimates of critical exponents, scaling relations and other details helping to understand a possible phase transition of flow regimes.

10.4.1 Critical exponents

The connection between percolation theory and cluster formation has been investigated previously by Ramstad and Hansen [40], using a similar network model. Since the increase in fractional flow of oil caused by wettability alterations seems to be caused by the breakdown of oil clusters, a connection between cluster strength in percolation theory and fractional flow is suspected. Assuming the transition in fractional flow can be described as a percolation transition, a similar relation between fractional flow and wetting angle as between percolation strength and percolation probability shown in eq.(34) is proposed.

$$F_{oil}(\theta) \propto |\theta - \theta_{crit}|^{\beta} \tag{73}$$

Hence, by plotting $log\, F_{oil}(\theta)$ vs. $log\,(|\theta - \theta_{crit}|)$ in the critical region, one can obtain an estimate for the critical exponent β. Shauffer and Aharony, [38].

In the following, the parameter $\Delta_\theta \equiv |\theta - \theta_{crit}|$ is introduced, and $log\, F_{oil}(\theta)$ vs. $log\, \Delta_\theta$ is then plotted. Also, one needs to know the critical wetting angle θ_{crit}. As mentioned in section 6.12, this can be shifted compared to the exact value due to finite size effects. However, in these plots the effective θ_{crit} is found from the inflection point of the curve ΔF_{oil} vs. θ_{min}, as seen in figure 40. Due to some uncertainty in determining θ_{crit} accurately, $log\, \Delta_\theta$ vs. $log\, F_{oil}(\theta)$ was plotted for $\theta_{crit} = 85, 84, 83, 82$. According to the suspected power law behavior from eq.(73), the data points should collapse to a linear curve. It was found that a value of $\theta_{crit} = 84$ gave the best linear fit when plotted on log-log scale. See figure 43.

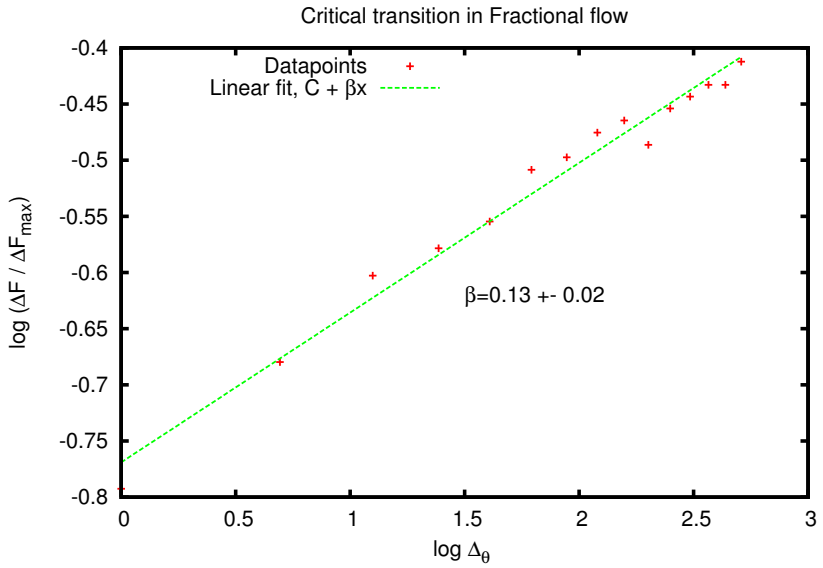

Figure 43: Plot of $log\, \Delta F_{oil}(\theta)$ vs. $log\, \Delta_\theta$, where $\Delta_\theta \equiv |\theta - \theta_{crit}|$. Showing a linear fit, obtaining an estimate for the critical exponent β. Δ_θ is in the range [1, 15], and each data point in the plot is the average value of 5 lattice initializations. Making the number of data points 75, rather then the apparent 15.

The estimate from the curve fitting is $\beta = 0.13 \pm 0.02$, which is close to the result from ordinary percolation, $\beta = 5/36 \approx 0,1388...$ However, the estimates for β are quite sensitive with respect to the choice of θ_{crit}, and the power law assumption is only valid in a narrow range. The limited domain of validity, can be seen in figure 44.

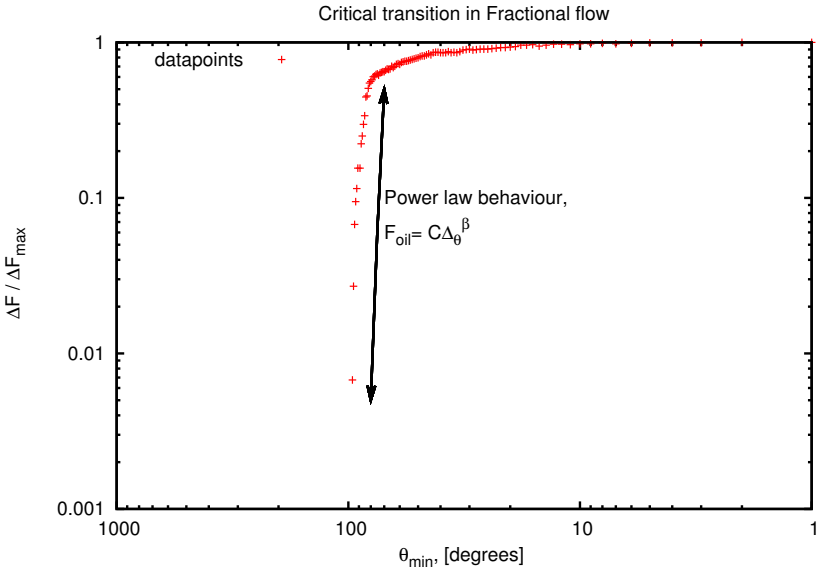

Figure 44: Showing the limited range of validity for the power law assumption. This is seen as the linear region of ΔF_{oil} plotted on logarithmic scale. In this case for $L = 40$ and $S_{oil} = 0.3$

In order to investigate the critical transition in more detail, it was decided to use relations from finite size scaling theory as derived in section 6.12 to investigate the system for various lattice sizes L, and from this obtain a better understanding of the critical behavior of the system.

Lattice size effects

Performing simulations with $S_{oil} = 0.3$ and lattice size L in the range $20 - 40$, gave indications of the dependence of finite size effects.

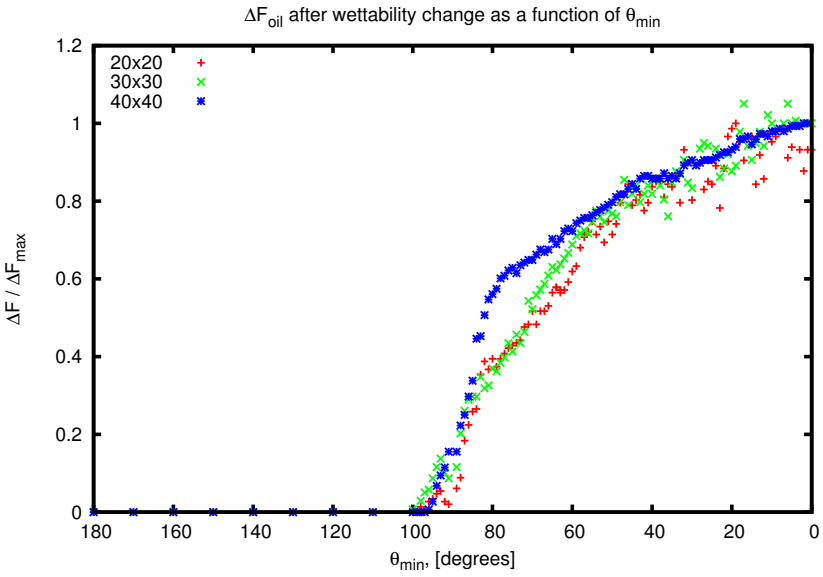

Figure 45: Change in fractional flow as a function of θ_{min} for lattice size $L = 20, 30, 40$

From figure 45 one notice that for a lattice size of $L = 40$, the transition is quite smooth, whereas for smaller lattice sizes, the fluctuations become more dominant. The transition was studied in more detail by investigating the derivative $\partial \left(\frac{\Delta F}{\Delta F_{max}} \right) / \partial \theta$ to estimate θ_{crit} from the inflection point, given as the maxima of the derivative.

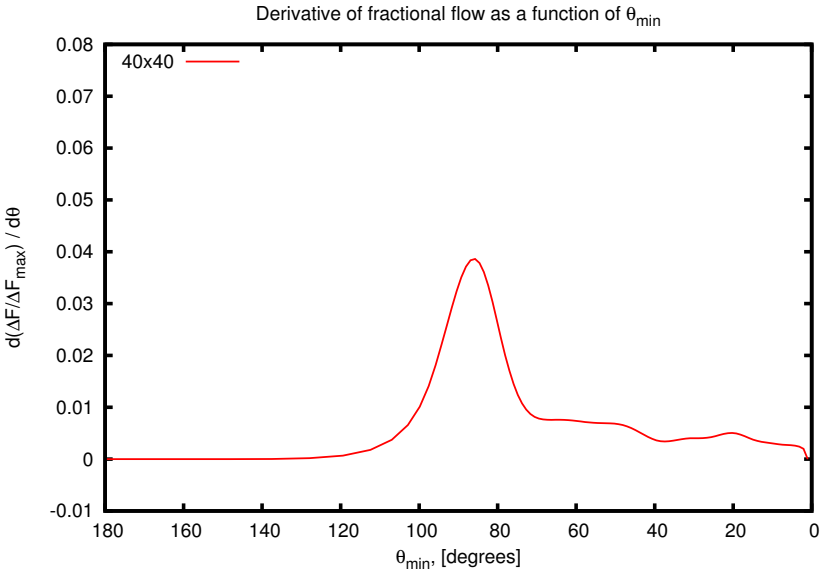

Figure 46: Derivative of the change in fractional flow as a function of θ_{min}, $\partial\left(\frac{\Delta F}{\Delta F_{max}}\right)/\partial\theta$. The peak indicating the inflection point, and thus the value of θ_{crit}. In this figure using a best fit curve for $L = 40$, and a central difference approximation to estimate the derivative

There are some fluctuations, but a distinct peak at $\theta \approx 85$ is seen in figure 46. Even when averaging over 5 samples there are some fluctuations, especially in the region after the critical transition. This becomes significantly worse as one decrease the lattice size L. Simulations were performed for $L = 20, 26, 30, 36, 40, 46$, and the fluctuations were dominating for small lattice sizes.

The transition is located in the region $\theta \approx 50 - 100$ degrees. From the fluctuations in this region for smaller lattice sizes, it was decided to neglect data for $L < 30$. Using only the data for $L > 30$ gave some better results, and the change in fractional flow for $L = 30$ and 40 can be seen in figure 47.

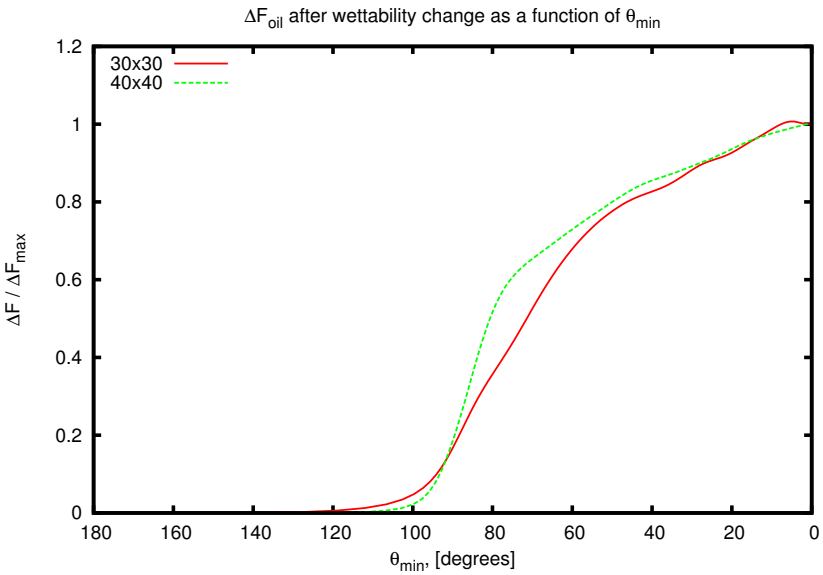

Figure 47: Change in fractional flow as a function of θ_{min} for $L = 30, 40$. In this figure, a best fit curve for the datapoints is used.

Comparing the curves for $L = 30$ and $L = 40$ in figure 47, one observes similar effects as that of finite size scaling for the percolation threshold seen in figure 41, that the transition is "smoothed out" over a larger region for smaller lattice sizes. From finite size scaling in percolation theory, as derived in section 6.12, the transition width Δ depends on the lattice size L:

$$\Delta \propto L^{-1/\nu} \tag{74}$$

Where ν is the correlation length critical exponent. If this system obeys similar scaling laws, this means that by investigating the width of the transition, Δ, one can estimate the correlation length critical exponent ν. Shauffer and Aharony [38]. The transition width Δ can be defined in any suitable way, and in this case it is simply defined as the difference between the value of θ_{min} where $\Delta F/\Delta F_{max}$ is 0.2 and 0.6, as shown in figure 48.

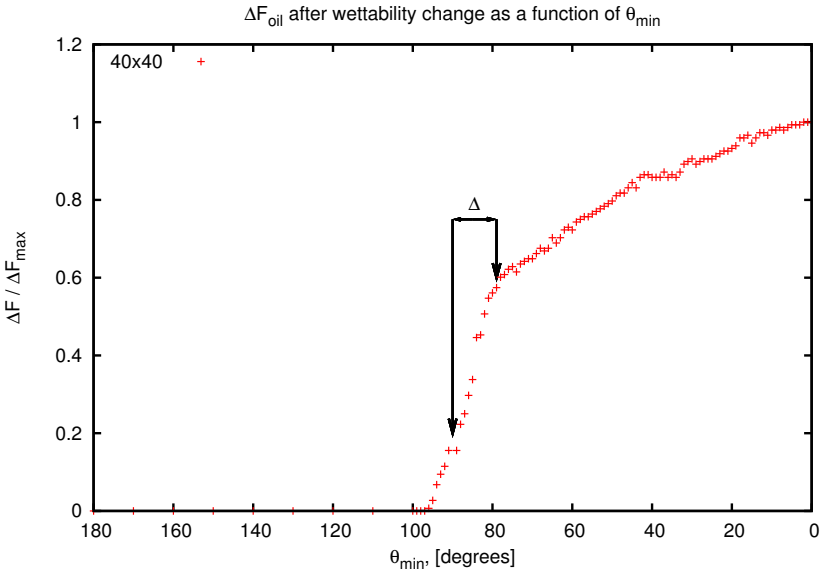

Figure 48: Figure indicating the definition of the transition width, Δ. Here shown for $L = 40$.

By plotting $\log(\Delta)$ vs $\log(L)$, for various lattice sizes L, one can thus extract an estimate for ν. Due to the large fluctuations in the results for small lattice size L, only data for $L = 30, 36, 40, 46$ was used.

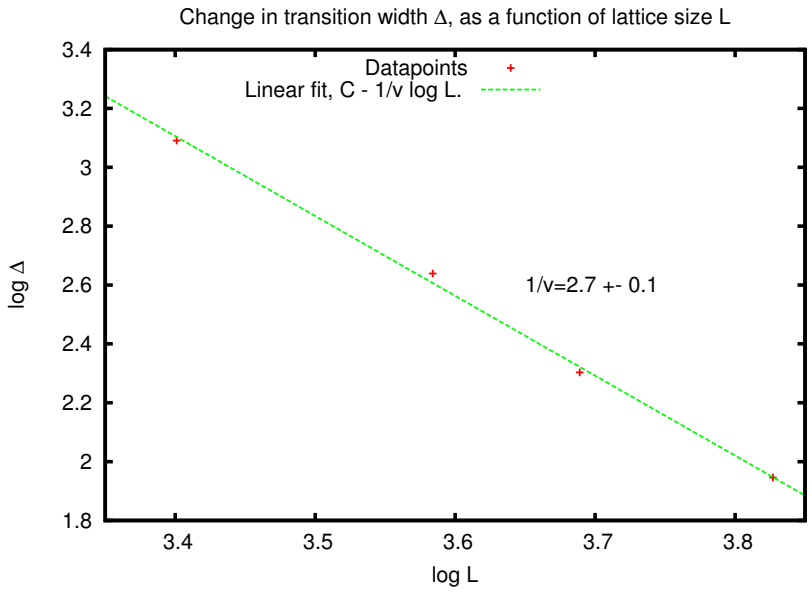

Figure 49: Change in transition width Δ as a function of lattice size L. Each data point is the average value obtained from 5 lattice initializations.

From the data used, the estimate for the correlation length critical exponent is $\nu \approx 0.4$. Compared to the result for ordinary percolation, $\nu = 4/3$, this is significantly smaller.

Another approach to obtain the critical exponents β and ν, is from the scaling law for the percolation strength, $P(L, \xi) \propto L^{\beta/\nu}$ at the critical point, Shauffer and Aharony [38]. If the transition in fractional flow obeys similar scaling laws as that of the percolation strength, one could expect the following relation at the critical transition point, θ_{crit}:

$$F_{oil}(L) \propto L^{\beta/\nu} \tag{75}$$

Meaning that the fractional flow of oil at θ_{crit} should depend on the lattice size L. Hence, by plotting $\log F_{oil}(L)$ vs. $\log L$, one can extract the ratio of the critical exponents, β/ν.

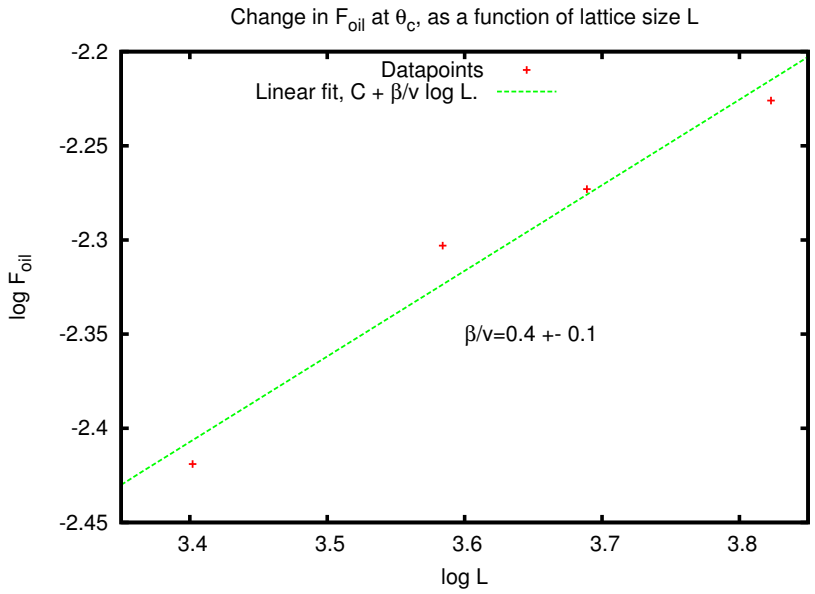

Figure 50: Change in fractional oil flow at θ_c as a function of lattice size L. Each data point is the average value obtained from 5 lattice initializations.

Using the result for β obtained in section 10.4.1, $\beta \approx 0.13$, one gets an estimate for the correlation length critical exponent consistent with the result using the transition width Δ, that $\nu \approx 0.4$. However, as seen in figure 50, the linear fit using this last method to extract β/ν is not as good as the one using the transition width Δ. The reason for this could be that in the estimation of F_{oil} at θ_{crit}, it has not been taken into account that the value of θ_{crit} might shift slightly depending on the lattice size, due to finite size effects as discussed in section 6.12. A more accurate determination of the critical point for the various lattice sizes, could thus yield a better fit to the expected power law behavior from eq.(75).

The estimate using these methods is far off the value from ordinary percolation, but the system still seems to obey similar scaling laws as a function of lattice size. The reason for this large difference in the estimates for ν, could be caused by the limited number of data points. The fluctuations at the critical transition, makes it important to perform many simulations in order to gather sufficient statistical data. In this case, only 5 simulations for each lattice size L were performed. This giving a total number of only 20 data points, which give large uncertainties in determining the critical exponents. It could be that performing more simulations, and for larger lattice sizes, would yield better data.

Saturation effects

In order to understand the transition better, investigating how the oil saturation affects the critical behavior is also important. Comparing simulations with oil saturations in the range $S_{oil} = 0.1 - 0.6$ yield some interesting results.

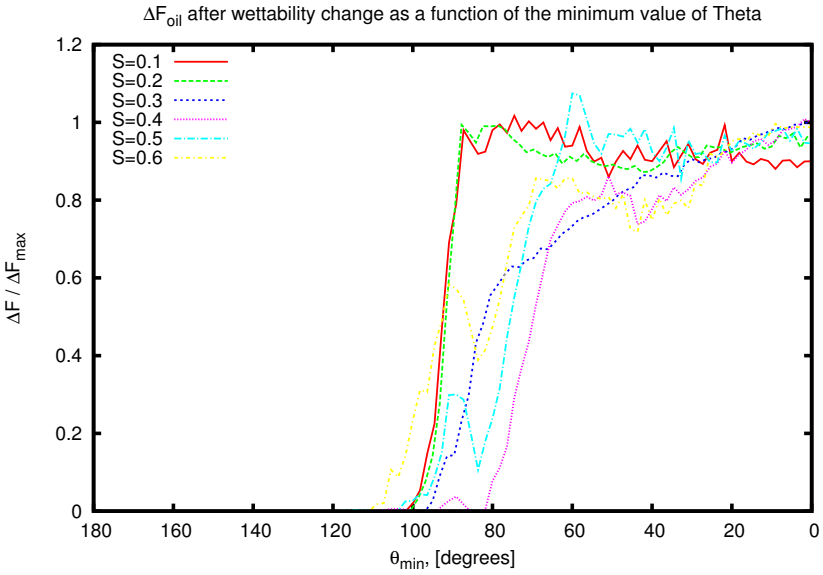

Figure 51: Change in fractional flow as a function of θ_{min}, indicating the critical transition for various oil saturations. Each data point used for the curve fitting, is the average value obtained from 5 different lattice initializations.

From figure 51, it is apparent that the transition is smoothest for an oil saturation of $S_{oil} \approx 0.3$. The behavior for $S_{oil} = 0.3$ and 0.4 are quite similar, even though there are more fluctuations for $S_{oil} = 0.4$. One notice that for oil saturations in the range $0.1 - 0.4$, the transition shifts to lower angles for higher saturations, before it increases for $S_{oil} = 0.5$ and 0.6. For $S_{oil} = 0.4 - 0.6$ there is a peak at $\approx$ 90 degrees, which is most likely due to numerical instabilities caused by the vanishing capillary pressure at this wetting angle.

The reason for the differences in critical transition depending on oil saturation is a bit unclear, but could be related to the saturation threshold in cluster formation, which according to work by Ramstad and Hansen [40] is for a non wetting saturation $S_{nw} \approx 0.7$ for $Ca = 10^{-3}$. This corresponds to an oil saturation, $S_{oil} \approx 0.3$ in this initially oil wet system. From this, it could be expected that cluster formation is most dominant for $S_{oil} \approx 0.3$, and that for higher oil saturations, the clusters should eventually disappear. Investigations for S_{oil} in the range 0.2-0.5 confirms this behavior.

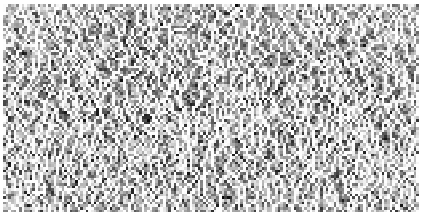

(a) Saturation, $S_{oil} = 0.2$

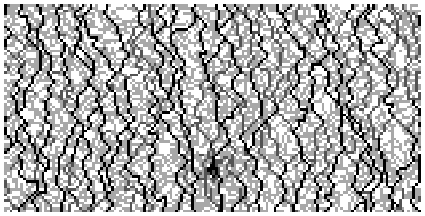

(b) Flowrates, $S_{oil} = 0.2$

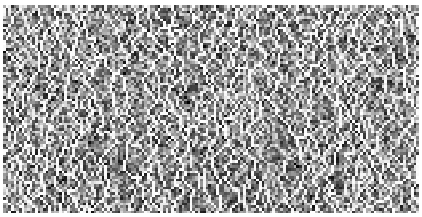

(c) Saturation, $S_{oil} = 0.3$

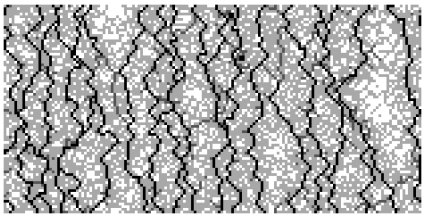

(d) Flowrates, $S_{oil} = 0.3$

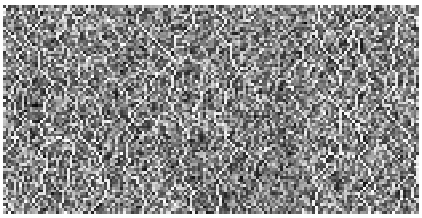

(e) Saturation, $S_{oil} = 0.4$

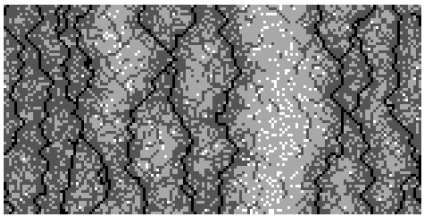

(f) Flowrates, $S_{oil} = 0.4$

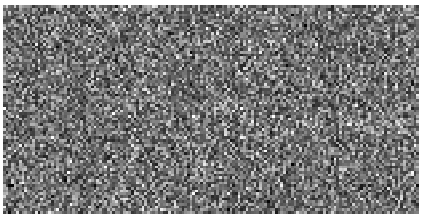

(g) Saturation, $S_{oil} = 0.5$

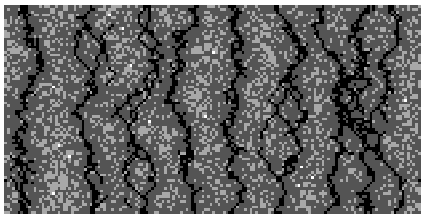

(h) Flowrates, $S_{oil} = 0.5$

Figure 52: Oil saturations and flow rates for S_{oil} in the range 0.2-0.5. Oil saturation pictures in the left column, and corresponding flow rate picture in the right column. Starting with $S_{oil} = 0.2$ at the top, and $S_{oil} = 0.5$ at the bottom.

In the case of $S_{oil} = 0.2$, one can see that the oil saturation is quite low, as the saturation picture is dominated by white paths through the system. However, one can still notice the presence of a few oil clusters in the network. The flow rates confirm what is seen in the saturation picture, that there are percolating paths dominating the total flow rate of the system, with small clusters in between. For $S_{oil} = 0.3$, the formation of clusters is easier to notice, seen as the dark regions surrounded by white paths in the saturation picture. In the flow

rate picture, one also notice the percolating paths, and the regions in between these paths which are almost immobile. As initially expected, the cluster formation become less apparent for the higher oil saturations of 0.4 and 0.5, For $S_{oil} = 0.4$, a few white percolating paths can be seen in the saturation picture, where as in the case of $S_{oil} = 0.5$, it seems oil and water is basically uniformly distributed in the system. This is also the case when noticing the flow rates, which is more uniform for higher oil saturations.

Connecting the behavior of this system to the percolation transition of cluster formation depending on $S_{non-wetting}$ as investigated by Ramstad and Hansen [40], can be understood by the fact that when adjusting the wetting angles of the system, one is basically determining which phase is the wetting phase in those tubes. In a region which is originally oil wet and has an oil saturation of 0.3, one could expect clusters to form according to the threshold value for $S_{oil} \approx 0.3$. Then, by adjusting the wetting angles in this region to a water wet system, one effectively changes the non wetting saturation from 0.7 to 0.3, as water is now the wetting phase. This moves the system away from the critical non wetting saturation, $S_{nw} \approx 0.7$ proposed by Ramstad and Hansen [40], and one would then expect clusters in this region to break up. This is consistent with what the results so far have shown. Comparing figures 27 and 28, one can clearly see that changes to the wetting properties of the system cause the initial clusters of oil in figure 27 to break up, and become mobilized.

10.5 Phase diagram

As seen in figure 51 in section 10.4.1, the transition in fractional flow depends on S_{oil}, where the critical region shifts for various values of the oil saturation. This can be seen as a "phase diagram", showing in which region the wettability alteration will have an effect on the fractional oil flow in the system.

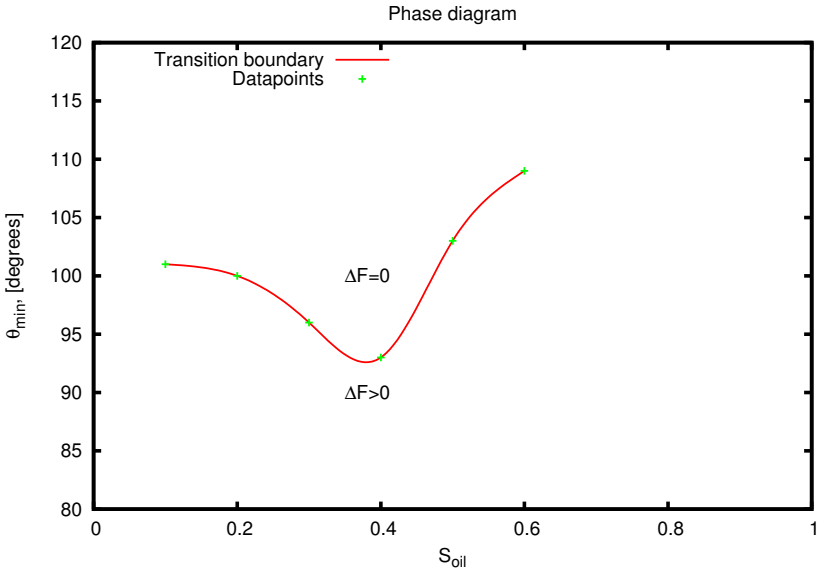

Figure 53: Phase diagram, showing when the system experience a change in F_{oil}, depending on the oil saturation

To get a better understanding of how both oil saturation and wetting angles affect the system, a plot of the fractional flow of oil as a function of both S_{oil} and the wetting angle θ_{min} is useful. As seen in figure 54.

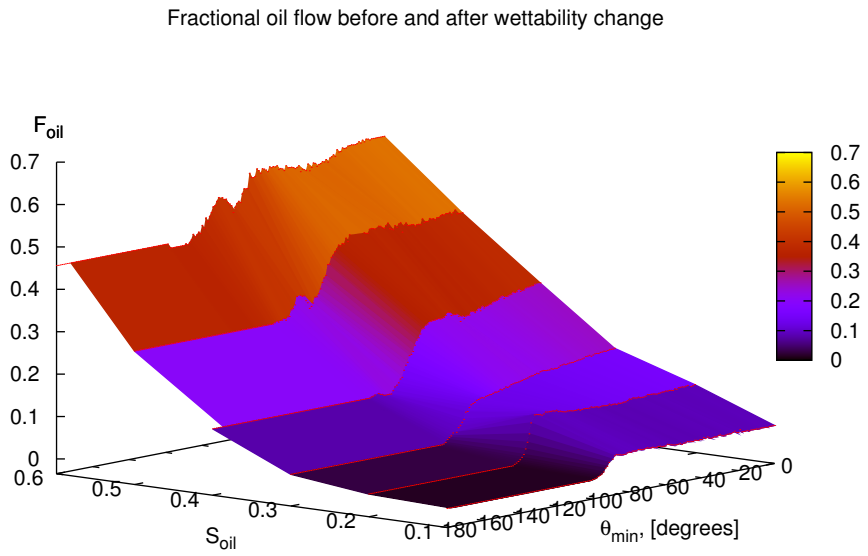

Figure 54: fractional flow of oil as a function of S_{oil} and the wetting angle θ_{min}.

Notice that for low oil saturations before the wettability is altered, $F_{oil} \approx 0$. This indicating that basically all oil in the system is contained in stuck clusters, as also seen in figure 52. When the wetting angle reach the critical region, these clusters become mobilized, which can be seen as a sudden increase in F_{oil} in figure 54. To better compare the various transition regions for different oil saturations, it is convenient to investigate the normalized change in fractional flow, $\Delta F/\Delta F_{max}$, as seen in figure 55.

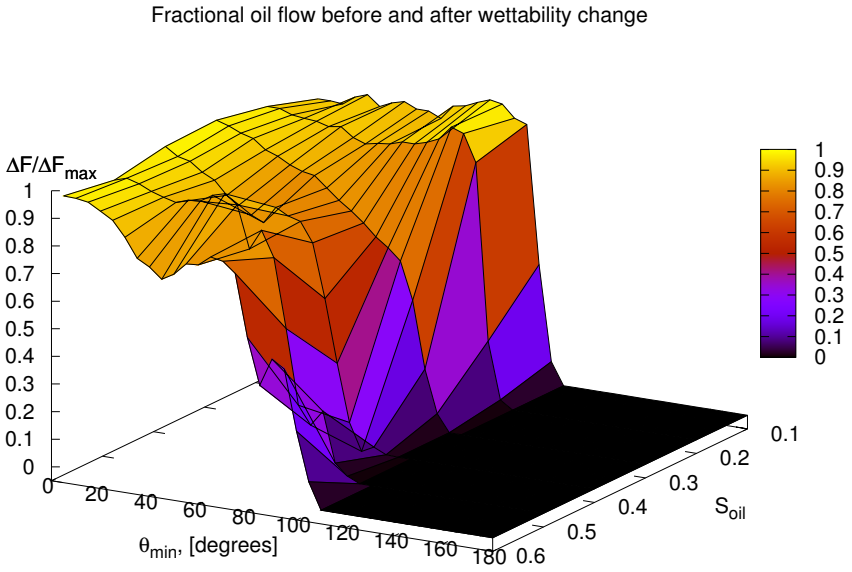

Figure 55: normalized change in fractional flow of oil, as a function of S_{oil} and the wetting angle θ_{min}.

From figure 55, one can se that the transition is smoothest for $S_{oil} \approx 0.3$, as discussed earlier. Also, the anomalies at $\theta_{min} \approx 90$ degrees become more dominant for $S_{oil} \geq 0.4$. However, as the focus is on the role of wettability alterations in re-mobilizing stuck oil clusters, the results for low oil saturations are of greatest interest. Due to the dominance of cluster formation at low oil saturations, it could be that the validity of describing changes in fractional flow using percolation theory is limited to this region.

Assuming that the transition in fractional flow obeys similar scaling laws as that of a percolation transition, and using the framework of percolation theory, the idea is that the correlation length ξ, diverge as the critical wetting angle is approached:

$$\xi \propto \Delta_\theta^{-\nu} \tag{76}$$

Where $\Delta_\theta \equiv |\theta - \theta_{crit}|$. This means the fractional flow of oil can be written as follows:

$$F_{oil}(\theta) = \begin{cases} \Delta_\theta^\beta f(L/\xi) & \text{for} \quad \theta < \theta_{crit} \\ 0 & \text{for} \quad \theta > \theta_{crit} \end{cases} \tag{77}$$

Where the scaling function $f(L/\xi)$ is defined as:

$$f(L/\xi) \propto \begin{cases} (L/\xi)^{-\beta/\nu} & \text{for} \quad L/\xi \ll 1 \\ const & \text{for} \quad L/\xi \gg 1 \end{cases} \tag{78}$$

10.6 Lattice disorder effects

The details concerning how the lattice disorder influence the system is interesting, as the chosen pore size distribution is what actually represents the real reservoir rock. In previous work by Ji and Robbins [49], it has been suggested that the critical behavior in similar systems to this one, is highly dependent on lattice disorder. Using a network model, they show a shift in the critical wetting angle as a function of lattice disorder R. Where R is defined as the ratio between the largest and smallest pore diameter d, $R \equiv d_{max}/d_{min}$. This effect can be seen in figure 56

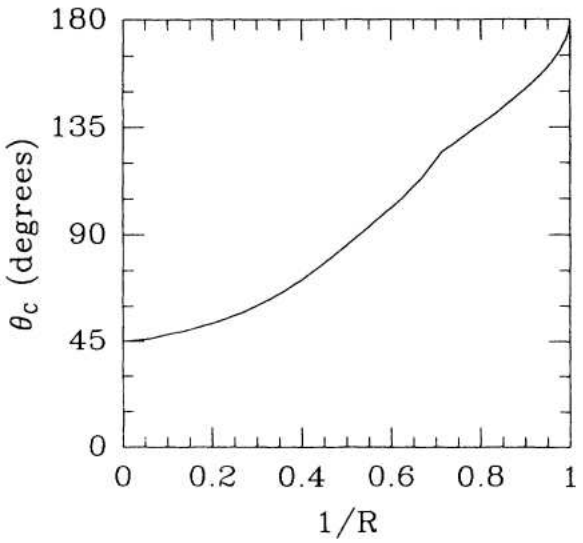

Figure 56: Shift in the critical wetting angle, θ_c, as a function of lattice disorder R. Figure from Ji and Robbins [49]

Their model, consisted of a 2D network of rectangular shaped ducts. With a disorder ratio of $R = 2$, they found a critical wetting angle $\theta_c = 86$ degrees. In this thesis work, a uniform pore radius distribution, $r\,\epsilon[0.1, 0.4]\,\mu m$ is used in most simulations. This would correspond to a disorder of $R = 4$, and the critical wetting angle was found to be $\theta_c \approx 84$ degrees. As this model investigates changes in fractional flow at steady state conditions rather than an invasion process, that difference is not unsuspected. However, doing simulations with other pore radius distributions and network disorder should show if there are any similar connections in this model.

11 summary

Through this thesis, results are shown that indicate dramatic influence on transport properties of porous media depending on the wettability of the system. In the first part, investigations whether a change in the system wettability causes sufficient perturbations to the system to re-mobilize previously stuck oil clusters were performed. Indicating it is indeed able to do so, following from the developed algorithm. The changes in fractional flow etc. agree with previous work by Ødegården [15]. In that case, the wettability altering mechanism was a simple flipping of the sign of the capillary pressure in randomly chosen tubes. Meaning the wettabiltiy could be changed also directly inside the stuck oil clusters, this possibly being the reason causing them to break down. In this model, there are correlations between wetting states in the various tubes, following from a more physically plausible mechanism. As this is based on the flow-rates of low salinity water through the network, it will not initially change the wettability inside the stuck oil clusters, which are not flooded by low salinity water. However, this mechanism is still able to cause sufficient perturbations to the system as to break down the clusters, and transform the system to one of a more uniform flow distribution. This showing that the effects of wettability alterations is still able to re-mobilize oil clusters when plausible correlations between the wetting properties throughout the network have been included.

Another interesting result, is the discovery of the systems critical behavior as a function of wetting angles. This was initially not expected, and investigation of these properties gave further insight to the problem. A possible link between a percolation threshold and changes in fractional oil flow was found. This connection, give the interesting possibility of using the theoretical framework of percolation theory to describe the system. Giving new ways of understanding the critical behavior, and the use of connections between various properties, scaling laws, universality etc. However, the link to percolation theory needs further investigation, as the amount of statistical data gathered so far seemed insufficient in accurately determining the critical exponents.

11.1 further work

The simulations performed were for systems with a constant Ca of 10^{-3}. The situation in a real reservoir is usually lower values of Ca, and this could be interesting to test in the model. It is suspected that wetting properties become increasingly important at lower capillary numbers, as the capillary forces will dominate over the viscous forces in the system. The main reason this is not performed yet, is due to the increase in computational time. The time it takes the system to reach steady state conditions, depends on the capillary nr., and for low values of Ca this time increase significantly. Also, for Ca $\leq 10^{-4}$, it is believed that thin film flow is important. This is not included in the present model, and the possible results for low Ca might then not be very reliable. The presence of wetting films is believed to be important in the context of wettability alterations, and it would be very interesting to upgrade the model to a 3D model including the effects of thin film flow. However, this model would be on a whole other level of complexity, and it is possible that the computational resources required for this would be very demanding.

Regarding the critical transition in fractional flow, it is possibly linked to a threshold in cluster formation as mentioned in work by Ramstad and Hansen [40]. It could thus be interesting to use a cluster identifying algorithm to investigate the connection between system wettability and cluster formation directly, rather than via the effect cluster formation has on changes in fractional flow. This could possibly yield more accurate results describing the critical behavior of the system, and give better estimates for the critical exponents. To clarify the connection to a percolation transition, needs further numerical work. A larger number of simulations in order to gather statistical data is thus recommended.

Due to lack of time, the full investigation of the dependence of lattice disorder was not performed. The details how this influence the system could be interesting, as the lattice is what actually represents the real reservoir rock. If the system is very dependent on the lattice disorder, this means one must use pore size distributions obtained from experiments in order to connect numerical simulations to real reservoir behavior.

As initially suspected, the progress made and the questions answered, have initiated more new questions than the ones answered. The way forward is still a long one before direct comparison between simulations and real life applications.

The future is indeed exciting!

References

[1] F.A.L. Dullien, *Fluid Transport and Pore Structure.* Academic press inc. 111 Fifth Avenue, New York. 1979

[2] W.Abdellah, J.S.Buckley, A.Carnegie, J.E.B.Herold, E.Fordham, A.Graue. T.H.N.S.C.Signer, H.Hussain, B.Montaron, M.Ziauddin, Schlumberger Oilfield Review, Summer, 44 *Fundamentals of wettability*, 2007

[3] J.Israelachvili, *Intermolecular and Surface Forces* Academic Press, 3rd ed. 2011

[4] A.R.Kovschek, H.Wong, C.J.Radke, AlChe Journal, 39, no.6, 1072 1993

[5] P.Roberts, *The end of oil: On the edge of a perilous new world* , Houghton Mifflin, New York 2005

[6] G.Q.Tang, N.R.Morrow, SPE Res. Engn. 12, 269, 1997

[7] D.C.Standnes, T.Austad, J. Petr. Sci. Eng. 28, 123, 2000

[8] A.Skauge, K.Spildo, L.Hiland, B.Vik, J. Petr. Sci. Engn. 57, 321 2007

[9] M.T.Tweheyo, T.Holt, O.Torster, J. Petr. Sci. Engn. 24, 179 1999

[10] R.Kaminsky, H. and C.J. Radke, SPE 39087, 13 1998

[11] J.S.Buckley, K.Takamura, N.R.Morrow, SPE Res. Engn. 4, 332 1989

[12] P.S.Laplace, Mechanique celeste, suppl. 10th vol 1806

[13] W.G.Anderson SPE, Conoco inc, *Wettability litterature survey - part 4. Effects of wettability on capillary pressure* 1987

[14] H.Anton and C.Rorres, Elementary Linear Algebra with Supplemental Applications 10th edition

[15] T.B.Ødegården, *Oil release and transport mechanism due to wettability change in a mixed-wet 2d porous medium*, Master thesis in physics, NTNU 2010

[16] G.G.Batrouni and A.Hansen, *Fourier acceleration of iterative processes in disordered systems*, J. Stat. Phys. 52, 747-773. 1988

[17] E.Aker, K.Måløy, A.Hansen, G.Batrouni, *A Two-Dimensional Network Simulator for Two-Phase Flow in Porous Media*, Transport in porous media 32: 163-186, 1998

[18] R.Booth, *Miscible Flow Through Porous Media.*, DPhil, Oxford, Sept. 2008

[19] E.W.Washburn, Phys Review 17 273 1921

[20] J.L.Barrat, L.Bocquet, phys Review Letters Volume 82, nr. 23 june 1999

[21] S.Berg, A.W.Cense, J.P.Hofman, R.M.M.Smits, *Two-Phase flow in porous media with slip boundary condition*, Transp. Porous Media 74, 275-292 2008

[22] H.A.Knudsen, E.Aker, A.Hansen, Transp. Porous Media 47, 99 (2002).

[23] Mathematica 5.2 Documentation

[24] R.Nasralla, M.Bataweel, H.Nasr-El-Din, *Investigation of Wettability alteration by low salinity water in sandstone rock*, SPE 146322, 2011

[25] R.N.Wenzel, Industrial and engineering chemistry vol 18, NO. 8, 1936

[26] K.S.Sorbie, I.R.Collins, *A proposed pore-scale mechanism for how low salinity waterflooding works*, SPE 129833 2010

[27] S.M.Rivet, W.Larry, G.A.Pope, *A Coreflood Investigation of Low-Salinity Enhanced Oil Recovery*, SPE 134297 2010

[28] F.M.White, *Fluid mechanics*, 6th edition, 2007

[29] R.Lenormand, C.Zarcone and A.Starr, *Mechanisms of the displacement of one fluid by another in a network of capillary ducts*, J.Fluid Mech 135:337-353 1983

[30] R.Lenormand, E.Touboul and C.Zarcone, *Numerical models and experiments on immiscible displacement in porous media*, J.Fluid Mech 189:165-187 1988

[31] L.Paterson, *Diffusion limited aggregation and two-fluid displacement in porous media*, Phys rev. Lett 52:1621-1624, 1984

[32] G.Batrouni, A.Hansen, *Fracture in three-dimensional fuse networks*, Phys. Rev. Lett. 80, 325-328. 1998

[33] J.D.Chen, D.Wilkinson, *Pore scale viscous fingering in porous media*, Phys rev. Lett 55:1882-1895, 1985

[34] K.J.Måløy, J.Feder, T.Jøssang, *Viscous fingering fractals in porous media*, Phys rev. Lett 55:2681-2691, 1985

[35] D.Wilkinson, J.F.Willemsen, *Invasion percolation, a new form of percolation theory*, J.Phys A 16:3365-3376 1983

[36] R.Lenormand, C.Zarcone, *Capillary Fingering: Percolation and Fractal Dimension*, Transport in Porous Media 4: 599-612 1989

[37] M.Cieplak, M.O.Robbins, *Dynamical Transition in Quasi static Fluid Invasion in Porous Media*, Physical review letters Vol 60, Nr. 20 , 1988

[38] D.Stauffer, A.Aharony, *Introduction to percolation theory, 2nd edition*, Taylor and Francis, London, Washington, DC 1992

[39] G.Tørå , T.Ramstad, A.Hansen, *Anomalous diffusion on clusters in steady-state two-phase flow in porous media in two dimensions*, EPL, 87 (2009) 54002

[40] T.Ramstad, A.Hansen, *Cluster evolution in steady-state two-phase flow in porous media*, Physical review E 73, 026306, 2006

[41] B.Berkowitz , R.P.Ewing, *Percolation theory and network modeling applications in soil physics*, Surveys in Geophysics 19: 23-72, 1998.

[42] Dr. Kim Christensen, *Percolation theory, Lecture notes*, Imperial College London 2002

[43] E.Aker, *A simulation model for two phase flow in porous media*, Master thesis, University of Oslo 1996

[44] G.M.Homsy, *Viscous fingering in porous media*, Ann. Rev. Fluid Mech 19:271-311, 1987

[45] Santanu Sinha, *Steady-state two-phase flow in porous media*, Powerpoint presentation Department of Physics, NTNU, Trondheim, Norway

[46] G.E.P.Box, M.E.Muller, *A Note on the Generation of Random Normal Deviates* , Annals Math. Star. 29, pp. 610-611, 1958

[47] S.E.Buckley, M.C.Leverett, *Mechanism of fluid displacement in sands*, Trans. AIME, 146, 107-116, 1942

[48] J.Kleppe, *TPG4150 Reservoir Recovery Techniques*, Lecture notes 2011

[49] B.Koiller, H.Ji, and M.O.Robbins, *Fluid wetting properties and the invasion of square networks*, Phys. Rev. B 45, 7762-7767 (1992)

[50] H.Ji and M.O.Robbins, *Transition from compact to self similar growth in disordered systems: Fluid invasion and magnetic-domain growth*, Phys. Rev. A 44, 2538-2542 (1991)

[51] E.Kreyszig, *Advanced engineering mathematics*, Wiley International 9th edition, 2006.

[52] W.H.Press, S.A.Teukolsky, W.T.Vetterling, B.P.Flannery, *Numerical recipes, The art of scientific computing* , 3rd edition, 2007

12 Appendix

12.1 Code

The code developed during this thesis was not included in the appendix, as the conversion to correct format would make it hard to read, and fill many pages. The complete code for the network model is included as an additional file in the electronic hand in of the thesis. Also, the author can be contacted at: vegardflovik@yahoo.no for access to the code.

12.2 Paper proposal

A preliminary proposal for a publication from the thesis work is appended.

The impact of wettability alterations on oil release and transport mechanisms in a 2D porous medium

Vegard Flovik[1,*]

[1]Department of Physics, Norwegian University of Science and Technology, N-7491 Trondheim, Norway

(Dated: July 20, 2012)

The effects of wettability alterations in a 2D network model of a porous media has been studied. By changing the wetting properties of the reservoir through a developed wettability changing algorithm, previously stuck regions in the network are re-mobilized, leading to significant changes in the steady state flow distribution of the model porous media This caused de-stabilization of percolating and trapped clusters as the wettability was changed from an oil wet to a mixed wet system. A critical transition at a certain wetting angle, depending on the initial saturation and lattice size of the system was found. This indicating a possible phase transition from a percolating flow regime to a more uniform flow distribution through the network model. A link between changes in fractional flow and a percolation transition is also suspected, and using the theoretical framework of percolation theory, D.Stauffer and A.Aharony [38], critical exponents were estimated. The best estimate for a critical exponent was $\beta = 0.13 \pm 0.02$, which is close to the result from ordinary percolation: $\beta = 5/36 \approx 0.1388...$ The critical transition in fractional flow, seems to obey similar scaling laws as that of ordinary percolation. The use of finite size scaling theory to investigate the system at various lattice sizes, yielded a rough estimate for the correlation length critical exponent, $\nu \approx 0.4$, which is significantly smaller compared to the result from ordinary percolation, $\nu = 4/3$.

PACS numbers: 47.56.+r,47.61.Jd

INTRODUCTION

The fact that some 20 to 60 percent of the oil remains in the reservoir after the end of oil production is a challenge of increasing importance in these times of dwindling oil reserves. Roberts [5]. The reason for this loss is the formation of oil clusters embedded in water and held in place by capillary forces, which in turn are controlled by the wetting properties of the reservoir fluids with respect to the matrix rock.

The production from oil reserves that today are considered immobile due to complex reservoirs will then be an important area of focus. Wetting properties of reservoirs is therefore an important topic within the field of Enhanced Oil Recovery, EOR, and the role of formation wettability has been reviewed during e.g. Schlumbergers Wettability Workshop in 2007, [2]

Sandstone is strongly water wet before oil migrates from a source rock into the reservoir. When oil enters a pore, it displaces water and form a water film sandwiched between the oil and rock surface. This film may be several nanometer thick, and results from balancing Van der Waals and electric double layer forces, capillary pressure and grain curvature. Israelachvili [3]. A permanent wettability alteration is believed to take place by adsorption of asphaltenes from the crude oil to the rock, and leads to high but slow recovery through continuous oil films. Kovschek et al. [4], Kaminsky et al. [10]. As the oil saturation drops, these films can become discontinuous, leaving immobile oil clusters held in place by capillary forces.

An important parameter which can determine the wetting properties of the reservoir, is the salinity of the pore water. At low salinities, perfect water wetting can be achieved. By changing the salinity level of the pore water, the wetting angle increase. Also, increase in temperature results in more water wetness of the reservoir, which increase the oil recovery. Skauge et al [8]. This could also be of great importance during e.g thermal recovery methods.

Changes in the reservoir from strongly oil wet to neutral wet or water wet conditions show a significant increase in oil recovery depending on the stage of recovery. Tweheyo, Holt and Torster [9]. New production methods, like low salinity water flooding show some promising results in increasing the recovery factor of reservoirs, and many mechanisms explaining this effect have been suggested. Correlations have been shown with wetting behavior to the electrostatic forces between the rock and oil surfaces. Buckley et al. [11]. But there is still no consensus on that what the dominating microscopic mechanism is. Research toward a deeper understanding of these effects could be an important effort towards a more complete understanding of transport properties in reservoirs, and has been a priority in the industry for years.

In this work, it is assumed that local wettability alterations take place, and the consequences of this on oil recovery by re-mobilizing stuck oil clusters is investigated. To study these effects, a two-dimensional pore scale network simulator model is used. Having bi-periodic boundary conditions, it allows the study of steady state flow, representing the flow behavior deep inside the reservoir. The effect of wettability alteration is introduced in the model through a developed wettability changing algorithm, continuously adjusting the wetting angles in the

network during simulation. The changes in steady state flow properties of the system as a result of this is then studied.

MODEL

The disorder of the system is incorporated using tubes of random radii from a chosen pore radius distribution to represent the porous medium. The network consists of capillary tubes oriented 45 degrees relative to the overall flow direction from bottom to top. The volume of both throats and pores is contained in the tubes, which then intersect in volumeless node points. With respect to the capillary pressure of menisci, the tubes are hour glass shaped. That is, the local capillary increase when menisci move into narrower parts of the tubes are taken into account. This makes the model closer to dynamics of drainage dominated flow, where thin film flow can be neglected. A modified Young Laplace equation give: Dullien [1]. Aker et al. [17]

$$p_c = \frac{2\gamma cos\theta}{r}(1 - cos(2\pi x)) \tag{1}$$

With the capillary pressure given by eq.(1), the local flow rate q is given by the Washburn equation. Washburn [19]

$$q_{ij} = -\frac{k_{ij}\pi r_{ij}^2}{\mu_{eff}}\frac{(\Delta p_{ij} - \sum p_c)}{l} \tag{2}$$

Where $k_{ij} = r_{ij}^2/8$ is the permeability, r_{ij} is the radius of the tube connecting node i and j, and $\Delta p_{ij} = p_j - p_i$ is the pressure difference between node i and j. $\sum p_c$ is the sum of the capillary pressures of the menisci in the tube and μ_{eff} is the weighted viscosity according to the volume fraction at the beginning of each time-step in each link. The reason for summing over the capillary pressures of the menisci, is because the present model allows for a total of 3 bubbles of oil/water in each tube. Menisci positions are changed according to a forward integration of eq.(2) (explicit Euler integration). There is a limit of maximum menisci movement of one tenth of the length of a single tube, l_{ij}, which limits the size of the time steps. When a menisci reaches the end of a tube it is redistributed among the neighboring tubes, where the basic processes of snap off and coalescence of bubbles have been considered. See Knudsen, Aker, and Hansen [22] for more detailed information.

The equations and assumptions mentioned above, give a large set of linear equations to be solved in order to calculate the local pressures in the nodes with respect to the global pressure drop across the network. These sets of equations are solved using a conjugate gradient method. Batrouni and Hansen [16].

Simulation is done considering a network of 40x40 nodes, which is sufficient to be in the asymptotic limit for the range of parameters used, and an average over 5 different samples has been taken for each simulation.

The simulations are performed under a constant flow rate Q_{tot} , which sets the capillary number. Initially, the system is purely oil-wet and filled with a given oil and water saturation, which remains constant throughout the simulation. Due to the bi-periodic boundary conditions both drainage and imbibition take place simultaneously, leaving wetting and non-wetting fluid clusters in the system. After reaching steady state, wettability alterations are introduced following from the developed algorithm.

Wettability alteration

In previous work by Ødegården [15], the wettability altering mechanism was a simple flipping of the sign of the capillary pressure to mimic a change in the wetting angle θ from 0 to 180 degrees in eq.(1), and occurred in randomly chosen capillary tubes. In this model, a more physical plausible mechanism to alter the wettability of the system is introduced. Instead of using a simple flip of the sign of the capillary pressure, a distribution function to mimic the effect of continuously changing wetting angles is implemented.

The idea behind this algorithm is that for wettability alterations to occur, the low salinity water needs to be in contact with the pore space. This claim is rather trivial, as one can not expect any change if the wettability altering agent is not present in the reservoir. The next assumption, is that the magnitude of change in the wetting angle depends on the cumulative flow of low salinity water that has passed through each pore. This means that if a certain pore is flooded by large amounts of fresh water, the wetting angle should change more than in a pore which has very little water flooded through. That is, all tubes in the model are initially oil wet, and by tracking the flow of low salinity water through each tube, a new wetting angle is assigned depending on this cumulative flow value, $Q_i(t)$ for tube i at time t.

This is implemented by summing up the flow rates in each capillary tube over a certain "wettability altering time span", $\tau = [t_0, t_1]$ (Illustrated in figure 3). t_0 is the time when the injection of low salinity water is initiated, and the algorithm starts tracking the flow rates in each tube. At time t_1, the system reaches a state with a static wetting angle distribution. To make sure that only the flow of low salinity water affects the wettability, and not the flow of oil, the flow rate in tube i at time t, $q_i(t)$, is multiplied with the water saturation in the tube at the same time step, $\Gamma_i(t)$. This gives the cumulative flow of low salinity water in tube i at time t:

$$Q_i(t) = \sum_{t_0}^{t \leq t_1} q_i(\tilde{t})\Gamma_i(\tilde{t})\Delta\tilde{t} \tag{3}$$

$Q_i(t)$ is then used to assign a continuously changing wetting angle for each tube, updated every time step in the range $[t_0, t_1]$ during simulation. This was done by replacing the $cos\,\theta$ term in eq.(1) by a distribution function depending on $Q_i(t)$. The distribution chosen has approximately the range [-1,1], to represent the $cos\,\theta$ term with θ in the range [180,0].

$$cos\,\theta \rightarrow \frac{2}{\pi} tan^{-1}\left[\frac{20}{Q_i^{thr}}(Q_i(t) - Q_i^{thr})\right] \tag{4}$$

The pre-factor $\frac{2}{\pi}$ is a normalization constant to set the range [-1,1], the nr. 20 is just a parameter to adjust the slope of the distribution function, and Q^{thr} a certain threshold value needed to significantly change the wetting angle.

The idea behind the Q^{thr} factor, is that in order to alter the pore wettability by injecting low salinity water, a certain amount needs to be injected before it significantly affects the wetting angle. Because of the random size distribution of the pore space in a porous media, this threshold value should also depend on the pore size. Intuitively, one expects that more low salinity water needs to be injected in a large pore compared to a small pore to alter the wettability significantly. This threshold value is thus defined as a constant η, times the corresponding pore volume.

$$Q_i^{thr} = \eta\pi r_i^2 l \tag{5}$$

where r_i is the pore radii of tube i, l is the pore length, and η is the parameter defining how many pore volumes of low salinity water needs to be injected through each pore to reach the threshold value.

As this model does not include thin film flow, the wetting angle will not be either 0 or 180 degrees. Rather, the starting point of $\approx$ 165 degrees was chosen. In this case, the threshold value Q^{thr} is the zero point of the distribution function, and represents the state when θ is changed from the initial value to 90 degrees.

This distribution gives the wetting angle for link nr i at time t, as a function of the amount of low salinity water injected, $Q_i(t)$. See figure 1.

With these changes, the capillary pressure given by eq.(1) is replaced by

$$p_c(t) \approx \frac{4\gamma}{\pi r_i} tan^{-1}\left[\frac{20}{Q_i^{thr}}(Q_i(t) - Q_i^{thr})\right](1 - cos(2\pi x)) \tag{6}$$

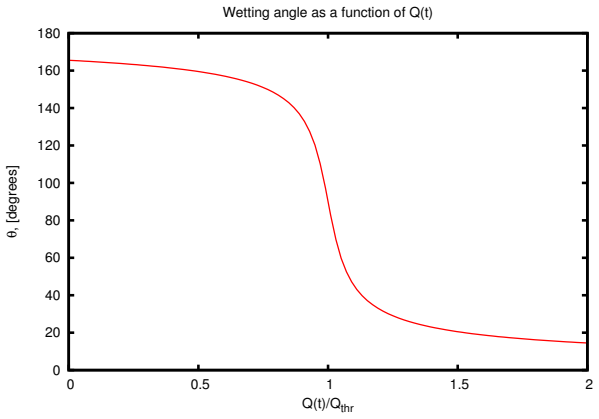

FIG. 1: Wetting angle for each tube as a function of $Q_i(t)$

Where $Q_i(t)$ is given by eq.(3). The value of $Q_i(t)$ is updated between each time step, meaning that the wettability is continuously changing as a function of time. This represents that the wetting angles are gradually changing in the various tubes, as more low salinity water has been in contact with the reservoir surface.

Q_{thr} is a fitting parameter, depending on how much low salinity water needs to be injected through a pore to cause a significant change in its wetting properties. This is a parameter which could possibly be fitted against experimental results. But, as such experiments have not been performed yet, this was treated as a tuning parameter in the following work.

The model is first run for a sufficient amount of time steps to reach steady state conditions. Then, the effect of wettability alterations is introduced following from the equations above. After a significant amount of time the system is set to static wetting properties, and the model is again run to steady state. This wettability alteration causes a perturbation to the system, and permanent changes in the static flow properties.

RESULTS

Changes in the network wettability caused significant perturbations to the system. As seen in figure 2, oil is initially located in stuck clusters surrounded by white percolating paths of water. This is also seen from the flow rates, which is dominated by a few paths where the flow rates are orders of magnitude greater than in the stuck clusters in between. The wettability alteration cause these percolating paths to break down, re-mobilizing the oil clusters and transforming the network to one with a more uniform flow distribution.

The re-mobilization of oil can also be seen as an increase in the fractional flow of oil, see figure 3. Where the fractional flow of oil is defined as the ratio be-

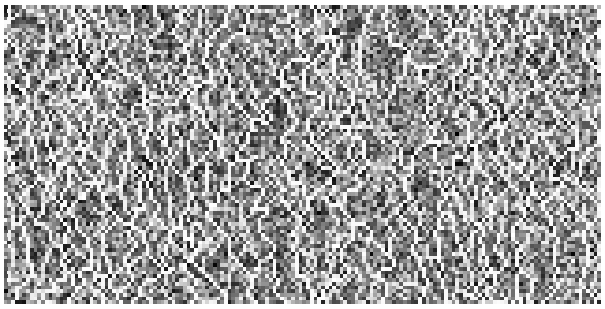

(a)Oil saturation before wettability alterations

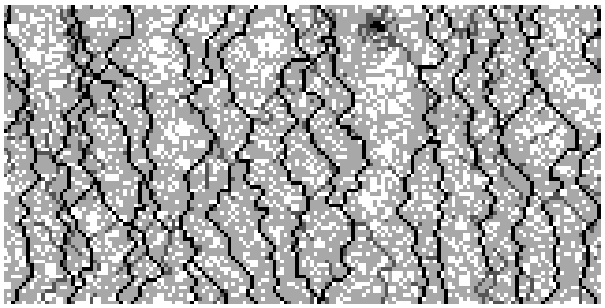

(b)Flowrates before wettability alterations

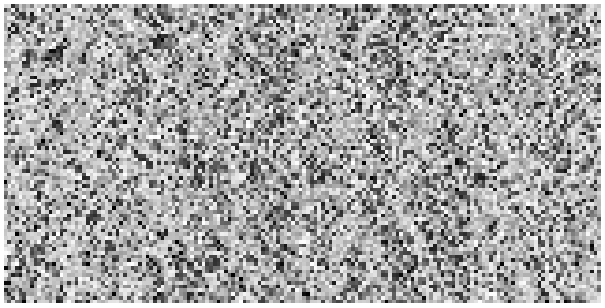

(c)Oil saturation after wettability alterations

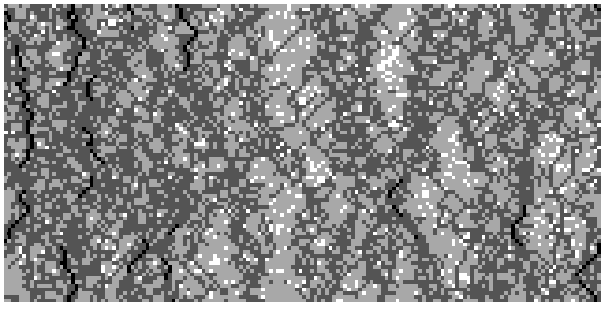

(d)Flowrates after wettability alterations

FIG. 2: Oil saturations and flow rates before and after wettability is altered. In the saturation pictures, oil is black and water white. The flow rate pictures are on a normalized logarithmic scale, with black=1 and white less then 10^{-4}.

tween the flow of oil, Q_{oil}, and the total flow Q_{tot}, as $F_{oil} \equiv Q_{oil}/Q_{tot}$.

For various oil saturations, these results can be summarized in a plot showing the change in fractional oil flow before and after wettability alteration, as seen in figure 4.

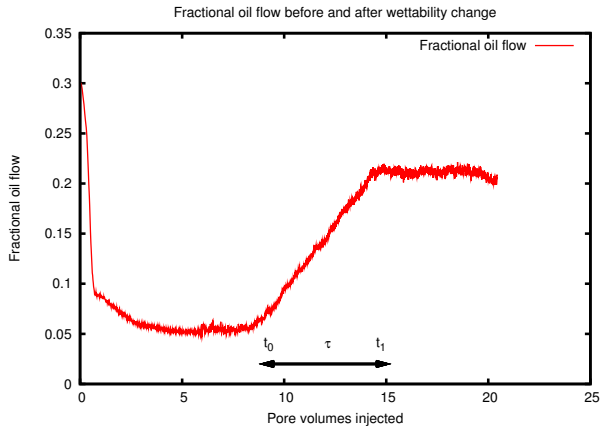

FIG. 3: Change in fractional oil flow for a 40x40 network with $S_{oil} = 0.3$. The system is starting to reach steady state after the injection of ≈ 5 pore volumes (total pore volume of the network). The wettability changing algorithm is activated after the injection of ≈ 8 pore volumes (t_0), and the system reaches a static wetting angle distribution after the injection of ≈ 15 pore volumes (t_1). It then settles in a new steady state, with a significant higher fractional flow of oil compared to before the change.

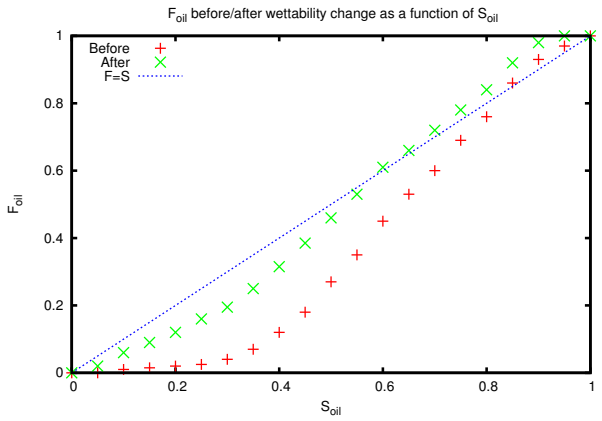

FIG. 4: Fractional flow of oil as a function of oil saturation in the range 0.1-0.9

The S-shape of these curves is resemblant of the ones found in Buckley-Leverett fractional flow. Dullien [1], Buckley and Leverett [47]. In figure 4, a diagonal line is added. This is the line where the fractional flow is equal to the oil saturation. A miscible fluid mixture would follow this line, and it is interesting to use as a reference to compare how the data points lie above or below this line.

To this point, the wetting angles of the final mixed wet system are in the approximate range of [165,0] degrees. However, the magnitude of wettability alteration due to low salinity water injection is not well understood. It is thus interesting to investigate how much the wetting angles have to change to cause any significant effect on the system. Instead of having the wettability altering algo-

rithm operating in the full range as shown in figure 1, a cutoff angle θ_{min} was introduced. As before, all angles initially start at 165 degrees. However, as the wetting angles are adjusted according to the algorithm, they are not allowed to change to values lower than θ_{min}. By doing many simulations with θ_{min} in the range between the initial 165 degrees and 0 degrees, a critical wetting angle was found. At angles above this critical value, the system is basically unaffected by the wettability alterations. When the wetting angles reach the critical value, this suddenly cause dramatic changes to the system, see figure 5

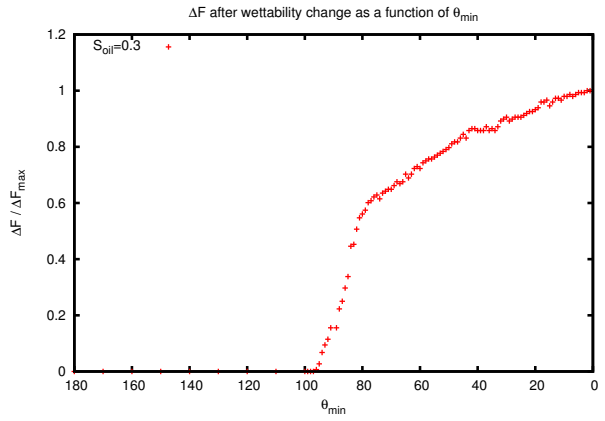

FIG. 5: Critical transition in fractional flow as a function of θ_{min}, indicating possible connections to a percolation threshold

The connection between percolation theory and cluster formation has been investigated previously by Ramstad and Hansen [40], using a similar network model. From figure 4 one notice that for oil saturations below $S_{oil} \approx 0.3$, basically all oil in the system is contained in stuck clusters, as $F_{oil} \approx 0$. Since the increase in fractional flow caused by wettability alterations seems to be caused by the breakdown of oil clusters, a connection between cluster strength in percolation theory and fractional flow is suspected. It could thus be possible to describe this transition using percolation theory when the oil saturation is low. Assuming the increase in fractional flow can be described as a percolation transition, a similar relation between fractional flow and wetting angle as between percolation strength and percolation probability is proposed, D.Stauffer and A.Aharony [38]

$$F_{oil}(\theta) \propto |\theta - \theta_{crit}|^{\beta} \tag{7}$$

Hence, by plotting $log\, F_{oil}(\theta)$ vs. $log\,(|\theta - \theta_{crit}|)$ in the critical region, one can obtain an estimate for the critical exponent β. In the following, the parameter $\Delta_\theta \equiv |\theta - \theta_{crit}|$ is introduced. The effective θ_{crit} is found from the inflection point of the curve ΔF_{oil} vs. θ_{min}, as seen in figure 5. According to the suspected power law behavior from eq.(7) the data points should collapse to a linear curve, where the critical exponent β is extracted from the slope. It was found that a value of $\theta_{crit} = 84$ gave the best linear fit when plotted on log-log scale. See figure 6.

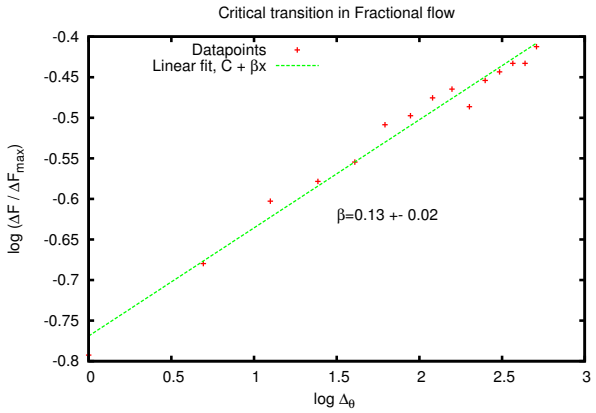

FIG. 6: Plot of $log\, \Delta F_{oil}(\theta)$ vs. $log\, \Delta_\theta$, where $\Delta_\theta \equiv |\theta - \theta_{crit}|$. Showing a linear fit, obtaining an estimate for the critical exponent β. Δ_θ is in the range [1, 15], and each data point in the plot is the average value of 5 lattice initializations.

The estimate from the curve fitting is $\beta = 0.13 \pm 0.02$, which is close to the result from ordinary percolation, $\beta = 5/36 \approx 0,1388...$

By investigating the model for various lattice sizes, similar effects as that from finite size scaling theory for ordinary percolation was found, that the transition is "smoothed out" over a larger region for small lattice sizes L. From finite size scaling analysis in percolation theory, the transition width Δ depends on the lattice size L, D.Stauffer and A.Aharony [38]:

$$\Delta \propto L^{-1/\nu} \tag{8}$$

Where ν is the correlation length critical exponent. If this system obeys similar scaling laws, this means that by investigating the width of the transition, one can estimate the correlation length critical exponent ν. The transition width Δ can be defined in any suitable way, and in this case it is simply defined as the difference between the value of θ_{min} where $\Delta F/\Delta F_{max}$ is 0.2 and 0.6.

From the data available, the estimate for the correlation length critical exponent is $\nu \approx 0.4$. Compared to the result for ordinary percolation, $\nu = 4/3$, this is significantly smaller.

Another approach to obtain the critical exponents β and ν, is from the fact that the percolation strength, $P(L, \xi) \propto L^{\beta/\nu}$ at the critical point, Shauffer and Aharony [38]. If the transition in fractional flow obeys similar scaling laws as that of ordinary percolation, one expects the following relation at the critical transition point, θ_{crit}:

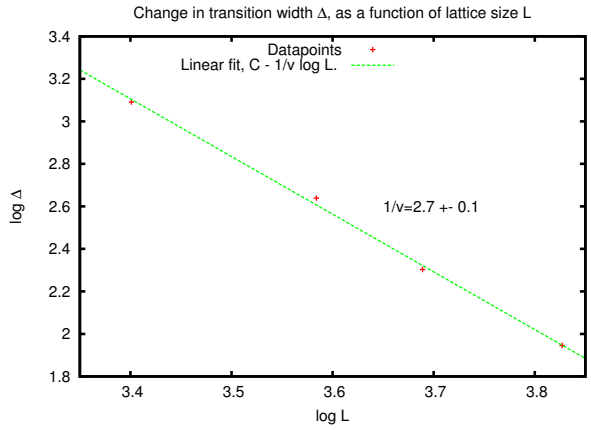

FIG. 7: Change in transition width Δ as a function of lattice size L. Simulations were performed for $L = 30, 36, 40, 46$, and each data point is the average value obtained from 5 lattice initializations.

$$F_{oil}(L) \propto L^{\beta/\nu} \tag{9}$$

Hence, by plotting $\log F_{oil}(L)$ vs. $\log L$, one can extract the ratio of the critical exponents, β/ν.

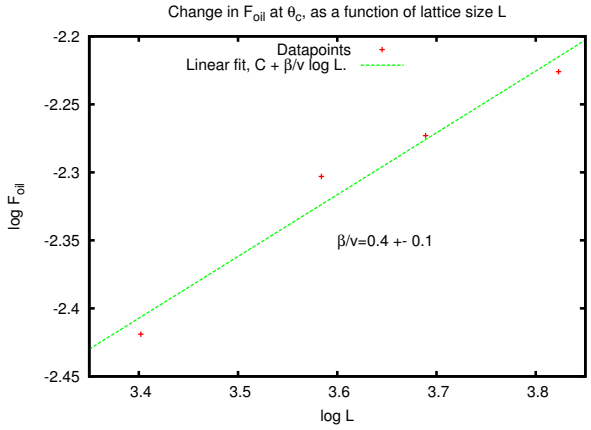

FIG. 8: Change in fractional oil flow at θ_c as a function of lattice size L. Simulations were performed for $L = 30, 36, 40, 46$, and each data point is the average value obtained from 5 lattice initializations.

Using the previous result, $\beta \approx 0.13$, this estimate for the correlation lenght critical exponent is consistent with the result using the transition width Δ, that $\nu \approx 0.4$. However, as seen in figure 8, the linear fit using this last method to extract β/ν is not as good as the one using the transition width Δ. The reason for this could be that in the estimation of F_{oil} at θ_{crit}, it has not been taken into account that the value of θ_{crit} might shift slightly depending on the lattice size, due to finite size effects. A more accurate determination of the critical point for the various lattice sizes, could thus yield a better fit to the expected power law behavior from eq.(9).

The estimates using these methods are small compared to the value from ordinary percolation, but the system still seems to obey similar scaling laws as a function of lattice size.

To get a better understanding of how both oil saturation and wetting angles affect the system, a plot of the fractional flow of oil as a function of both S_{oil} and the wetting angle θ_{min} is useful, as seen in figure 9.

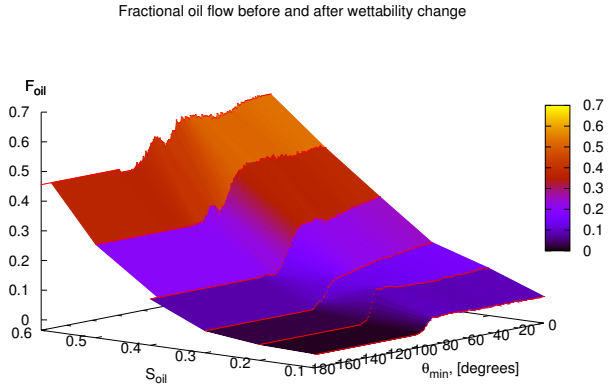

FIG. 9: fractional flow of oil as a function of S_{oil} and the θ_{min}.

Notice that for low oil saturations before the wettability is altered, $F_{oil} \approx 0$. This indicating that basically all oil in the system is contained in stuck clusters, as also seen in figure 2. When the wetting angle reach the critical region, these clusters become mobilized, which can be seen as a sudden increase in F_{oil} in figure 9. To better compare the various transition regions for different oil saturations, it is convenient to investigate the normalized change in fractional flow, $\Delta F/\Delta F_{max}$, as seen in figure 10.

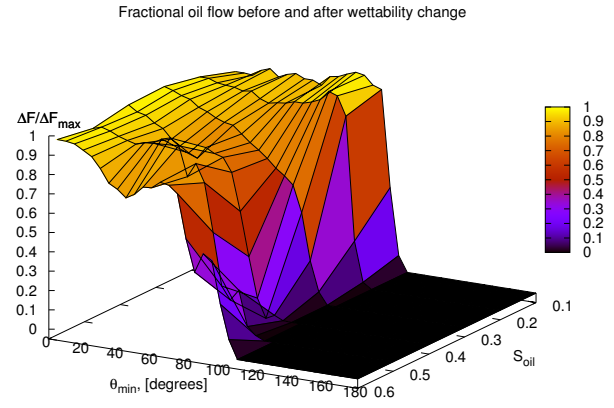

FIG. 10: Normalized change in fractional flow of oil, as a function of S_{oil} and the wetting angle θ_{min}.

From figure 10, one notice some anomalies at $\theta_{min} \approx 90$ for $S_{oil} \geq 0.4$. This is probably caused by numerical instabilities due to the vanishing capillary pressure at this wetting angle. However, as the focus is on the role of wettability alterations in re-mobilizing stuck oil clusters, the results for low oil saturations are of greatest interest.

As seen in figure 9, for saturations below $S_{oil} \approx 0.3$, $F_{oil} \approx 0$ for $\theta > \theta_{crit}$. Before wettability alterations, basically all oil in the system is contained in stuck clusters at such low oil saturations. Due to the dominance of cluster formation at low oil saturations, it could be that the validity of describing changes in fractional flow using percolation theory is limited to this region.

Assuming that the transition in fractional flow obeys similar scaling laws as that of a percolation transition, and using the framework of percolation theory, D.Stauffer and A.Aharony [38], the idea is that the correlation length ξ, diverge as the critical wetting angle is approached:

$$\xi \propto \Delta_\theta^{-\nu} \tag{10}$$

Where $\Delta_\theta \equiv |\theta - \theta_{crit}|$. This means the fractional flow of oil can be written as follows:

$$F_{oil}(\theta) = \begin{cases} \Delta_\theta^\beta \, f(L/\xi) & \text{for } \theta < \theta_{crit} \\ 0 & \text{for } \theta > \theta_{crit} \end{cases} \tag{11}$$

Where the scaling function is defined as:

$$f(L/\xi) \propto \begin{cases} (L/\xi)^{-\beta/\nu} & \text{for } L/\xi \ll 1 \\ const & \text{for } L/\xi \gg 1 \end{cases} \tag{12}$$

CONCLUSIONS

In this paper, results are shown that indicate dramatic influence on transport properties in porous media depending on the wetting properties of the system. In the first part, investigations whether a change in the system wettability is able to re-mobilize previously immobile oil clusters was performed. Indicating it is indeed able to do so, following from the developed wettability altering algorithm. Changing the wetting properties cause significant perturbations to the systems flow distribution, and destabilize percolating and trapped clusters appearing in the steady state.

Another interesting result, is the discovery of the systems critical behavior as a function of wetting angles. A possible link between a percolation threshold and changes in fractional oil flow was found, and critical exponents were estimated. Several critical exponents were investigated, but due to lack of sufficient data, not all estimates were reliable. The best exponent obtained, was $\beta = 0.13 \pm 0.02$, which is close to the result from ordinary percolation: $\beta = 5/36 \approx 0.1388..$ The critical transition in fractional flow, seems to obey similar scaling laws as that of ordinary percolation. The use of finite size scaling theory to investigate the system at various lattice sizes, yielded a rough estimate for the correlation length critical exponent, $\nu \approx 0.4$, which is significantly smaller compared to the result from ordinary percolation, $\nu = 4/3$

The reason for this large difference in the estimates for ν, could be caused by the limited number of data points. The fluctuations at the critical transition, makes it important to perform many simulations in order to gather sufficient statistical data. In this case, only 5 simulations for each lattice size L were performed. This giving a total number of only 20 data points, which give large uncertainties in determining the critical exponent. It could be that performing more simulations, and for larger lattice sizes, would yield better data.

This connection give the interesting possibility to use the theoretical framework of percolation theory to describe the system. However, this needs to be investigated further, as the amount of statistical data gathered so far showed insufficient in accurately estimating the critical exponents.

* Electronic address: vegardflovik@yahoo.no

[1] F.A.L. Dullien, *Fluid Transport and Pore Structure*. Academic press inc. 111 Fifth Avenue, New York. 1979

[2] W.Abdellah, J.S.Buckley, A.Carnegie, J.E.B.Herold, E.Fordham, A.Graue. T.H.N.S.C.Signer, H.Hussain, B.Montaron, M.Ziauddin, Schlumberger Oilfield Review, Summer, 44 *Fundamentals of wettability*, 2007

[3] J.Israelachvili, *Intermolecular and Surface Forces* Academic Press, 3rd ed. 2011

[4] A.R.Kovschek, H.Wong, C.J.Radke, AlChe Journal, 39, no.6, 1072 1993

[5] P.Roberts, *The end of oil: On the edge of a perilious new world* , Houghton Mifflin, New York 2005

[6] G.Q.Tang, N.R.Morrow, SPE Res. Engn. 12, 269, 1997

[7] D.C.Standnes, T.Austad, J. Petr. Sci. Eng. 28, 123, 2000

[8] A.Skauge, K.Spildo, L.Hiland, B.Vik, J. Petr. Sci. Engn. 57, 321 2007

[9] M.T.Tweheyo, T.Holt, O.Torster, J. Petr. Sci. Engn. 24, 179 1999

[10] R.Kaminsky, H. and C.J. Radke, SPE 39087, 13 1998

[11] J.S.Buckley, K.Takamura, N.R.Morrow, SPE Res. Engn. 4, 332 1989

[12] P.S.Laplace, Mechanique celeste, suppl. 10th vol 1806

[13] W.G.Anderson SPE, Conoco inc, *Wettability litterature survey - part 4. Effects of wettability on capillary pressure* 1987

[14] H.Anton and C.Rorres, Elementary Linear Algebra with

Supplemental Applications 10th edition
[15] T.B.Ødegården, *Oil release and transport mechanism due to wettability change in a mixed-wet 2d porous medium*, Master thesis in physics, NTNU 2010
[16] G.G.Batrouni and A.Hansen, *Fourier acceleration of iterative processes in disordered systems*, J. Stat. Phys. 52, 747-773. 1988
[17] E.Aker, K.Måløy, A.Hansen, G.Batrouni, *A Two-Dimensional Network Simulator for Two-Phase Flow in Porous Media*, Transport in porous media 32: 163-186, 1998
[18] R.Booth, *Miscible Flow Through Porous Media.*, DPhil, Oxford, Sept. 2008
[19] E.W.Washburn, Phys Review 17 273 1921
[20] J.L.Barrat, L.Bocquet, phys Review Letters Volume 82, nr. 23 june 1999
[21] S.Berg, A.W.Cense, J.P.Hofman, R.M.M.Smits, *Two-Phase flow in porous media with slip boundary condition*, Transp. Porous Media 74, 275-292 2008
[22] H.A.Knudsen, E.Aker, A.Hansen, Transp. Porous Media 47, 99 (2002).
[23] Mathematica 5.2 Documentation
[24] R.Nasralla, M.Bataweel, H.Nasr-El-Din, *Investigation of Wettability alteration by low salinity water in sandstone rock*, SPE 146322, 2011
[25] R.N.Wenzel, Industrial and engineering chemistry vol 18, NO. 8, 1936
[26] K.S.Sorbie, I.R.Collins, *A proposed pore-scale mechanism for how low salinity waterflooding works*, SPE 129833 2010
[27] S.M.Rivet, W.Larry, G.A.Pope, *A Coreflood Investigation of Low-Salinity Enhanced Oil Recovery*, SPE 134297 2010
[28] F.M.White, *Fluid mechanics*, 6th edition, 2007
[29] R.Lenormand, C.Zarcone and A.Starr, *Mechanisms of the displacement of one fluid by another in a network of capillary ducts*, J.Fluid Mech 135:337-353 1983
[30] R.Lenormand, E.Touboul and C.Zarcone, *Numerical models and experiments on immiscible displacement in porous media*, J.Fluid Mech 189:165-187 1988
[31] L.Paterson, *Diffusion limited aggregation and two-fluid displacement in porous media*, Phys rev. Lett 52:1621-1624, 1984
[32] G.Batrouni, A.Hansen, *Fracture in three-dimensional fuse networks*, Phys. Rev. Lett. 80, 325-328. 1998
[33] J.D.Chen, D.Wilkinson, *Pore scale viscous fingering in porous media*, Phys rev. Lett 55:1882-1895, 1985
[34] K.J.Måløy, J.Feder, T.Jøssang, *Viscous fingering fractals in porous media*, Phys rev. Lett 55:2681-2691, 1985
[35] D.Wilkinson, J.F.Willemsen, *Invasion percolation, a new form of percolation theory*, J.Phys A 16:3365-3376 1983
[36] R.Lenormand, C.Zarcone, *Capillary Fingering: Percolation and Fractal Dimension*, Transport in Porous Media 4: 599-612 1989
[37] M.Cieplak, M.O.Robbins, *Dynamical Transition in Quasistatic Fluid Invasion in Porous Media*, Physical review letters Vol 60, Nr. 20 , 1988
[38] D.Stauffer, A.Aharony, *Introduction to percolation theory, 2nd edition*, Taylor and Francis, London, Washington, DC 1992
[39] G.Tørå , T.Ramstad, A.Hansen, *Anomalous diffusion on clusters in steady-state two-phase flow in porous media in two dimensions*, EPL, 87 (2009) 54002
[40] T.Ramstad, A.Hansen, *Cluster evolution in steady-state two-phase flow in porous media*, Physical review E 73, 026306, 2006
[41] B.Berkowitz , R.P.Ewing, *Percolation theory and network modeling applications in soil physics*, Surveys in Geophysics 19: 23-72, 1998.
[42] Dr. Kim Christensen, *Percolation theory, Lecture notes*, Imperial College London 2002
[43] E.Aker, *A simulation model for two phase flow in porous media*, Master thesis, University of Oslo 1996
[44] G.M.Homsy, *Viscous fingering in porous media*, Ann. Rev. Fluid Mech 19:271-311, 1987
[45] Santanu Sinha, *Steady-state two-phase flow in porous media*, Powerpoint presentation Department of Physics, NTNU, Trondheim, Norway
[46] G.E.P.Box, M.E.Muller, *A Note on the Generation of Random Normal Deviates* , Annals Math. Star. 29, pp. 610-611, 1958
[47] S.E.Buckley, M.C.Leverett, *Mechanism of fluid displacement in sands*, Trans. AIME, 146, 107-116, 1942
[48] J.Kleppe, *TPG4150 Reservoir Recovery Techniques*, Lecture notes 2011
[49] B.Koiller, H.Ji, and M.O.Robbins, *Fluid wetting properties and the invasion of square networks*, Phys. Rev. B 45, 7762-7767 (1992)
[50] H.Ji and M.O.Robbins, *Transition from compact to self similar growth in disordered systems: Fluid invasion and magnetic-domain growth*, Phys. Rev. A 44, 2538-2542 (1991)
[51] E.Kreyszig, *Advanced engineering mathematics*, Wiley International 9th edition, 2006.
[52] W.H.Press, S.A.Teukolsky, W.T.Vetterling, B.P.Flannery, *Numerical recipes, The art of scientific computing* , 3rd edition, 2007